An Investigation of Inkjet Printing of Polycaprolactone Based Inks

By

Yinfeng He

A Doctoral Thesis Submitted in Partial Fulfilment of the Requirements for the Award of Doctor of Philosophy of Nottingham University

Department of Mechanical, Materials and Manufacturing Engineering

March, 2016

Abstract

Traditional manufacturing methods like moulding or subtractive manufacturing place significant limitations on structures which could be manufactured in a single process. These limitations can now be overcome by a new manufacturing technology—Additive Manufacturing (AM), which provides the users much more freedom to design and produce structures in one piece. Additive manufacturing refers to a range of processing technologies, which fabricate 3D parts by adding successive layers. With this technology, complex 3D structures can be produced directly following the production of a geometric data. Additive manufacturing also enables production without the need of tooling, which brings the prospect of a revolution in the manufacturing industry.

Material jetting is one of the additive manufacturing techniques, which generates material layers through inkjet printing. This technology also allows the user to build structures consisting of more than one material, which further expands the capability of additive manufacturing to include the production of multi-functional products. However, due to the strict requirements on the rheology of usable inks, there is a limited number of materials available for use in this technology.

This research aims to develop a novel polycaprolactone based ink which is suitable for material jetting and could be potentially used for fabricating scaffolds. The bespoke nature of these devices often require a complex structures, customized design and small batch sizes, which all together make the product costly when using the traditional manufacturing methods. Additive manufacturing technology can reduce these costs, in the main due to the nil

marginal cost (e.g. tooling cost, mould design etc.) when changing product design. In addition, material jetting can also incorporate multi-materials or multi-functional devices, mixing several materials at micron level, potentially enabling more advanced and intelligent functions to be incorporated into the final devices.

In this project, Polycaprolactone (PCL), commonly used for its biodegradable properties, was investigated as a candidate for material jetting. Both solvent based and UV reaction based jetting techniques were attempted to build up an understanding of the aspects and parameters involved in material jetting ink development and jetting parameter optimization.

For solvent based PCL ink, PCL flakes were dissolved into various solvents with different concentrations to prepare a low viscosity ink which could be printed. Volatility, viscosity and surface tension were investigated to confirm that the prepared ink was suitable for jetting. PCL with 5wt% in 1,4-dioxane was successfully jetted by using a Dimatix material printer. A range of experiments were carried out to investigate the ink's printability under different conditions. During the study, efficiency limitation for solvent based ink was also realized. In order to meet the printing viscosity limit of the inkjet printheads, the loading level of a solute in a solvent ink as well as the efficiency of stacking precipitated layers were both restricted. This curbed the possibility of solvent based ink be applied in making large 3D parts.

For UV reaction based inks, the printed ink can fully solidify to form structures after UV illumination, which overcame the processing efficiency limitation of the initial solvent based inks. Pure PCL is not UV curable and therefore

chemical modifications were made to graft UV curable functional groups into the PCL structure. The rheology of synthesized UV curable PCL polymers were studied and modified to make them suitable for material jetting. Different photoinitiators were also investigated to work out the suitable composition to achieve real-time curing. Oxygen inhibition was found to be the main side effect which inhibited the curing reaction in an air environment. Type II photoinitiators can help overcome this effect and 3D structures were able to be obtained in both air and nitrogen. It was also found that a nitrogen environment can improve the properties of the printed specimens and the printed samples showed better hardness and modulus than those in printed in air. It was also noted that the increasing concentration of the photoinitiator can improve the curing speed of the ink printed in air. However the samples with higher concentration of photoinitiators manifested a reduction of hardness and modulus. A post-curing procedure, carried out using further UV illumination, was shown to help improve both the hardness and the modulus, but this improvement was limited to the directly illuminated surface.

Acknowledgement

I would like to express my deepest appreciation to my supervisors Professor Ricky Wildman and Professor Christopher Tuck for their guidance, suggestions and supervision throughout my whole PhD period. It has been my honour to be a research student under their patient supervision and receive their valuable comments to my researches, papers and thesis. I am also highly indebted to Dr Christie Steven, Dr Stephen Edmondson and Sam Kilsby for their support in completing the project.

Thanks to Loughborough University, Nottingham University and Engineering and Physical Sciences Research Council (EPSRC) for covering all of my university tuition fees and living expenses and financial support for attending internal conferences. My thanks and appreciations also go to Prof, Richard Hague, who accepted my e-mail and gave me a chance when I was seeking for a PhD opportunity.

I would like to express my gratitude towards to all the staff of the Faculty of engineering, Nottingham University for their support and help, especially Thomas Buss, Mark Daine, Martin Roe, David Mee, Calum Welsh and Hassan Rashidi. I would also like to express my special gratitude and thanks to all the members of the Additive Manufacturing Research Group (AMRG). I am sincerely grateful to Mark East, Mark Hardy, Joseph White, Dr. Bochuan Liu, Dr. Jiaming Bai, Dr. Xuesheng Chen, Dr Belen Begines and Dr. Hongyi Yang for their kindness help and encouragement.

List of Publications

Published

Yinfeng He, Ricky D. Wildman, Chris J. Tuck, Steven D.R. Christle, and Steven Edmonson, An Investigation of the Behaviour of Solvent Based Polycaprolactone Ink Developed for Material Jetting, (*Scientific Report*)

Manuscript submitted

Yinfeng He, Chris J Tuck, Elisabetta Prina, Sam Kilsby, Steve DR Christie, Steven Edmondson, Richard JM Hague , Felicity RAJ Rose, and Ricky D Wildman, A New Photocrosslinkable Polycaprolactone based ink for 3D Inkjet Printing

Conference Presentations

Yinfeng He, Sam Kilsby, Chris J.Tuck, Ricky D. Wildman, Steven D.R. Christie, Hongyi Yang, Steven Edmondson, An Study of 3D Printing on Processing Biodegradable Polycaprolactone, *Solid Freeform Fabrication*, 2013

Yinfeng He, Chris J. Tuck, Ricky D. Wildman, Steven D.R. Christie, Steven Edmondson, Hongyi Yang, An Study of Processing Biodegradable PCL through 3D Printing, *European Conference on Biomaterials,2013*

Yinfeng He, Sam Kilsby, Chris J. Tuck, Ricky D. Wildman, Steven D.R. Christie, Hongyi Yang, Steven Edmondson, 3D Jetting of UV Curing Based Bioresorbable Polycaprolactone, *Solid Freeform Fabrication*, 2014

Yinfeng He, Sam Kilsby, Chris J. Tuck, Ricky D. Wildman, Steven R.D. Christie, Steven Edmondson,A Biodegradable Polycaprolactone Based Ink Developed for 3D Inkjet Printing, *Society for the Advancement of Material and Process Engineering*, 2014

Contents

List of Figures

List of Table

Chapter 1. Introduction

1.1 Background

3D Printing or Additive Manufacturing (AM) is an advanced manufacturing technology that relies on addition of material, rather than subtraction. Starting out as a prototyping methodology, recent efforts have focused on it becoming a process that is able to manufacture end-use products. One of the potential applications for AM is in the making of medical devices with inbuilt functions such as tailored drug release or degradation speed. Such biomedical devices often require a customized design to meet the needs of the patient, achieve enhanced cell adhesion and growth (Bobyn et al., 1999; Hacking et al., 2002; Bobyn et al., 2005). These requirements are difficult and/or costly through current manufacturing techniques. However, AM offers a potential for these difficulties to be overcome, either reducing the cost or improve the performance of the product. Unlike subtractive methods, AM allows for the manufacture of complex, bespoke products, with little to no marginal cost, opening up a vista of products previously unachievable.

Polycaprolactone (PCL) is widely used in the biomedical area, which can slowly decompose, usually through random hydrolytic chain scission of the ester groups (Pitt, 1984). Previous attempts to build PCL structures with AM have included Powder Bed Fusion (i.e. laser sintering) or material extrusion (Ramanath et al., 2008; Williams et al., 2005; Eshraghi and Das, 2010).

However, these processes are limited in terms of embedded functionality and resolution. In comparison to the other techniques, material jetting has the potential for producing multi-material products within a single process cycle and achieving controllable micron level material distribution in the final product. This capability can offer more extensive functionality, for example the manufacture of products with a localized drug distribution or degradation speed. As a consequence, this work will focus on understanding routes to the development of printable PCL formulations that in the future could lead to its use in the manufacture of biomedical products.

1.2 Aims and Objectives

Aims:

This PhD project will develop the requisite understanding to enable the printing of polycaprolactone based formulations.

Objectives:

- To develop printable formulations based on polycaprolactone.
- To optimize printing conditions to allow for reliable printing polycaprolactone based formulations through drop on demand piezo based ink jet printers.
- To characterize the quality of printed polycaprolactone samples.

1.3 Research Concept

Material jetting has a highly constrained dependence on the rheology and solidification of the ink. The viscosity of melted high molecular weight PCL is normally several hundred times higher than most commercial piezo based

printheads' viscosity limit, as a result of polymer chain entanglement. This makes such materials hard to be jetted directly by melting. In order to satisfy the printing viscosity requirement, two potential methods could be used. The first method is to dissolve polymerized PCL into a solvent to create an ink with sufficiently low viscosity. After being deposited on to the target surface, the solvent can be evaporated and the dissolved PCL will precipitate to form a solid layer. The second method is to print a low viscosity oligomer of PCL, which normally has relatively low viscosity and can be manipulated by varying the environmental conditions or ink composition to satisfy the printing viscosity range. After deposition, a polymerization reaction can be triggered by applying external energy source such as UV light or heat to achieve solidification.

1.4 Structure of the Thesis

A brief description of the thesis structure is given below:

Chapter 2 Literature Review provides a brief review of the basic concepts for additive manufacturing. Previous studies about jetting will then be reviewed including the printhead design, ink development requirements, jetting parameters and potential problems which may happen during the jetting process. To finish, current research about Polycaprolactone, AM manufactured PCL structures and PCL derivatives will be reviewed.

Chapter 3: Methodology and Experimental Setup introduces the research approaches for this project following by an introduction to the main equipment used for ink development and jetting. Preparation protocols for the inks based on different solidification concepts will be described. The synthesis of UV curable Polycaprolactone will be described.

Chapter 4: Polycaprolactone Solvent Based Ink will introduce the attempts of printing Polycaprolactone (PCL) by dissolving it into specific solvents. In this chapter, the printability of PCL solvent based inks and printing parameters will be studied and modified to improve the ink's printing stability. Layered PCL structures will be printed.

Chapter 5: Polycaprolactone UV Curing Based Ink will study the printing of chemically modified UV curable Polycaprolactone. The rheology behaviour will be studied and modifications will be made to improve the ink's printability. Different kinds of photoinitiators and their performances will be tested to identify the most suitable for material jetting. The influence of the post-curing procedures on the products' properties will be studied. Further experiments will also investigate how photoinitiator concentrations as well as the printing environment will influence the properties of the printed sample.

Chapter 6: General Discussion will discuss the advantages as well as potential risks of different ink formulations. The properties of fabricated samples will also be compared with the samples fabricated by the commonly used AM techniques in the literature to highlight the improvements proposed by the methods proposed in this research.

Chapter 7 Conclusion and Future Work provides the main conclusions from this project and the suggestions for future work.

Chapter 2. Literature Review

2.1 Development of Additive Manufacturing

The concept of Additive Manufacturing (AM) first appeared in the 20th century under the name of rapid prototyping (RP). Traditional processing methods may need days or even months in tooling design and preparation which is costly for realizing preliminary ideas. AM, by contrast, is a mould-free processing technique, which skips the costly tooling design and allows users to produce prototypes quicker and more economy. The processing cycle is able to be reduced from several days down to several hours. More important, as a layer based mould free manufacturing method, AM can overcome many design limitations and provide the users with more design freedom.

In the early stages, limitations regarding materials meant that AM was only applied in the production of models or prototypes, since the achievable materials' mechanical properties were poor by engineering standards (Gibbons et al., 2010). In recent years, the development of materials science and processing technology has improved AM product properties as well as accuracy, which has greatly expanded the application of AM (Dimitrov et al., 2006; Stopp et al., 2008). As a consequence, AM now is also used for the production of small batches of customized products with complex or unique shapes which are hard to realize by traditional manufacturing methods. Although AM products are more expensive when compared to mass

manufacturing, when comparing to small batches, the unit cost is significantly lower (Gibson, 2010).

ASTM has classified the commercial AM techniques into seven categories including (ASTM, 2012):

- Binder Jetting
- Directed Energy Deposition
- Material Extrusion
- Material Jetting
- Powder Bed Fusion
- Sheet lamination
- Vat Photopolymerization

All these techniques are layer based manufacturing methods but using very different initial materials including reactive oligomer liquid (material jetting and vat polymerization), powders (binder jetting and powder bed fusion), polymers strips (directed energy deposition and material extrusion) and solid sheets (sheet lamination). The technique used in this PhD project belongs to the material jetting category. For details of other techniques, the reader is referred to the work of Gibson, Wohlers and Hopkinson (Gibson, 2010; Wohlers, 2007; Hopkinson, 2006).

AM techniques normally share the same generic processes which include 8 steps. They are (Gibson, 2010):

- Conceptualization or CAD
- Stereolithography (STL) Convert

- Transfer the STL file to AM machine
- Machine setup
- Removal and Cleanup
- Post-process
- Application

With the help of computer, a 3D model can be created by three-dimensional Computer Aided Design (3D CAD). Then, the model will be converted into an STL file, during which the 3D model is converted into a range of 2D layers of sample cross-section (where the number of layers depends on the resolution of processing). AM machines can then reproduce the original design by building the product layer by layer. Thinner layer thickness provides higher resolution in the *z* direction, which allows the product to have smoother surfaces and the appearance is closer to the original design. Sometimes post-processes such as polishing or post-curing may be carried out to improve the product's surface finishing or mechanical properties.

2.2 Material Jetting

In the ASTM classification, material jetting is defined as:

"…*an additive manufacturing process in which droplets of build material are selectively deposited*." (ASTM, 2012).

The droplets mentioned in the definition are normally generated by one or more printheads which following similar principles to the 2D printing.

In general the inks being printed can have a range of states including molten materials, monomers or oligomers. Printed layers are then solidified by natural

cooling or polymerization reactions and stacked up until the product is formed. Figure 2.1 is a schematic of how material jetting works. The build platform will move downward after each layer is finished. Several printheads can be assembled together in one printer to print structural materials and support materials simultaneously.

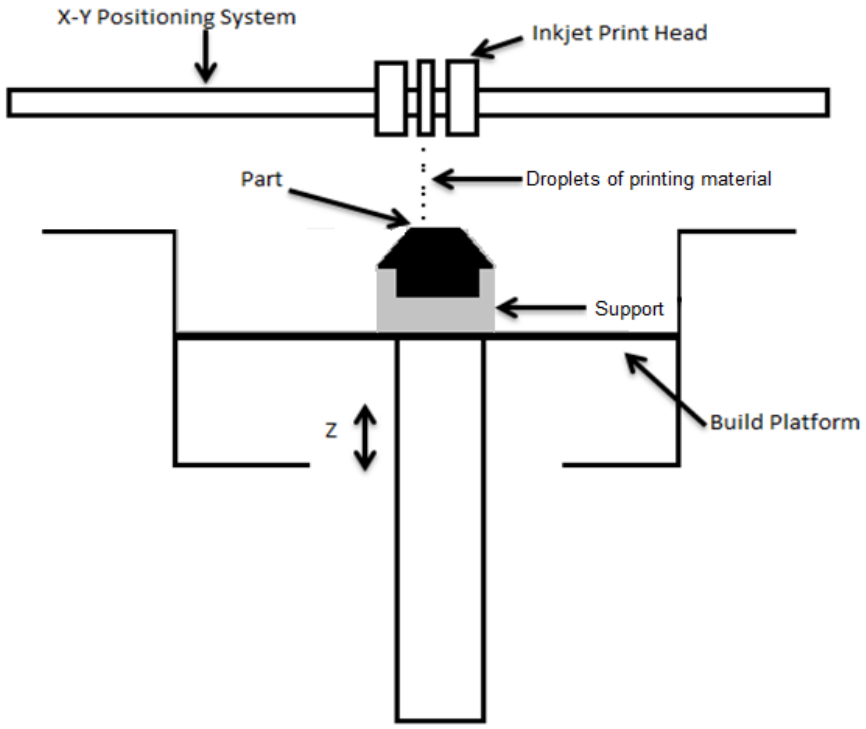

Figure 2.1: Schematic of material jetting modified from Objet datasheet (Objet, 2012)

Comparing with the other AM techniques, material jetting process is able to achieve lower layer thickness and finer multi-material distribution. Layer thickness is one of the parameters which can be used to judge resolution in *z* direction. The layer thickness of a powder bed fusion system (such as selective laser sintering and selective laser melting) is normally between 20μm to 100μm (EOS, 2014; Renishaw, 2014), while material extrusion is typically 100μm to 200μm (Stratasys, 2014; Makerbot, 2014). The layer

thickness of material jetting in commercial systems can be 16μm or smaller (Stratasys, 2014), which will provide better surface finishing. As each material is printed by an independent printhead, material jetting can produce specimens with two or more materials within a single process. Meanwhile, as each material was deposited dropwise (20-80μm droplet diameter), the distribution can be controlled at the micron level which makes this technique superior to others. Currently, there are a limited number of processes, which can produce multi-material samples for example, material extrusion, direct energy deposition (DED) and material jetting. In comparison, material jetting has a much better resolution than material extrusion and is capable of processing polymeric materials.

2.3 Printhead

The printhead is one of the most important units in material jetting technology, and it also determines product resolution, processing speed and printing materials. Most of the commercial printheads are based on Drop-On-Demand mode. Continuous mode printhead is also available but not widely used. In the following section, the mechanism of each mode will be introduced respectively.

2.3.1 Continuous Mode

Figure 2.2 is a schematic of continuous mode printhead. Material is pumped into the printhead from a material reservoir and a continuous stream of ink is ejected from the nozzle. Due to the Rayleigh instability effect, the stream breaks into droplets after leaving the nozzles. Extra procedures such as vibration may be applied to help produce more consistent and uniform droplets (Gibson, 2010). The droplets then pass through a charging field and

obtain an electrostatic charge. After that, the charged droplets will enter a deflection field, which will determine whether droplets are going to be deposited on the substrate or collected by droplet catcher by controlling the deflection field's voltage signal

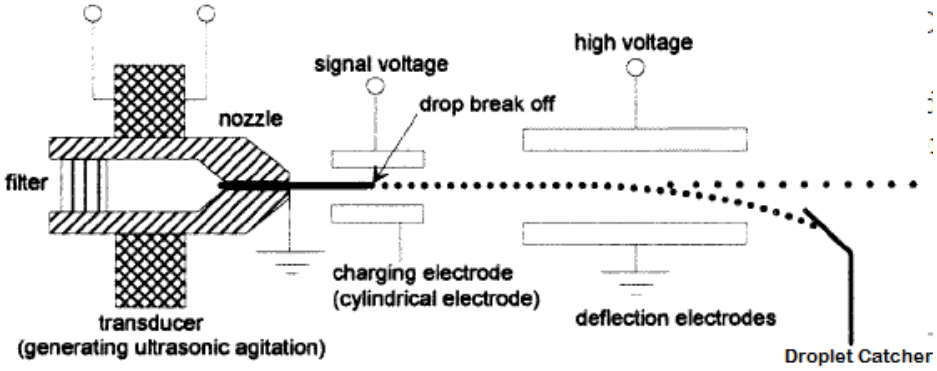

Figure 2.2: Schematic of continuous mode jetting (Deipold et al., 1998)

2.3.2 Drop-on-Demand Mode

Drop-on-demand (DOD) mode is the most widely used printhead mode in commercial printing machines. Droplets are ejected whenever it is demanded by generating a pressure wave inside the ink channel of a printhead. The internal pressure wave can be generated by either a piezoelectric or a thermal actuator. Comparing with continuous mode, the structure of DOD mode can be applied to more materials as electrostatic charge is not required and less ink wastage.

Figure 2.3 shows the mechanisms of the both piezoelectric and thermal actuators. For thermal actuator based printhead, the internal pressure wave is generated by localized heating up the ink and letting bubbles nucleate at the heating surface. The bubble will lead to a pressure rise in the chamber, which

push the ink out from the orifice. For piezoelectric actuator, the internal pressure is generated by physical deformation of the piezo-ceramic. When a voltage pulse is applied, the piezo-ceramic inside the printhead will deform to squeeze the ink out. By varying the voltage pulse intensity, length and frequency, the formation of droplet will be varied.

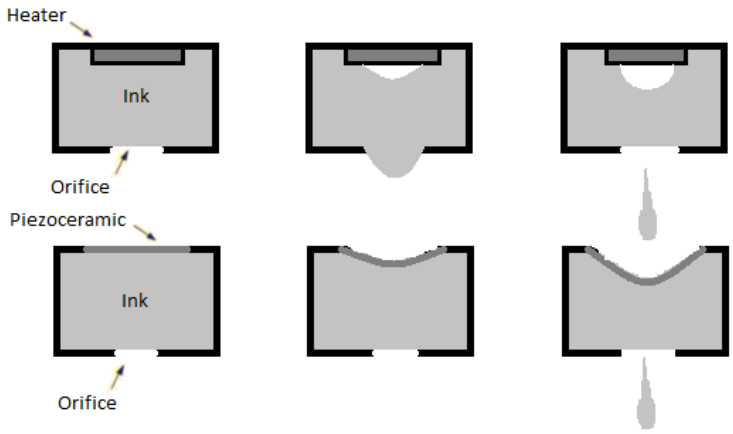

Figure 2.3: Schematic of piezoelectric and thermal actuators (Gibson, 2010)

There are four types of commercial piezo-ceramic actuator, which are: Squeeze mode, Shear mode, Push mode and Bend mode (Brunahl, 2003):

Squeeze Mode

A piezo-ceramic tube, which can deform radially, is used as an actuator to connect the ink channel and the nozzle. Ink from the reservoir will go through the channel and fill up the ceramic tube, then reach the nozzle. When a voltage pulse is applied, the piezo-ceramic tube will contract to squeeze the ink out. After that, when the voltage is removed, the ceramic tube will recover to the original state, which will create a negative pressure inside to refill the cavity with fresh ink.

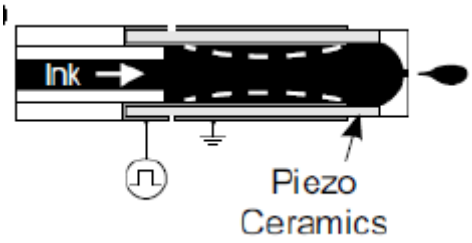

Figure 2.4: Schematic of the squeeze mode piezo-ceramic actuator (Brunahl, 2003)

Shear Mode

In the shear mode, the deformation direction of piezo-ceramic is designed to be perpendicular to the printing direction, which generates shearing force to squeeze the ink out. As shown in Figure 2.5, the mechanism of the shear mode is similar to the squeeze mode. However, instead of using a piezo-ceramic tube, piezo-ceramic plates are used and arranged in parallel with each other to form channels. When a voltage pulse is applied, piezo-ceramic plates will deform and generate shearing forces to create an ink droplet. When opposite voltage pulses were applied to the two piezo-ceramic walls, it will cause transient volume change inside the channel (increase or decrease) and therefore generate an internal pressure wave that forms a droplet (Figure 2.5). This shear mode is mainly used by Xaar.

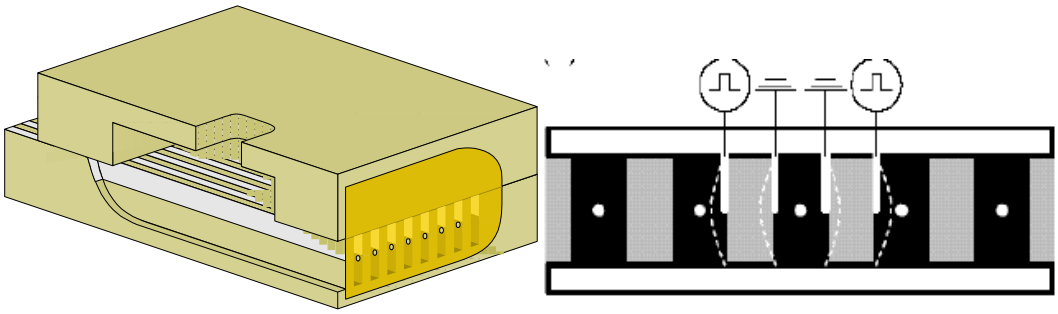

Figure 2.5: Schematic of shear mode piezoelectric actuator (Brunahl, 2003)

Push Mode

A schematic of Push mode is shown below in Figure 2.6. The piezo-ceramic plate is placed directly above the nozzle. When a voltage is applied, the piezo-ceramic plate will deform to cause a volume change inside the ink channel, which generates an internal pressure wave and form droplets.

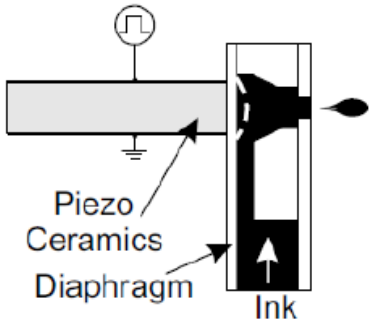

Figure 2.6: Schematic of push mode piezo-ceramic actuator (Brunahl, 2003)

Bend Mode

The structure of a bend mode printhead is very similar to push mode. However, the piezo-ceramic is not directly facing the nozzle. A pressure chamber is introduced with piezo-ceramics attached to one side of it. When a voltage pulse is applied, piezo-ceramics will bend inward and cause a pressure rise that expels a droplet through the nozzle. When the voltage pulse is withdrawn, the piezo-ceramics will recover and therefore, generate negative pressure which helps ink refilling.

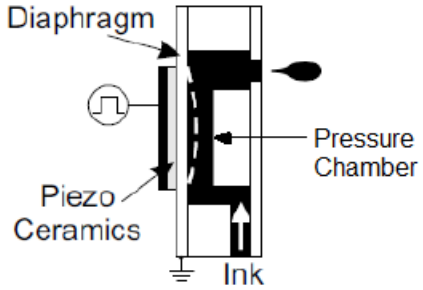

Figure 2.7: Schematic of bend mode piezoelectric actuator (Brunahl, 2003)

2.3.3 Comparison of Two Printing Modes

Continuous mode printhead is one of the oldest inkjet technologies which have relatively high droplet ejection frequency and better nozzle stability when printing volatile inks. However, it is not widely used in the market now due to the limitations of the compatible ink and the ink wastage during the process. As mentioned before, the continuous mode printhead requires the ink is able to carrying charges while this is not requisite for the DOD mode printhead. Therefore, the DOD mode printhead provides more design freedom for ink formulations and less restrictions in materials selection, which makes the idea of developing new functional inks jetting more feasible. In the meantime, DOD mode printhead provide better controlling of the ink ejection and less ink wastage as it only ejects ink droplets whenever it is required, while for continuous mode printhead, the ink is jetted constantly. As a consequence of these, most of the commercial printheads are based on DOD mode.

2.4 Material Jetting Technology

Material jetting aims to print the target material directly. There are two kinds of material jetting technologies: direct printing and reactive printing. These technologies are going to be introduced in the following section.

2.4.1 Direct Printing

Direct printing is the printing of materials directly through a printhead without any chemical reaction included. The material falls into a printable viscosity range by either melting or dissolved into a solvent.

In 1994, Sanders Prototype developed the first commercial material jetting machine named ModelMake, which used melt wax as the structural material. In 1996, 3D Systems developed Actua2100 later known as Thermojet, which was another wax-based 3D printing machine (Gibson, 2010). All the machines above are based on direct printing technology and primarily use wax. By heating wax up to 95-115°C, it will transform into low viscosity melt and then solidified rapidly by natural cooling after being printed onto target surface.

Though high molecular weight polymers usually have good mechanical properties and they are good candidates for material jetting (Gowariker, 1986; Williams, 1971; Ebewele, 2000), the viscosity of their melt are hundreds or even thousands of centipoise (cp) due to long polymer chains and entanglement. This makes most of the thermoplastic polymers is unprintable. Solvent based deposition is a potential method for the processing of high molecular weight polymers. Ink could be prepared by dissolving high molecular weight polymers into low viscosity solvents to reduce the mixture

viscosity. After deposition, the solvent can be removed (normally by evaporation), leaving a layer of polymer.

Metals are normally small molecules, but commercial metal material's melting points are much greater than a normal printhead's processing temperature range (around 100°C). It is possible, however, to use DOD printing to deposit low melting point metals. Yamaguchi et al. (Yamaguchi et al., 2000; Yamaguchi et al., 2003) developed an alloy (Bi-Pb-Sn-Cd-In) with 47°C melting point, which was successfully jetted from nozzles with 200 μm, 50 μm and less than 8 μm in diameter at 55°C.

2.4.2 Reactive Printing

As the viscosities of many pure polymers are too high to be printed, low viscosity oligomers or monomers are potential candidates for reactive inks. Such an ink is polymerized after being deposited onto a target surface. Currently, the most widely used reaction is an Ultraviolet (UV) light curing reaction, which can trigger oligomers to crosslink and solidify within seconds in the presence of photo initiators. 3D printing machines based on reactive printing were brought onto the market by *Objet*. Photocurable oligomers were the chief structural materials used for reactive jetting. By varying an oligomer's backbone structure, side groups and ink additives, reactive jetting can produce a range of products with very different properties ranging from rubbery opaque to solid glassy. UV light is introduced after droplets were deposited on to the target surface to initiate the polymerization reaction. The liquid form oligomers then crosslink and solidify within seconds.

The mechanical properties of UV cured polymers are superior to wax based materials. However, these polymers formed by the crosslink reaction are thermoset polymers and the curing is irreversible. Therefore, these materials are difficult to be recycled after curing.

2.5 Optimizing the Printing Process

Optimizing the printing process includes three stages: printability assessment, droplet formation optimization and deposition optimization. There are many parameters and side effects that need to be addressed in these three stages in order to work out a practical ink formulation for a material jetting process.

2.5.1 Printability assessment

Generally, in order to assess whether an ink is printable or not, the most important properties which need to be characterized are the viscosity and surface tension. Printhead manufacturers usually will provide a printing viscosity and surface tension range for specific versions of a printhead to help the users identify if a liquid is able to be printed or not.

Viscosity

Viscosity is the key factor in judging whether or not a liquid is printable. It is defined by the resistance to deformation under shearing or tension. As viscosity is increased, more energy will be dissipated through internal friction when forming a droplet. Whenever the piezo-ceramic cannot provide enough energy within its working voltage limit, ink will not be printable.

Surface Tension

Surface tension is another factor that will influence the amount of energy required at the droplet formation stage. Forming a droplet will create new surface area and the energy required for creating unit area of new surface is defined as the surface energy (Chan, 1993). Normally, this energy varies with the different kinds of molecules used to in an ink and it is possible to be manipulated by using surfactant.

Printing Indicator

Viscosity and surface tension can be used to roughly judge whether an ink is printable or not. Ainsley et al. promote a printing indicator equation to help assess an ink's printability with the consideration of both viscosity and surface tension. This equation is based on Reynolds Number and Weber Number (Ainsley et al., 2002)

$$Z = \frac{Re}{We^{\frac{1}{2}}} = \frac{\sqrt{\rho r \gamma}}{\mu} \qquad \text{Equation 2.1}$$

where ρ is density, r is characteristic length, γ is surface tension of the fluid and μ is viscosity of ink. They suggested that when the value of printing indicator falls between 1 and 10, an ink could be identified as printable. This indicator, however, is still only a guide and not suitable for all inks. Take water as an example, it has high surface tension and low viscosity, so the value of printing indicator is above 10. Water, however, is printable and ttherefore, this indicator cannot be used as a general law (Gibson, 2010).

2.5.2 Jetting Parameters

The stability of ink droplet formation during jetting process is an important factor which influences the resolution and consistency of the printed structures. This is controlled by the jetting parameters during the printing process, which includes jetting voltage, jetting temperature and jetting waveform.

Jetting Voltage

At the droplet formation stage, the jetting voltage is directly related to the energy imparted to generate a droplet. As described before, the amplitude of the piezo-ceramic deformation is positively related to the amplitude of jetting voltage. It will then determine the level of volume change inside the printhead channels and therefore influence the energy imparted to form a droplet. Typically, the imparted energy will convert into three parts as shown in following equation (Gibson, 2010):

$$E_{imparted} = E_{loss} + E_{surface} + E_{kinetic} \qquad \text{Equation 2.2}$$

E_{loss} represents the energy loss, usually associated with viscous heating. $E_{surface}$ is the energy required to form the new droplet surfaces and is directly related to an ink's surface energy. $E_{kinetic}$ represents the energy required to expel an ink droplet at a given velocity. The imparted energy that can be provided by a piezo-ceramic actuator will determine a printhead's printable range of viscosity and surface tension.

Jetting Temperature

The printing temperature will also affect the droplet formation by influencing the ink's physical properties. It has been recognized that the viscosity and surface tension of a liquid is directly related to the temperature and for most of the materials, as temperature increases, both viscosity and surface tension will drop (Palit, 1956; Seeton, 2006). Taking Equation 2.2 into consideration, as an ink's surface tension and viscosity decreases when the temperature is increased, the viscous dissipation as well as energy associated with creating a new droplet surface will both decrease and thus E_{loss} and $E_{surface}$ will both decrease. This concept will be quite helpful when dealing with inks which are slightly out of a printhead's printable range at a certain temperature. By increasing the jetting temperature, a non-printable ink may fall into the printable range.

Jetting Waveform

The precise details of the change in pressure, controlled by the applied voltage to the actuator, can affect the release of the droplet from the nozzle. By varying the level and time length of the voltage pulses, the deformation of the actuator can be controlled, which influences the droplet formation state as well as stability. Different piezo-ceramic actuator deformation sequences will generate different pressure wave inside a printhead, which can be used to manipulate the droplet formation. Previous studies have shown that a suitable waveform can help control droplet volume as well as suppress satellite effects.

Gan et al. (Gan et al., 2009) showed that by varying the waveform, the volume of the droplet can also be controlled. As shown in Figure 2.8 and 2.9,

they investigated 4 types of waveform including unipolar waveform, bipolar waveform, M-shape waveform and W-shape waveform, which showed totally different droplet volume when printing with the same printhead and printing voltage. They suggested that during the printing studies, the volume of droplet need to be taken into consideration during the comparision of printing qualities between different jetting waveforms. Meanwhile, the jetting waveform is a potential way to manipulate the deposited droplet size, which may potentially increase or decrease the jetting resolution.

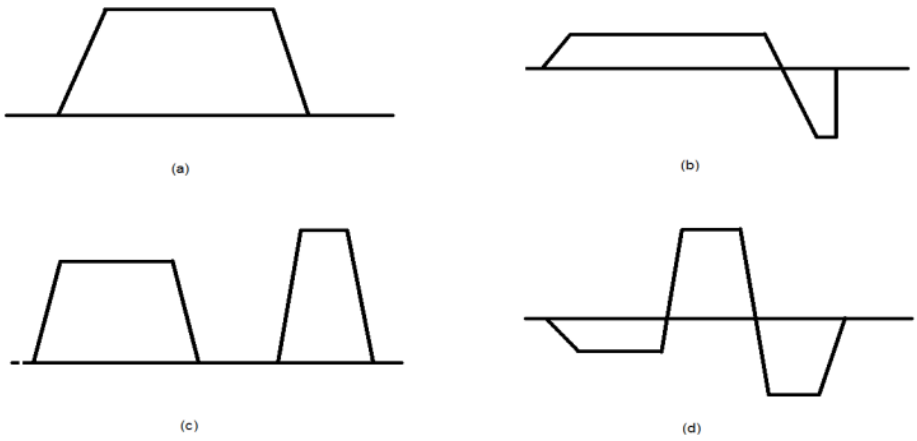

Figure 2.8: Four types of waveform Gao et al. investigated: (a) Unipolar waveform, (b) Bipolar waveform, (c) M-shape waveform (d) W-shape waveform (Gan et al., 2009)

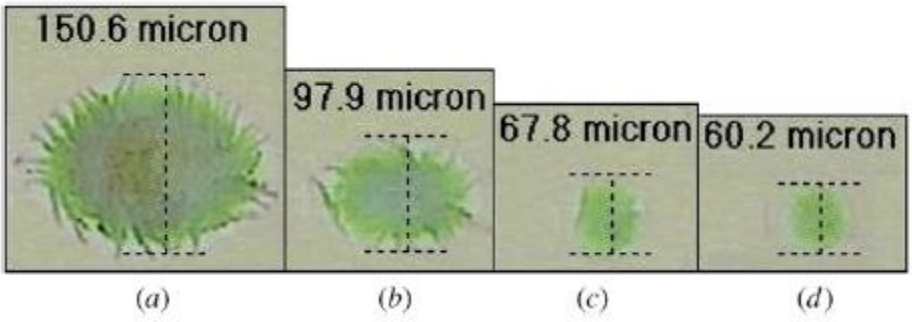

Figure 2.9: Comparison of deposited droplet volume with different jetting waveform: (a) Unipolar waveform, (b) Bipolar waveform, (c) M-shape waveform, (d) W-shape waveform. (Gan et al., 2009)

Satellite Effect

When a droplet pinches off from the nozzle, the liquid thread may break up into one primary droplet and one or several satellite droplets (Figure 2.10). This is known as the satellite effect, which is one of the phenomena that may happen during droplet formation. These satellite droplets may deposit on or around the primary droplet and are detrimental to the printing accuracy. It began to gain attention in the 1970s during continuous jetting when printing technology started to be widely introduced (Pimbley and Lee, 1977; Eggers and Villermaux, 2008). Although piezo-ceramic based DOD printhead mode has more control over an individual droplet, it still suffers from this effect and many efforts have been carried out to suppress this effect by manipulating the printing waveform.

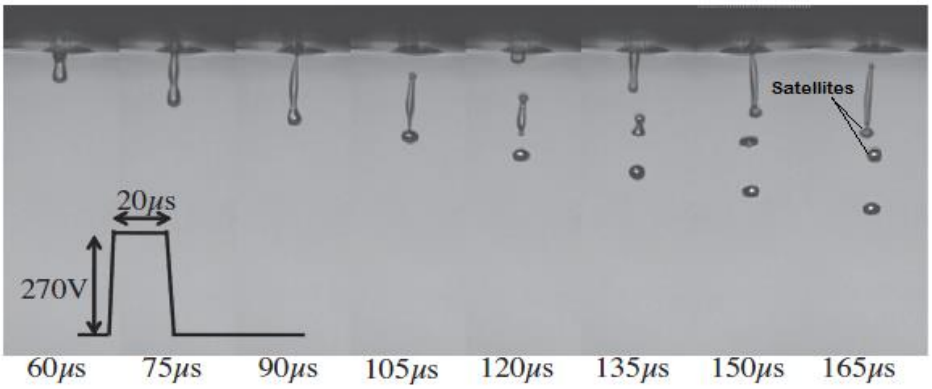

Figure 2.10: A droplet formed with satellite effect (Shin et al., 2011)

Prior studies have shown that the satellite effect of low viscosity inks can be significantly suppressed by introducing a double pulse waveform within a droplet formation cycle (Shin et al., 2011; Dong et al., 2006).

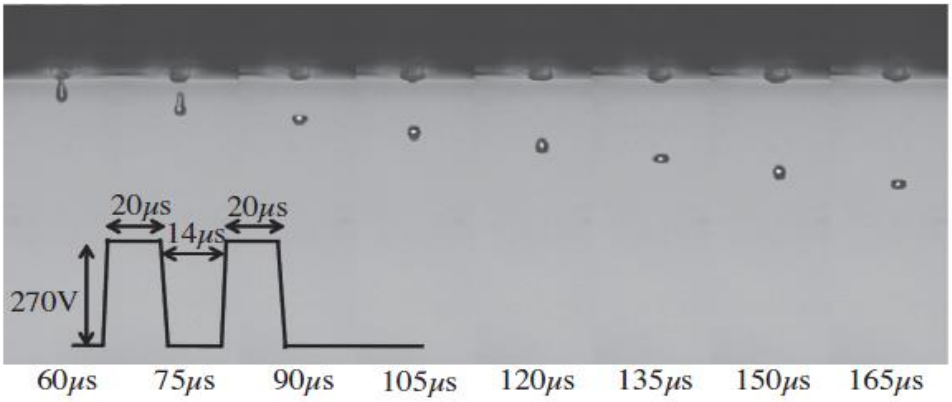

Figure 2.11: Droplet formation image of double peak waveform (Shin et al., 2011)

Figure 2.10 and Figure 2.11 shows that by adding another voltage pulse, the droplet tail as well as satellite effect disappeared. Similar results were also obtained by Dong (Dong et al., 2006) as shown in Figure 2.12. Dong suggested that by adding another small voltage wave, a small pressure was produced, which promoted the separation of the droplet.

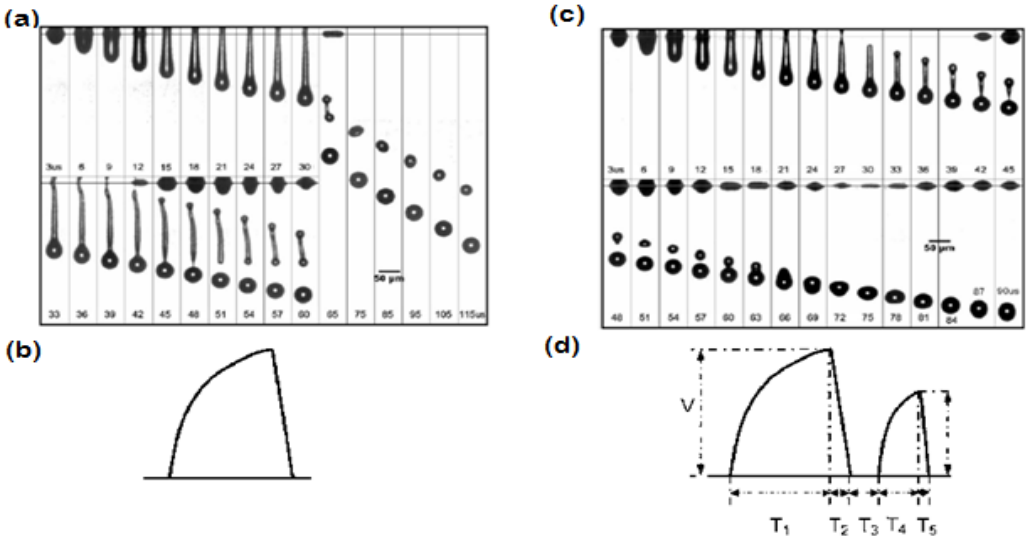

Figure 2.12 droplet formation image comparing of single and double waveform, (a) Droplet formation of single voltage wave,(b) Single voltage wave form, (c) Droplet formation of double voltage wave,(d) Double voltage waveform (Dong et al., 2006)

These studies suggested that whether satellite effect happened or not depended on the thread length and primary droplet speed when the thread broke up. They demonstrated that the retreating speed of the thread tail is almost constant for an ink while the primary droplet speed was related to printing voltage and waveform. When the retreating speed is lower than the primary droplet speed, satellite droplet without recombination will happen. If the satellite effect happens during the actual jetting process, one may minimise it by adjustment of the printing waveform.

2.5.3 Droplet Deposition

After the droplet is formed, it will be deposited on the target surface to form the designed pattern. During the deposition, there are also a few factors which will decide whether a desired pattern can be achieved or not. These factors

mainly include: droplet spacing, substrate temperature and the coffee ring effect (to be introduced in the following section).

Droplet Spacing

Droplet spacing is a very important factor, which influences whether the target pattern can be formed precisely. Normally, in order to form a continuous ink thread or film, the droplet spacing should be smaller than the droplet diameter so that the deposited droplet can overlap with each other and fully cover a target area.

Gao and Sonin printed a series of wax lines with different droplet spacing by varying the printing frequency (shown in Figure 2.13) (Gao and Sonin, 1994). As the droplet spacing approached a droplets' diameter, separate individual droplets started to combine together and form a continuous uniform thread. However if the droplet space was too small, the ink thread became unstable again and began to swell. Therefore, finding the optimum droplet spacing during inkjet printing is a very important step to produce a uniform pattern.

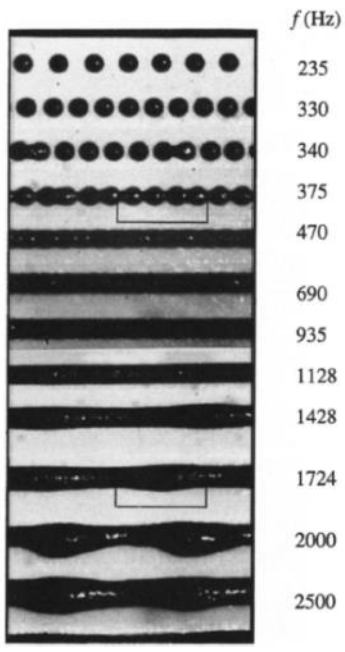

Figure 2.13: Top view of printed wax droplet with different voltage frequency (Gao and Sonin, 1994)

Gao and Sonin (Gao and Sonin, 1994) also suggested that in order to make sure droplets overlap with each other, the droplet spacing must be smaller than the deposited droplet radius R_c which in turn is related to the contact angle on a specific substrate (as shown in Figure 2.14). Therefore, in order to work out the starting droplet spacing gap to form a continuous pattern, it is necessary to study the morphology of deposited individual droplets.

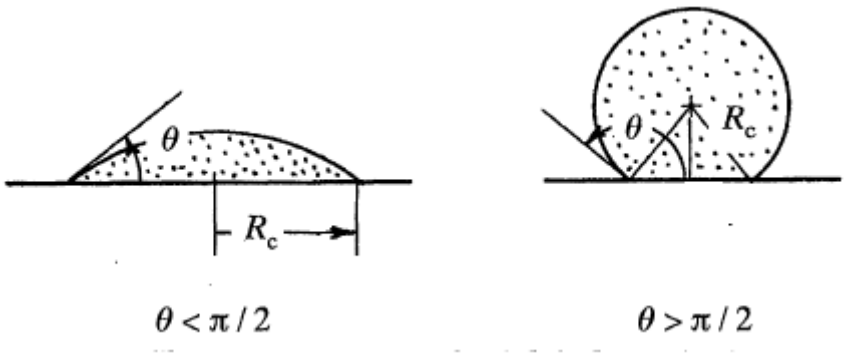

Figure 2.14: The definition of Rc with different contact angle (Gao and Sonin, 1994)

Substrate Temperature

For the inks, whose solidification relies on evaporation, the substrate temperature will determine the evaporation or solidification speed of deposited ink droplets and therefore influence the morphology of the printed pattern.

Teichler et al. (Teichler et al., 2011) performed a series of experiments to investigate the influences of substrate temperature on the printed film quality. Figure 2-15 shows the printed film morphology of the solvent ink printed with the same droplet spacing on to the substrates with different temperatures

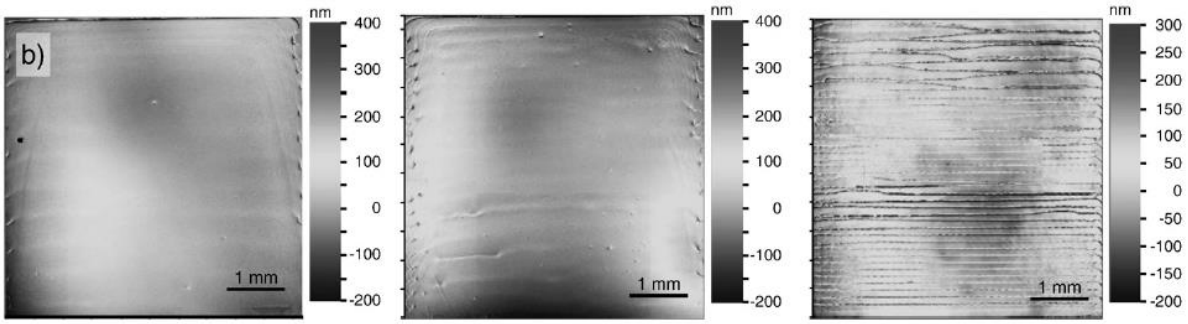

Figure 2.15: Surface appearance of films with different plate temperature room temperature, 35°c and 50°c (Teichler et al., 2011)

From Figure 2.15, it can be seen that as the temperature increases, the boundaries between different ink threads became more significant and influenced the printed film's surface quality. The formation of these boundaries is mainly due to a thread of ink solidified before the next thread is printed.

Lee et al. (Lee et al., 2011) also showed that by increasing the substrate temperature, the boundaries between two threads became more regular and clearer (as shown in Figure 2.16) while at lower substrate temperature, printed threads tended to dissolve and merge with previously printed structures. They explained that this was because by increasing the substrate temperature, the printed ink droplet evaporated quickly and the solvent inside the ink did not have time to dissolve and merge with the solute precipitated from previous thread. Therefore, the thread was pinned at the location where it is printed, making the pattern more regular.

As shown in these works, different ink properties leads to different dependencies on the the plate temperature. It may improve the print quality or

make it worse. Therefore, deciding the substrate temperature is a very important step in optimizing the printing quality.

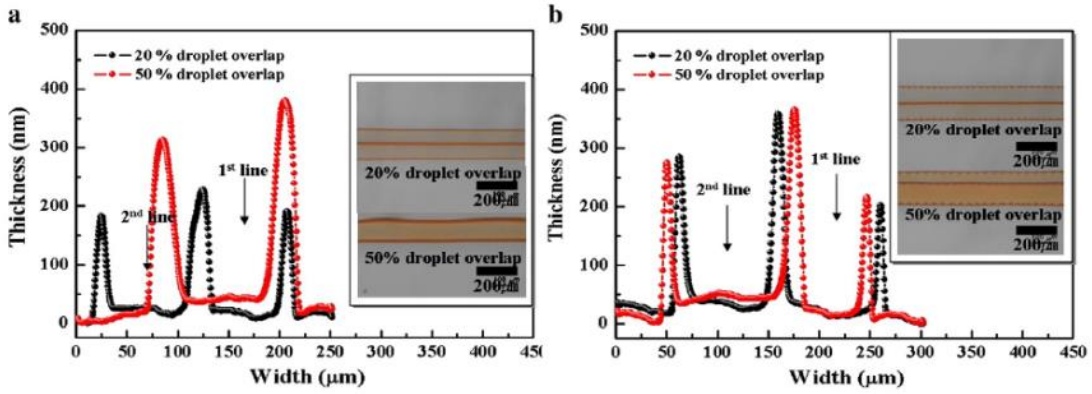

Figure 2.16: Surface profiling and optical microscope image of printed double line with different droplet spacing and plate temperature: left) 25°C, right) 40°C (Lee et al., 2011)

Coffee Ring Effect

The coffee ring effect (Lee et al., 2011; Deegan et al., 1997; Deegan et al., 2000) is an effect which influences the distribution of the dispersed or precipitated material and reduces a printed layer's uniformity during the drying process. When a coffee droplet is deposited on a solid substrate, the coffee particles tend to move outward during the evaporation of water and finally form a ring stain. This phenomenon also appears in suspension or in a volatile solution based solvent.

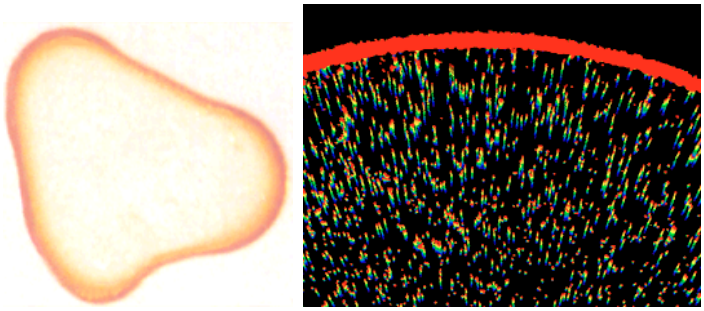

Figure 2.17: Coffee Ring stain and migration track (blue spot are the earliest position and red spots are the final position) (Deegan et al., 1997)

Deegan et al. (Deegan et al., 2000) suggested this effect was due to localized evaporation volume variation on the droplet surface and the pinned contact line.

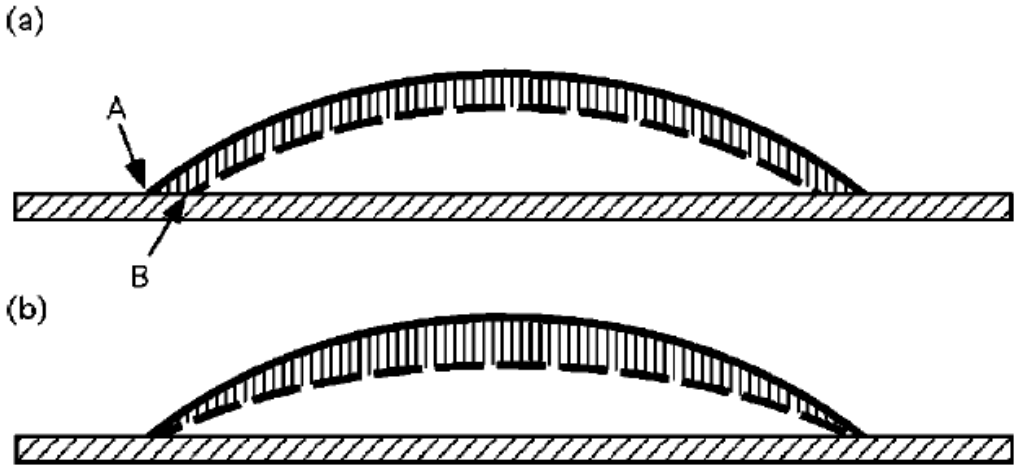

Figure 2.18: Mechanism of coffee ring effect (a) theoretical situation where the contact line is not pinned (b) real situation that contact line at the edge is pined (Deegan et al., 2000)

Deegan et al suggested that for a deposited droplet, the evaporation speed is higher at the outer rim than in the central circle. In Figure 2.8, situation (a) is the theoretical situation where the contact line is not pinned and no internal flow happens. At this situation, the contact line will move inward as evaporation continues and the coffee ring effect will not appear. However in

the reality, the contact line is pinned as shown in Figure 2.18(b) (Deegan et al., 2000; Parisse and Allain, 1996). The motion of the contact line from A to B is prevented by an outflow of the solution to refill the solvent evaporated from the edge. The solute particle which is distributed in the solvent will then move outward together with the liquid, which makes amount of particles higher at outer ring and finally form ring stains.

Lee et al. (Lee et al., 2011) also found that different solute concentrations influence the strength of the coffee ring effect; solvent with higher solute concentration suffered more serious coffee ring effects (Figure 2.19).

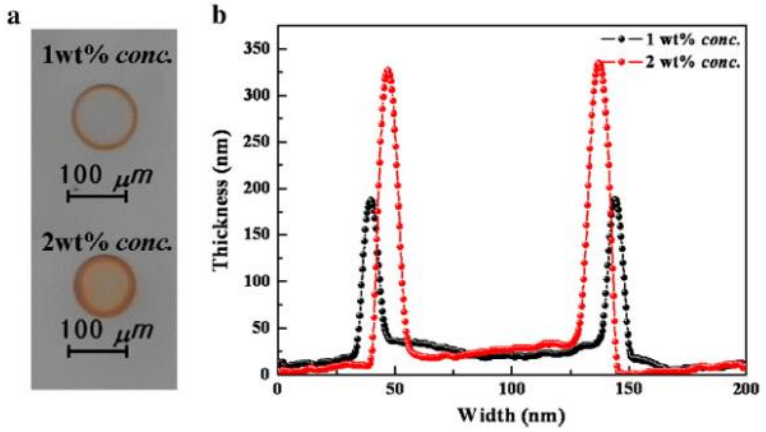

Figure 2.19 Coffee ring effect of different solute concentration (Lee et al., 2011)

Figure 2.19 shows that as solvent concentration increases, more solute is pushed to the edge during evaporation. However, the central thickness of the solidified structure stays almost the same for samples with different concentrations.

The Marangoni effect was used as one of the methods to help minimize the coffee ring effect (Kim et al., 2006; Kajiya and Doi, 2011). The Marangoni

effect is a convective motion of the fluid caused by the variation of surface tension. The surface tension variation could be induced by temperature (thermocapillarity) or surfactant (solutal Marangoni effect). This effect happens along the surface of the liquid and will lead to flow in the bulk. (Baround, 2013)

Kim et al. (Kim et al., 2006) implied that by using a multi-solvent system, the coffee ring effect can be minimized by the Marangoni effect (as shown in Figure 2.20). The principle is to utilize the driving force of surface tension gradient at the droplet surface. Instead of barely relying on surface tension variation initiated by temperature gradient, they use a multi-solvent system to enhance the driving force. Ethylene glycol (EG), a solvent with relatively lower surface tension but much higher boiling point (EG T_b=197, γ=48.5 mN/m) than their ink mixture (48-80wt% water, 10wt% n-propanol, 10wt% ethanol) helped reducing the coffee ring effect. They suggested that the outward flow and enhancement of the solvent evaporation near the contact line leads to higher concentration of EG at the rim of the droplet than that in the centre. This concentration variation led to surface tension gradients that created an anti-coffee ring flow at the droplet surface.

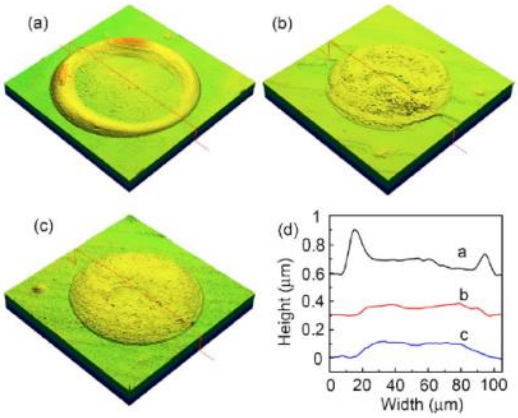

Figure 2.20: 3D images of droplets with different composition. (a) 0wt% (b) 16wt% and (c) 32wt% EG (Kim et al., 2006)

Kajiya and Doi (Kajiya and Doi, 2011) introduced the use of surfactant to minimize the coffee ring effect, which is also based on the usage of the Marangoni effect as Kim et al. did to create surface gradient at a deposited droplet's surface The mechanism is shown in the figure below. They suggested that the outward flow will increase the polymer and surfactant concentration at the edge which will generation surface tension gradient to minimize coffee ring effect.

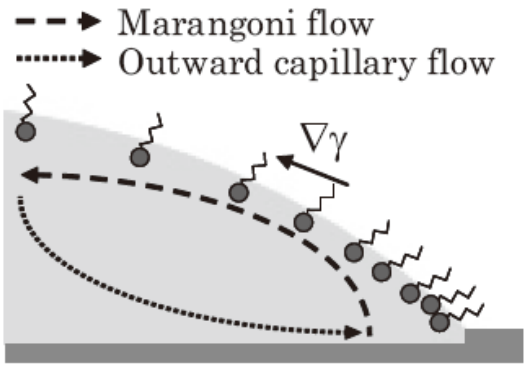

Figure 2.21: Surfactant working mechanism on reducing coffee ring effect (Kajiya and Doi, 2011)

These studies showed that coffee ring effect is a potential side effect which may happen during solvent ink jetting, but that its effect could be minimised with the use of a multi-solvent system or by adding surfactant.

2.6 Free Radical based UV Curing Reaction

2.6.1 Basic Concept

Free radical based UV curing reaction based approaches are widely used solidification methods for the commercial material jetting process. Table 2.1 (Wang, 2001) gives a typical formulation of the UV ink. Oligomers or monomers containing unsaturated acrylate or methacrylate structures can be used to prepare UV curable inks. These unsaturated oligomers or monomers may occupy up to 97wt% of the whole ink and they are the key determinants of the final product properties or functions.

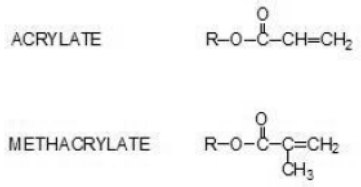

Figure 2.22: Types of free radical based UV curable groups (Arceneaus and Willard, 2014)

The photoinitiator (PI) is another indispensable component of a UV curable ink. The required concentration of PI could be influences by a lot of factors such as initiation mechanism, processing conditions, UV intensity and so on. The main function of PI is to initiate the crosslinking (or curing) reaction.

In order to satisfy the viscosity requirements for jetting, a diluent may be added to modify the overall viscosity. Acrylated monomers are commonly used as a diluent and are often monofunctional acrylated monomers or multifunctional acrylated monomers (Arceneaus and Willard, 2014). The diluent monomer participates in the UV curing reaction and becomes part of the final product. Therefore, final product properties will vary as different types and amount of diluent being added.

With different processing environments or product requirements, some other additives may also be added to modify an ink's processability and the final product's properties. These additives can include surfactants, photosensitizers, accelerators and pigments.

T*able 2.1: Typical formulation for a UV curable ink (Wang, 2001)*

Name	Function	Concentration
Monomer or Oligomer	Body of the ink which will decide the main function of cured materials	>40wt%
Photoinitiator	Absorb UV light and initiate polymerization	<10wt%
Diluent	Adjust the ink viscosity	20-50wt%
Other Additives	Modify ink properties	0-30wt%

Free radical based UV curing reactions include three stages, which are initiation, propagation and termination (as shown in Figure 2.23) (Wang, 2001). During the initiation stage, the PI will be activated by absorbing the energy from UV light and generate free radical species. These free radical species

will then attack unsaturated acrylate groups R (containing C=C double bond) and form PIR• free radicals which will then initialize chain propagation. During the chain propagation, PIR• free radical species will attack other unsaturated R groups to propagate and form new species. Through the whole of the polymerization sequence, the free radicals (PI• or R•) always have chances to terminate with another free radical. However, in the initial stage of reaction, the concentration of reactant R is much higher than the free radicals, so the reaction tends to propagate instead of terminate. As the polymerization reaction goes on, the free radical concentration keeps increasing while the concentration of unreacted R reduces. Thus the possibility that a free radical meets the other one and terminates will increase and the reaction will then gradually enter termination stage (Pappas, 1980).

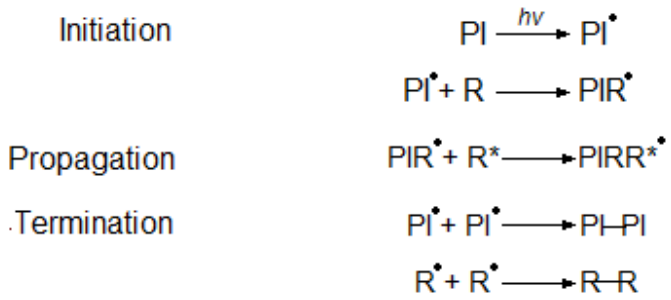

Figure 2.23: UV curing free radical polymerization process (Pappas, 1980)

2.6.2 Photoinitiator (Type I & Type II)

A photoinitiator is a chemical which can easily break into free radicals when certain wavelength of UV light is applied. Photoinitiators can be catalogued into a Type I and Type II (Davidson, 1999) based on their mechanism of radical production.

For Type I photoinitiator, the σ bonding between C-C beside the carbonyl group will break and split into two free radicals when exposed under UV light (Wang, 2001). Normally only one of the free radicals is able to initialize a polymerization reaction (Arceneaus and Willard, 2014).

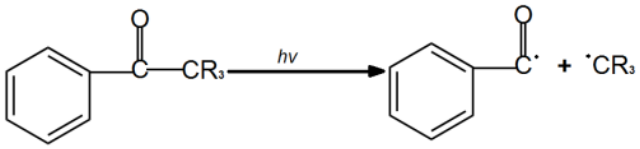

Figure 2.24: A schematic of type I photoinitiator split under UV light

Type II photoinitiation systems consist of two components which are photoinitiator and accelerator. When the photoinitiator is excited under UV light, instead of splitting into two free radicals, it will abstract an electron from accelerator (or synergist) and generate two reactive free radicals. Take Benzophenone as an example, which is a typical type II photoinitiator, it will undergo a series of reactions as shown in Figure 2.25.

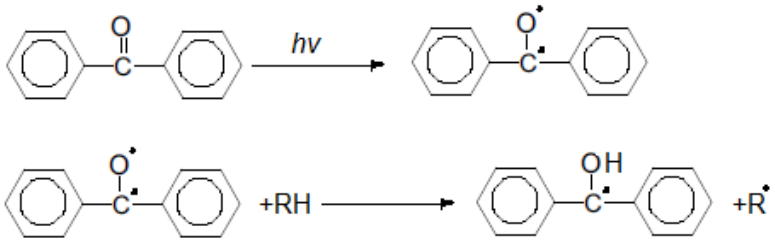

Figure 2.25: A schematic of Benzophenone (Type II photo initiator) under UV light

RH in Figure 2.25 represents an accelerator and works as an electron supplier. The most commonly used accelerators are tertiary amines, which

can incorporate with benzophenone efficiently. The free radicals generated from tertiary amines are more reactive with Oxygen than the other free radicals. Therefore, the accelerator can help protect the free radicals being oxidized through oxygen inhibition.

2.6.3 Oxygen Inhibition

Oxygen is an effective inhibitor which widely exists in the environment. Oxygen molecules may come from ambient air or dissolved Oxygen in raw materials. As shown in Figure 2.26, Oxygen can inhibit the polymerization reaction through the all of the polymerization stages. During the initiation stage, Oxygen can react with excited initiators and transform it into an unreactive state. At the chain propagation stage, Oxygen will react and form stable peroxide free radicals, hence inhibiting the chain growth. The reaction rate constant (a number which can help decide the reaction priority) between free radical R● and Oxygen is about 104-105 times larger than that between R● and monomer (Wang, 2001), and as a consequence the reaction between R● and Oxygen is more likely to happen. Therefore, even small amounts of Oxygen can inhibit the polymerization reaction considerably.

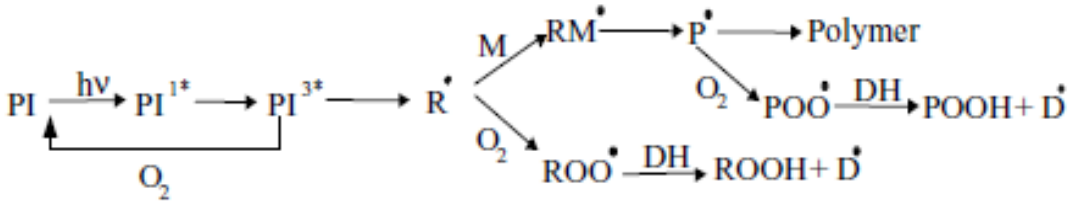

Figure 2.26: Oxygen inhibition at different polymerization stages (Wang, 2001)

There are several options to overcome the Oxygen inhibition problem including changing the polymerization mechanism, modifying the process

conditions, increasing free radical concentration and using type II photoinitiators.

Changing the Polymerization Mechanism

There are two kinds of UV curing polymerization mechanisms:

1. Free radical polymerization.
2. Cationic polymerization.

Cationic polymerisation, another kind of UV curing polymerization, is not sensitive to Oxygen (Table 2.2), however it can only be used for certain polymers and it is limited to moisture which is even harder to deal with comparing with oxygen.

Table 2.2: Comparison of free radical and cationic polymerization (Wang, 2001), (Davidson, 1999)

	Free Radical Polymerization	Cationic Polymerization
Resin	Acrylate, unsaturated resin	Alicyclic epoxy compound, vinyl ether
Initiator	Free Radical	Cationic (Strong Acid)
Reaction Speed	Fast	epoxy: medium vinyl: Fast
Oxygen sensitivity	Strong	None
Moisture sensitivity	None	Strong
Odour	Strong	Low
Price	Low	High

Adjusting the Processing Condition

A direct method to avoid Oxygen inhibition is to use an inert atmosphere which protects the reactant from contact with Oxygen. Both nitrogen and carbon dioxide are examples of atmospheres that can be used. However this method brings higher cost and complexity in the system design. Experiments have shown that adding wax into a UV ink can also reduce Oxygen inhibition (Norman, 1996). When a UV ink is spread on to the target substrate, the wax inside will gradually transfer to the surface and form a protective film. This method requires a slow curing speed to allow enough time for the wax to transfer which will influence the processing efficiency and limit its applications.

Increasing the Free Radical Concentration

By increasing free radical concentration, there will be more reactive species generated during polymerization, which means even though some of the reactive species are oxidized, the reaction can still continue. There are two methods to increase the free radical concentration: increase the photoinitiator concentration or increase the intensity of UV radiation. Both methods can increase the concentration of excited photoinitiator and therefore minimize the Oxygen inhibition effect (Davidson, 1999). However, high initiator concentration may also cause reduction of a final product's molecular weight (Clay and Gilbert, 1995). So increasing the intensity of UV radiation is preferred.

Using Type II Photo Initiators

As mentioned in the previous section, type II photo initiators are a type of photo initiator system which consists of both photoinitiator and accelerator. And the excited accelerator preferentially reacts with Oxygen molecules as shown below and forms peroxide radical ROO●. The peroxide radical can then abstract a hydrogen atom from another amine molecule to generate another excited reactive amine free radical (Norman, 1996). Through this procedure, the excited accelerator can keep capturing Oxygen molecules and maintain the free radical concentration inside the reactant.

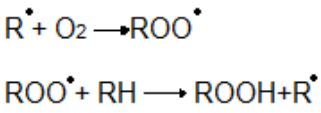

Figure 2.27: Schematic of active free radical generated by oxidized accelerator.

2.7 Polycaprolactone

Polycaprolactone (PCL), poly (lactic acid) (PLA), poly (glycolic acid) (PGA) and Polydioxanone (PDS) are widely used aliphatic polymer based bio-materials (Hogue et al., 2009, Peter et al, 2004). These polymer materials are complementary and serve different application in tissue engineering and medical fields (Middleton and Tipton, 2000). In these polymers, PCL has been reported to have relatively low synthesis cost, long degradation period, good processability, high permeability to drugs and blend-compatibility with other polymers. (Labet and Thiele, 2009, Merkli et al., 1998, Middleton and Tipton, 2000, Sinha et al., 2004). These properties provide PCL with the potential to be manipulated to suit different requirements. These advantageous properties

also make it a very competitive candidate for a 3D printable biomaterial, and a starting point for developing biodegradable polymers for 3D inkjet printing or material jetting processes.

Table 2.3: Physical, mechanical and degradation of PCL, PDLA family and PGA (Modified from Middleton and Tipton, 2000, Peter et al, 2004)

Polymer	Glass transition temperature (°C)	Modulus (GPa)	Degradation time (months)
PGA	35 to 40	7.0	6 to12
PDLA	55 to 60	1.9	12 to 16
PCL	-65 to -60	0.4	>24
PDS	-10 to 0	1.5	6 to 12

PCL is an aliphatic polyester compound of hexanoate repeat unit (as shown in Figure 2.28). It is normally synthesized through ring opening polymerization (Figure 2.29), however it could also be synthesized through polycondensation polymerization in some case (Labet and Thiele, 2009). It is a hydrophobic semi-crystalline polymer, the crystallinity of which can reach 69% (Iroh, 1999). Therefore PCL has good resistance to the water molecules and manifest relatively low degradation speed through hydrolysis degradation.

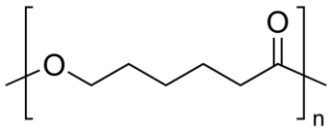

Figure 2.28: Chemical structure of Polycaprolactone

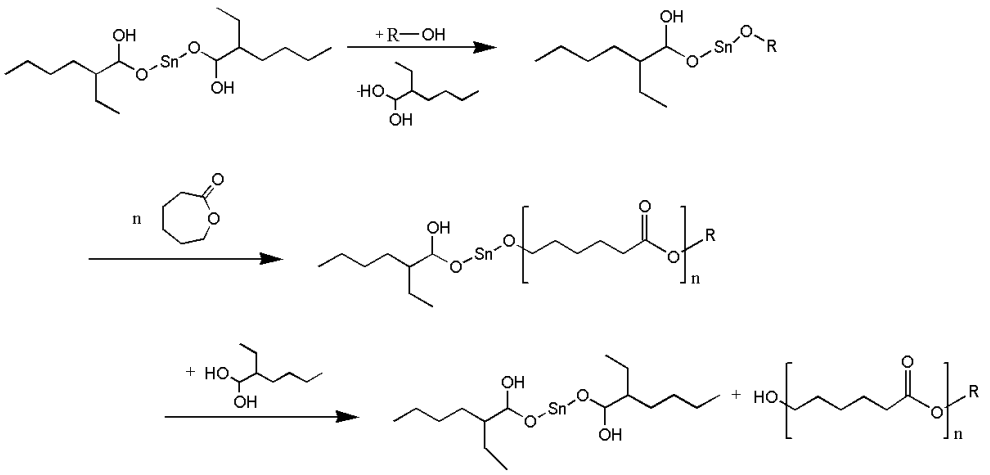

Figure 2.29: An example of ring opening polymerization to synthesis Polycaprolactone with tin(II) catalyst. (Modified from Labet and Thiele, 2009)

Pure PCL normally degrades within a range of 2 to 4 years (molecular weight dependant) (Gunatillake and Adhikari, 2003, Middleton and Tipton, 2000). Based on current understanding, it can be concluded that the degradation of PCL includes two stages which are non-enzymatic hydrolytic cleavage of ester groups at the very beginning which mainly happens at the amorphous phase and then intracellular degradation within the residual highly crystalline phase (Woodward et al., 1985, Sun et al., 2006). Chen et al. also suggested that the degradation of PCL is a homogeneous process as they found that the physical shape of the PCL specimen did not show obvious effect on the degradation rate (Chen et al., 2000).

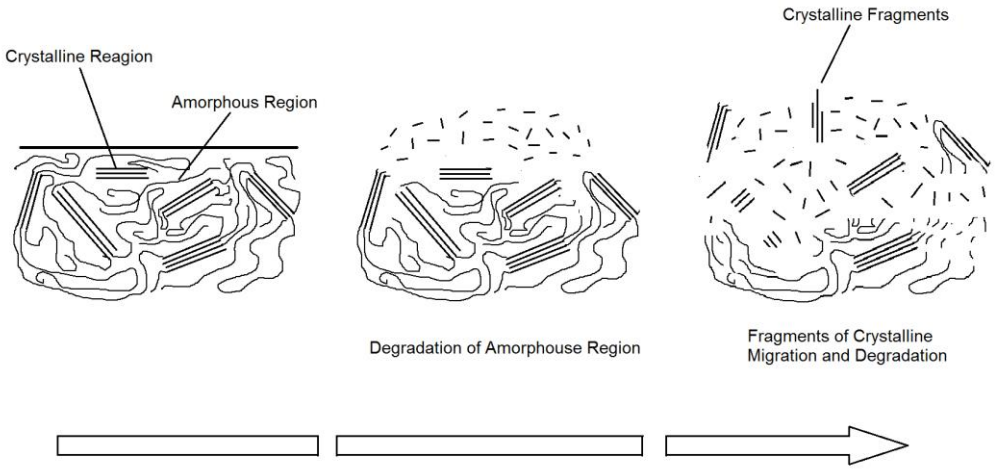

Figure 2.30: Schematic of PCL degradation (Modified from Lam et al. 2008)

PCL also has exceptional blend-compatibility with other kinds of bio-polymers which makes it possible to manipulate the PCL co-polymer's degradation kinetics and mechanical properties. Due to the slower degradation rate, PCL and its copolymers were originally used in drug-delivery devices which remain active for over 1 year. Owing to its exceptional processability, relatively low production cost compared with other aliphatic polyester polymers, a wide range of fabrication studies on PCL scaffold were carried out in 2000s. Meanwhile, a number of drug-delivery devices fabricated with PCL have been approved by FDA, which accelerated the step of the developmentof PCL based products (Woodruff and Hutmacher, 2010).

2.7.1 Fabrication of PCL in AM

PCL as a biodegradable polymer has drawn special attention in 2000s, especially in the additive manufacturing field, due to its good processing ability and thermal stability (Ciapetti et al., 2003; Zein et al., 2002). The processing window of PCL can reach 240ºC; the melting temperature of PCL

is about 60ºC and the decomposition temperature is above 300 ºC (Hogue et al, 2009). AM is viewed as a platform for fabrication of a new generation of scaffolds with high reproducibility and compositional variation (Woodruff and Hutmacher, 2010).

Fusion Deposition Modelling

The majority of papers addressing the processing PCL scaffolds through additive manufacturing are mainly based on the Fused Deposition Modelling (FDM) technique and its derivatives.

Zein et al (2002) carried out a range of studies on FDM technique to produce novel scaffold architectures for tissue engineering applications. They mainly focused on the optimization of fabrication parameters and scaffold design to study their influences on the final product's morphology, mechanical properties. In their work, they managed to produce scaffolds with channel size down to 160µm and filament diameter down to 260µm with a compressive modulus ranged from 4 to 77MPa.

Part et al. (2008) produced a range of scaffolds with different nozzle size to study the potential influences of pore and filament diameter on the performance of scaffold. They compared the scaffold with 200µm/300µm 250µm/500µm, 330µm/700µm (filament size/pore size) and concluded that the 200µm/300µm manifest the best compressive modulus while 330µm/700µm performed best cell ingrowth in the in vitro test.

Shor et al. (2009) have developed PCL scaffolds for bone tissue engineering to provide viable substitutes for bone regeneration. They presented a novel

modified FDM technique called Precision Extruding Deposition (PED), which they claimed that it is possible to produce scaffolds with pore sizes of 350µm. The mechanical properties of the prepared scaffold were measured, which manifest compressive modulus of 59MPa and compressive strength of 5.3MPa. Both in vitro cell-scaffold and in vivo study were carried out with the printed scaffold structure. The in vivo study was established in a mouse model and they found that the osseous ingrowth was increased during the 8 weeks study and osteoblast cells were able to attach and proliferate on the PCL scaffold.

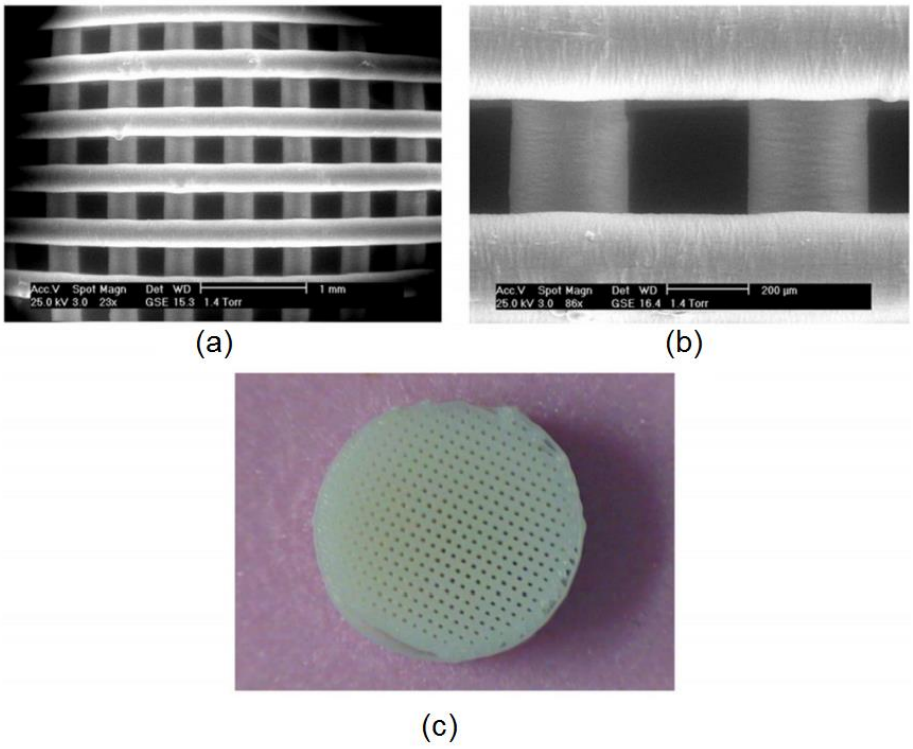

Figure 2.31: (a) and (b) SEM picture of the fabricated scaffold structure (c) appearance of the scaffold. (Modified from Shor et al, 2009)

Ahn et al (2011) presented processing PCL scaffold with Electrohydrodynamic (EHD) direct writing technique, which has a working principle similar to FDM.

It was claimed that EHD direct writing produced fine threads (<50µm). 10wt%, 15wt% and 20wt% PCL solution was used as the printing material and the minimum filament size they achieved was 200µm with 350µm pore size. The modulus of EHD processed PCL was between 6.3 to 41MPa depending on the porosity, and a modulus from 38MPa to 130MPa, which was claimed to be suitable for fabricating scaffold for trabecular bone regeneration. They carried out in vitro test with osteoblast-like cells (MG63) and evaluated the cell viability that adhered and proliferated on the scaffolds, during which the EHD plotted PCL scaffold manifested very positive results.

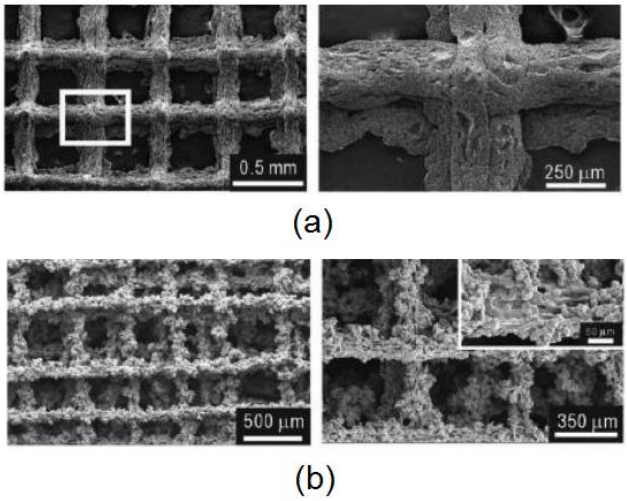

Figure 2.32: (a) SEM picture of strut produced through normal EHD printing (b) SEM picture of highly roughened surface produced on the PEO solution batch. (Modified from Ahn et al.2011)

Selective Laser Sintering (SLS)

Recently, the research focused more on investigating the possibility of fabricating polycaprolactone scaffolds for tissue engineering applications with selective laser sintering technique.

William et al. (2005), investigated the ability of using SLS to fabricate PCL scaffolds with different porous architecture that have sufficient mechanical properties for bone tissue engineering. In their paper, they managed to produce PCL scaffolds with 6 different internal pore architectures and porosities with pore diameters between 1.75mm and 2.50mm and porosity between 63% and 79%. The compressive modulus and strength of the produced PCL scaffold specimens ranged from 52MPa to 62MPa and 2.0MPa to 3.2MPa respectively, which is within the lower range of properties for human trabecular bone. From the in vivo test, they suggested that PCL scaffolds fabricated via SLS enhanced tissue ingrowth and showed advantageous for bone and cartilage tissue engineering in the future.

Yeong et al. (2010) tried to fabricate porous polycaprolactone scaffold for cardiac tissue engineering with SLS technique. CAPA 6501 PCL powder was used in their study. They suggested that the undensified PCL powder can work for microporosity (40-100μm), which helps allow adequate medium and waste exchange flow through the scaffold. The minimum strut width demonstrated was around 600μm. An in vitro test was carried out with C2C12 myoblast cells for 21 days, during which cells were found to have proliferated around the strut and in the micropores. They declared that differentiation of C2C12 cells into multinucleated myotubes during the in vitro study, which demonstrated the biocompatibility of this scaffold for cardiac tissue engineering.

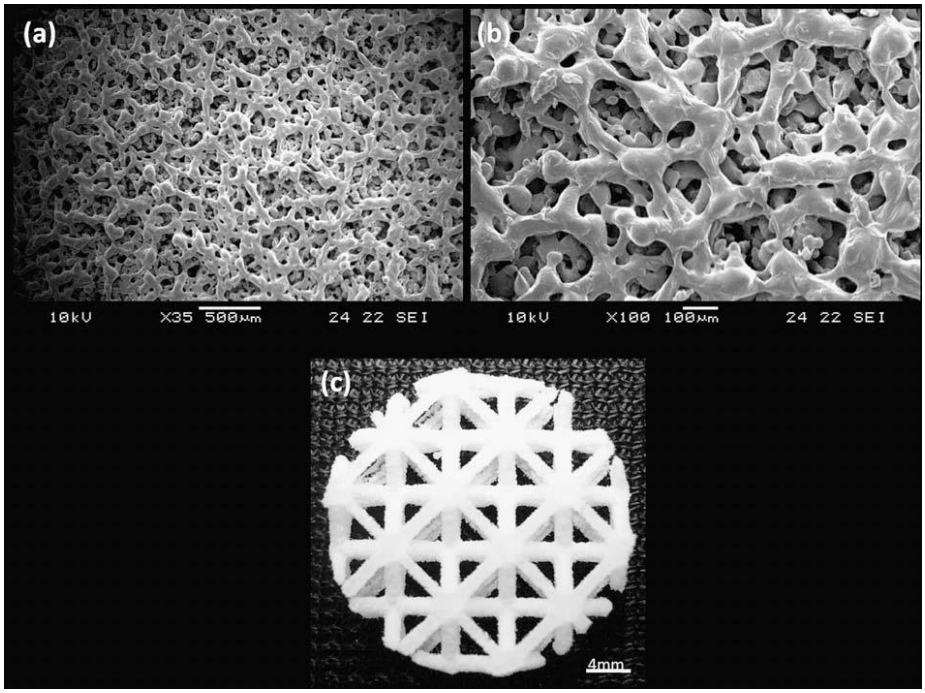

Figure 2.33: (a) SEM image of the micropores 35X, (b) SEM image of the micropores 100X, (c) scaffold appearance (Yeong et al. 2010)

Mazzoli et al. (2015) also presented processing PCL bone scaffolds for bone tissue engineering with SLS. They carried out a range of characterization on the PCL powder's physical properties, particle size distribution, compression properties of PCL scaffold and SEM observation of produced PCL scaffold. The strength of manufactured scaffold was around 3.6MPa, which they also suggested applications for human trabecular bone. A scaffold with 500µm pores was produced with SLS, while rather undensified PCL particles were also observed on the specimen. They suggested this was mainly due to the limitation of the SLS technique that the particles are only partially melted and complete elimination of porosity is generally not possible. In the in vitro test, human mesenchymal stem cells (MSCs) were used to obtain biocompatibility data with SLS manufactured PCL scaffold. Adhesion of cells on the specimen

was examined with SEM that both rounded cells and stretched cells were observed. However more systematic in vitro studies were not included.

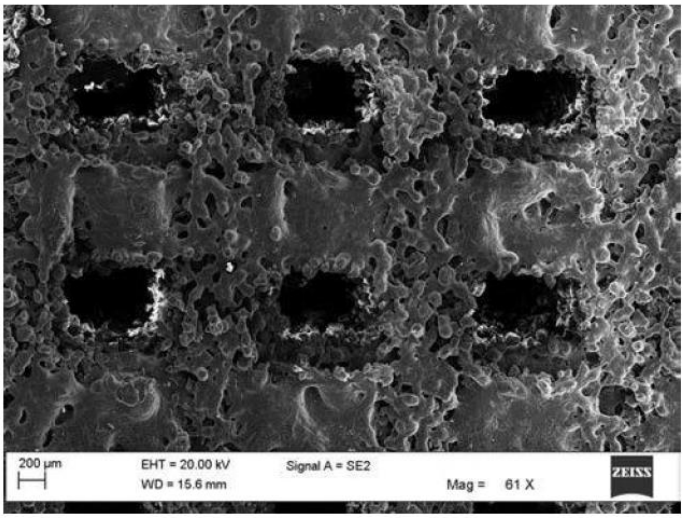

Figure 2.34: SEM picture of fabricated PCL scaffold (Mazzoli et al. 2015)

Partee et al. (2006) inspected the optimization of SLS processing parameters for a commercial PCL powder CAPA 6501 to manufacture a bone tissue engineering scaffold. They claimed that 94% dense relative to full density structure was able to be produced. The minimum strut size that was demonstrated in this paper was around 700µm.

Lohfeld et al. (2010) also studied the optimization of SLS processing parameters in order to fabricate small features on PCL scaffolds for tissue engineering. They managed to produce PCL constructs with strut width of 500µm (x-direction) and 800µm (y-direction), and pore sizes of around 400µm. They also noted that with commercial polyamide powder, the strut size can go down to 350µm and the anisotropy in strut size was reduced.

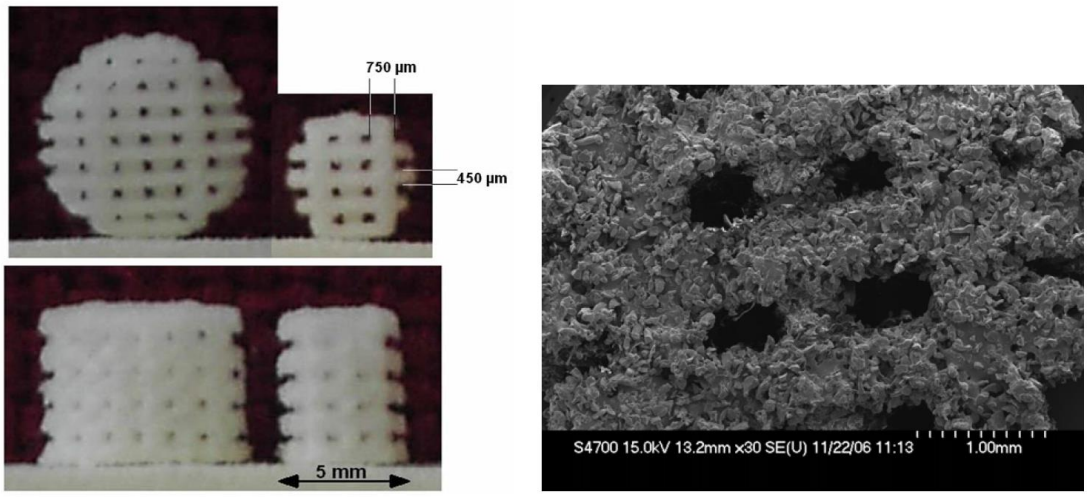

Figure 2.35: (a) Processed PCL scaffold which showed strut size differentiation in x and y direction and (b) SEM image of the scaffold surface (modified from Lohfeld et al. 2010)

2.7.2 PEG-PCL Copolymer

Poly ethylene glycol is a polymer which can be potentially used to prepare copolymer with PCL and manipulate the properties of PCL. PEG and PCL are both biocompatible and have been used in several FDA approved products. Polyester-polyether block copolymers composed of PCL and PEG attracted much attention as PEG is a hydrophilic polymer while PCL is hydrophobic, which offered the possibility of varying the ratio of hydrophobic/hydrophilic constituents to manipulate the degradability and hydrophilicity of the product (Li et al, 2002, Huang et al. 2004)

Gong (Gong et al, 2009) and Yin (Yin et al., 2010) performed biodegradability tests of PEG-PCL-PEG copolymer in mice. Gong et al injected PEG-PCL-PEG hydrogel into mice thigh to observe the degradation behaviour. They found that PEG-PCL-PEG hydrogel totally degraded on the 14th day after

subcutaneous injection (As shown in Figure 2.36). Similar work was carried out by Yin et al. (Yin et al., 2010), they injected PEG-PCL-PEG hydrogel into mice's eyes to investigate the degradation. Most of the injected materials were decomposed within 15 days and no mortality occurred during the whole observation period.

Figure 2.36: PEG-PCL-PEG hydrogel degradation from A to F showed photo at 0,1st, 3rd, 7th, 10th and 14th day (Gong et al., 2009)

Other than hydrogel applications, Hogue et al. and Jiang et al. also tried to extend the application of PEG-PCL copolymer into the scaffolds field (Jiang et al., 2011; Hogue et al., 2009). Both of them tried to produce scaffold through FDM. In vitro test was carried out with skin fibroblast cells from one month old mice. Figure 2.37 showed the processing schematic presented by Jiang et al. and the picture beside it shows the cell morphology of fibroblast cells in the pore of the scaffold made from PEG-PCL copolymer. They suggested that with the presence of PEG segment in the polymer backbone, the hydrophilicity of copolymer increased which is advantageous for improving cell attachment.

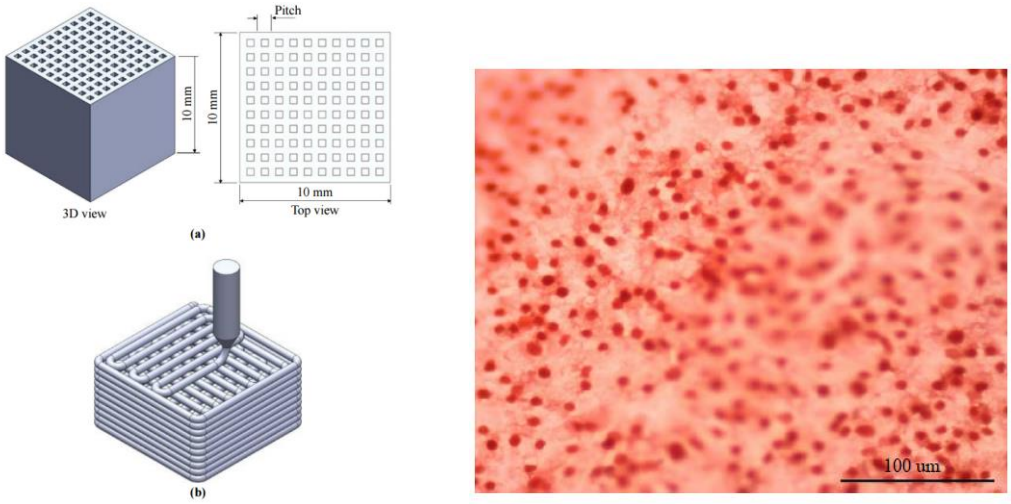

Figure 2.37: Fabrication of PEG-PCL-PEG scaffold and cell attachment (Jiang et al., 2011).

2.7.3 UV Curable Poly (ethylene glycol) and Polycaprolactone

In previous section, PEG-PCL copolymer showed the advantageous for tuneable hydrophilicity and degradability. There is little research in preparing PEG-PCL copolymer through UV curing reaction. As mentioned before, UV curing reaction is a relatively easy and quick reaction to prepare crosslinked polymers. Meanwhile, it is a promising reaction, which has been widely used in the material jetting field. These provide the potentials of fabricating PCL-PEG copolymer through material jetting process.

A number of studies have been done to show the capability of UV curable PEG: polyethylene glycol diacrylated (PEGDA) being applied in tissue engineering (Zhu, 2010; Hoffman, 2012) or drug delivery parts (Aimetti et al., 2009). PCL itself is not UV curable, but by attaching acrylate groups onto the PCL's backbone through condensation polymerization, UV curable polycaprolactone can be synthesized. Several different methods to prepare

Polycaprolactone with UV curing functional groups have been published (Feng and Snaping, 2003; Park et al., 2007; Ferreira et al., 2008). Both Feng et al. and Park et al. used the method that is based on condensation polymerization and used acryloyl chloride as a reactant to provide a UV curable functional group. The main differences are the solvent system to dissolve PCL and the reaction temperature. Ferreira used 2-isocyanatoethyl methacrylate instead of methacryloyl, which will not generate small molecules during the reaction; whilst preparation procedures were simplified. However, 2-isocyanatoethyl methacrylate is very sensitive to water and has more critical requirements for the reaction environment conditions.

UV curable polycaprolactone can solidify by crosslinking reaction of the grafted acrylate groups. These crosslinked sections of acrylate groups, even though they only occupy a small volume of the whole crosslinking network, will restrict the behaviour of polycaprolactone segment, which will influence the degradability of the cured sample.

Kweon et al. (Kweon et al., 2003) synthesized UV curable Polycaprolactone acrylate through a condensation reaction by letting PCL react with acryloyl. Their degradation tests were done with UV cured PCL diacrylate as shown in Figure 2.38. It was found that the degradation speed of a UV cured PCL network was significantly promoted. They suggested that pure PCL is a highly crystallized and hydrophobic polymer, and therefore the degradation speed is considerably reduced. This is mainly because water, the main component to initiate random hydrolytic chain scission for degradation, cannot penetrate the sample easily. The existence of crosslinking largely restricted the polymer

chains and prevents them from stacking and crystallizing. The degradation speed is therefore accelerated.

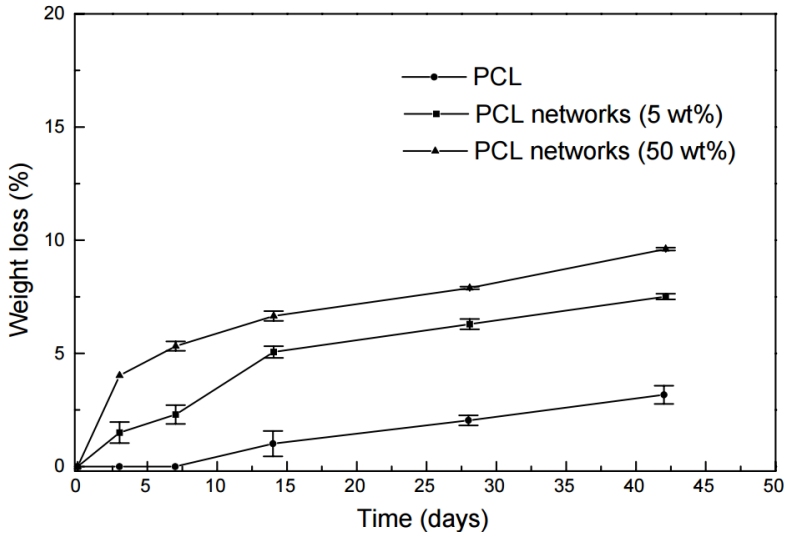

Figure 2.38: Degradation of PCL and PCL networks (pH7.4, 37°C) (Kweon et al., 2003)

However, in the other situation, if the crosslink density of the product is too high, it will restrict the progress of hydrolysis reaction, which will reduce the biodegradability of the final product.

A potential risk of using UV curable Polycaprolactone is that the unreacted acrylate monomer or oligomer will influence the biocompatibility of the product. Acrylic based materials have been widely used in dental practice (Bhola et al. 2010, Goncalves et al. 2008, Harrison and Huggett, 1992, Ivkovic et al. 2013, Tsuchiya et al. 1994) and residual monomers have caused concern regarding hypersensitivity and allergic reactions. One of the methods is to avoid residual monomer content is to manipulate the polymerization reaction to minimize the unreacted content, but a more effective way is to carry out post-processing to remove the residual reactant. This is not realistic for some of the dental

applications as the paste-like reactant is deposited to the target dental position and then polymerized to make sure it fits in the cavity, and is not able to be taken out for post-processing. However in 3D printing this is a possible route, since the sample is fabricated in a material printer.

2.8 Characterization and Removal of Chemical Residuals

The amount of chemical residuals in the final product is a factor that also needs to be taken into consideration especially during the fabrication of products for biomedical applications. Grodowska and Parczewski (2010) reviewed the potential risks of residual organic solvent in the pharmaceutical industry. They suggested that removing the unwanted solvent residuals was not only for reducing toxicity, improve biocompatibility, but also improve the physical and chemical stability of some desired active substance in the final product. A guideline of the concentration limit as well as daily dosage limit for some commonly used organic solvents was also presented.

2.8.1 Sources of Chemical Residuals in Material Jetting

Material jetting, as mentioned before (section 2.4), can be categorized into two techniques: direct or melt printing and reactive printing. The products fabricated through these two techniques have different source of chemical residuals.

For direct printing, polymers are often printed with solvent-based inks, which would be prepared by dissolving the target polymer into a organic solvent. Therefore, the main source of chemical residuals is the residual solvent in the precipitated and solidified polymer structure after evaporation.

For reactive printing, the monomer or oligomer form of target polymer was normally used for ink preparation. Initiator(s) (or catalyst) sometimes is also added to help triggering the polymerization reaction after jetting to form solid polymer structures. Therefore, the main source of the chemical residuals in this case is the unreacted monomer or oligomer as well as initiator (or catalyst), if it has been added.

2.8.2 Characterization and Removal

In order to characterize the amount of chemical residuals in the product, a number of chemical analytical techniques can be applied (B'Hymer, 2003, Grodowska and Parczewski, 2010, O'D onnell and McGinity, 1997).

Gas Chromatography (GC)

GC is a very useful and commonly used technique for residual solvent analysis. It is mainly applied to analyse the chemicals which can be vaporized without decomposition. This technique could be used to carry out both qualitative and quantitative analysis.

Mass spectrometry (MS)

Mass spectrometry is normally incorporated with GC to help analyse the amount of residual solvent or unreacted monomer inside synthesized polymer. It can also incorporate with other separation techniques than GC, such as Liquid Chromatography, to expand its capabilities to different specimens.

Infrared Spectroscopy (IR)

Infrared Spectroscopy is another technique to detect the residual chemicals. However, it is normally used for qualitative analysis. Quantitative analysis can also be carried out, but the resolution is not as good as GC. Meanwhile, IR can only be applied to selected solvents or chemicals.

Nuclear Magnetic Resonance (NMR)

Nuclear magnetic resonance is a technique which can carry out more quantitative characterization compared with IR. Still, similar to IR, this technique can only be applied to selected chemicals as well.

Other techniques such as Thermal gravimetric analysis (TGA), Differential Scanning Calorimetry (DSC) are also potential characterization methods to determine the chemical residuals.

The normally used techniques in the industry for removing the chemical residuals are static bed drying, fluidized bed drying, spray drying and turbo bed drying. During the drying procedure, the dryer will be sealed and vacuumed to help removed the chemicals. If necessary, heating (e.g. microwave, infrared lamp) and nitrogen can be applied to accelerate the process as well as protecting desired content. In the laboratory level, vacuum oven is commonly used for removal of chemical residuals. If the residual chemical is hard to vaporize, chemical wash can be used as an assistant method before vacuum drying (Stjerndahl et al, 2007). Also carrying out post-curing procedure is a potential way to improve the completion of the reaction and reduce the residual amount of unreacted monomer, oligomer or initiators.

2.9 Summary

PCL is a biodegradable polymer that has relatively low synthesis cost, long degradation period, good processability, high permeability to drugs and blend-compatibility with other polymers. Polycaprolactone has been proposed as a AM material previously, but to date its use in material jetting has not been explored.

It has been demonstrated that it is possible to process Polycaprolactone through additive manufacturing and a new generation of scaffolds with reproducible and compositional variation structures have been demonstrated. Most of these works suggested PCL scaffold fabricated by additive manufacturing was suitable for bone tissue engineering. The compressive modulus and strength of the scaffold fell into the range of 30MPa to 70MPa and 2.0MPa to 6.0MPa respectively, which can be applied in human trabecular bone (Goulet et al., 1994, Mazzoli et al. 2015, Shor et al, 2009, William et al, 2005).

However, current research focused on two AM techniques: FDM and SLS, both of which have their own limitations in manufacturing.

Resolution: the strut size can go down to 200μm for FDM while for SLS, the limit is around 500μm during the manufacturing of PCL scaffold.

Multi-Material: To include more than one material in a product provide the possibility of producing multi-functional structure with localized properties such as degradation speed, ingredient concentration etc. With SLS, only one material can be applied in a process and therefore it is not realistic to fabricate scaffold with several materials. For FDM, even though more than one nozzle

can be used during the process to deposit different materials in the same sample, due to resolution limitation, the distribution of different materials is limited to a level of several hundred microns.

Scalability: For SLS, in order to scale up the process and increasing the number of laser source is required, which is quite costly. For FDM, it is more scalable than SLS by assembling several nozzles, however the processing speed is still limited as it is a filament based extrusion process and the moving speed of the nozzle is limited.

In comparison, material jetting manifests superior performance and the potential to overcome the limitations faced by SLS and FDM. For example, the volume of a droplet during material jetting can go down to 1 pico-lite which realises a deposit of around 30μm in diameter on the target substrate. Similarly material jetting is well suited to multi-material object production via multi-head printing. Meanwhile, as different materials are deposited and mixed at pico-liter level and controlled by DOD printhead, the distribution of different materials can be more accurate. Moreover, for reaction based material jetting, as the monomer inks are used and the polymerization reaction is carried out after the deposition, it is possible to manipulate the composition of the co-polymer in different location of the product within the fabrication process. Finally, and perhaps most importantly, material jetting can be scaled up by assembling an array of printheads. As a consequence, a suitable biomaterial based ink being made available for material jetting will open up the vista of applications for AM to the field of tissue engineering.

Based on the study of previous literatures, it was concluded that the potential methods of printing PCL includes dissolving PCL into a suitable solvent to prepare a solvent based ink or print monomer or oligomer form of PCL as a reaction based ink and polymerize it afterwards. Several potential challenges are still faced in developing such an ink including viscosity limitation of the printhead, solidification efficiency of the ink, processing side effects of the jetting process etc. PCL is a promising starting point, but PCL based ink's printability needs to be determined and the routes to formulating it need to be established. The effect of processing parameters and ink formulations on the sample properties as well as the risks associated with residual chemicals remaining within the object post creation need to be addressed. The focus of this project will be to meet the challenge of finding suitable PCL formulations and understanding the mechanisms for film and object formation. The complex fluid and solid mechanics, intertwined with materials science and chemistry present a significant challenge, but it can potentially yield in substantial benefit in the fields of fabricating biomaterial based scaffold through material jetting.

Chapter 3. Methodology and Experimental Setup

3.1 Research Approach

In this section, the research approach will be introduced. In this thesis, the development of an ink for material jetting was classified into six stages, described as follows:

Stage 1: Solidification Method Assessment

Firstly, to prepare an ink for material jetting, the solidification method needs to be assessed and determined in advance, this is to ensure each layer of ink can solidify effectively and stack up into a 3D structure. There are two potential solidification methods: evaporation based solidification and reaction based solidification.

Inks for evaporation based solidification were prepared by dissolving the target polymer into a solvent. Following ink deposition, the solvent will be evaporated leaving a layer of precipitated polymer. This procedure could be accelerated by applying an external heat source such as substrate heating or infrared heating. When choosing a solvent, the solubility and evaporation speed need to be taken into consideration.

For reaction based inks, the solidification reaction needs to be decided and tested to ensure the ink can solidify with the chosen reaction. Monomer or

oligomers of the target structure material are normally used together with an initiator to prepare a reactive ink. The reservoir and printhead environment also need to be carefully controlled to prevent the ink from solidifying before jetting and damaging the printhead. The reaction will then need to be initiated after each droplet or layer of ink is deposited on to the target surface. Commonly used initiation sources include heat and UV radiation, depending on the solidification reaction.

Stage 2: Ink Preparation

Preparation of inks with good dispersion of the polymer or monomer that avoids contamination is the key to the production of an ink with good printability and final deposition properties. Bubbles or agglomerated particles within the ink will cause unstable droplet formation, nozzle failure or clogging during printing. After all the ingredients are mixed together, the ink also needs to be filtered to minimize contaminants and large particles. The filtered ink should be settled for a period of time or vacuumed to remove existing bubbles before filling the printhead reservoir.

Stage 3: Printability Assessment

Piezo based drop-on-demand (DOD) printing has strict requirements on the ink's viscosity and surface tension. Therefore, both of these properties need to be characterized to confirm if they fall into a printable range. Modifications are required to help adjust an ink's viscosity and surface tension. This can be achieved by a number of methods such as increasing printing temperature, adding diluents or other additives. To develop a printable ink, all of these

properties need to be investigated to help determine the appropriate mixture composition and printing condition.

Stage 4: Droplet Formation Optimization

At the droplet formation stage, the focus is to achieve consistent stable droplet formation, whilst avoiding satellite effects and nozzle failure. The formulated ink is printed within a certain temperature range determined at stage 3 with different printing parameters such as printing voltage and waveform. A drop view system was used to monitor droplet states, which helps further narrow down and define the optimum printing parameters.

Stage 5: Droplet Deposition and Solidification

In order to achieve a stable and continuous pattern, the droplet spacing needs to be smaller than a deposited droplet's equilibrium diameter. The deposited droplet diameter is related to an ink's contact angle and solidification speed. When a droplet reaches the target surface, it will gradually spread and solidify. Spreading and solidification of a droplet are competing phenomena so that fast solidification may cause droplet diameter reduction. Therefore controlling the solidification speed will influence the droplet spacing and the quality of the printed pattern.

Stage 6: Characterization of Final Product

Different printing parameters influence droplet formation, deposition and solidification, which will be reflected by the morphology and mechanical properties of the printed specimens. Due to sample size limitations, mechanical properties were analysed by nano-indentation.

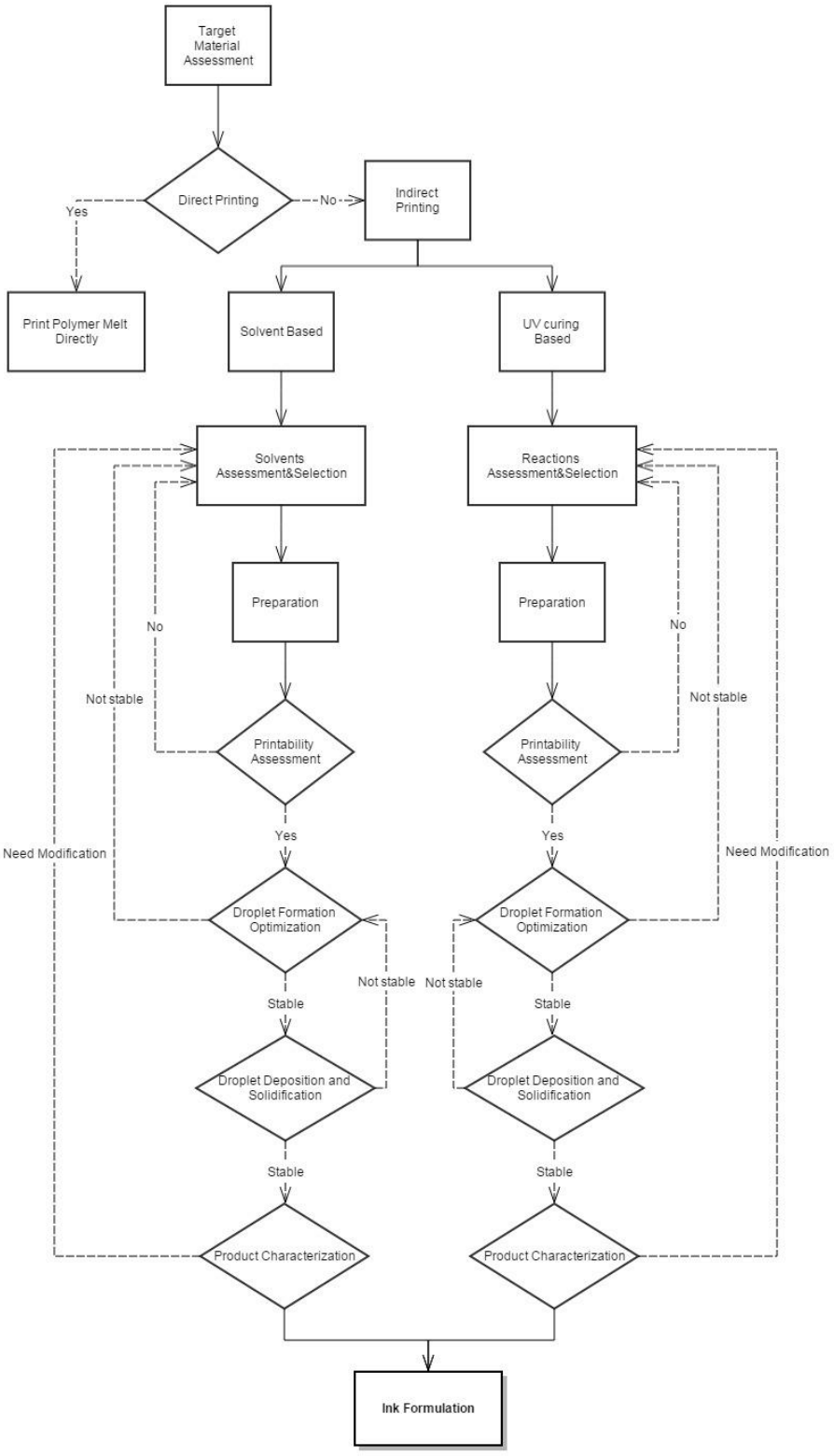

Figure 3.1: Overall methodology of the ink development and modification

3.2 Jetting Device

The jetting device used in this thesis was a Dimatix DMP-2830 produced by Fujifilm. The printhead is disposable, which is ideal for the initial ink development. A UV curing unit was added and the whole facility was contained in an environmental chamber that could be flushed with different gasses (i.e. for production of inert atmospheres).

(a) (b)

Figure 3.2: (a) Dimatix DMP-2830 appearance (b) Disposable printhead and printing unit. (Dimatix, 2014)

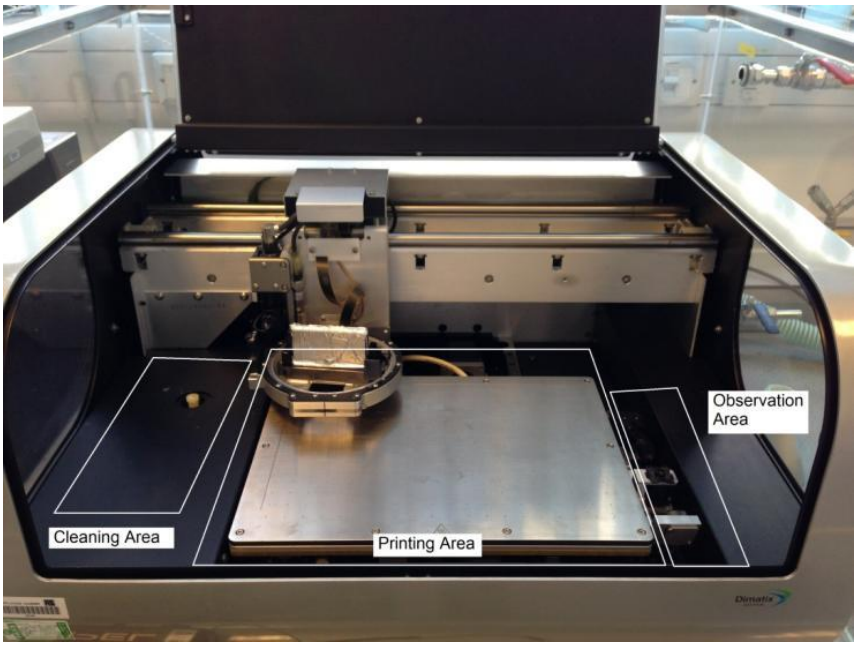

Figure 3.3: Printing area division inside the printer

As mentioned, the DMP-2830 uses a disposable printhead this is placed in a cartridge holder with pressure supply system and a cartridge alignment scale.

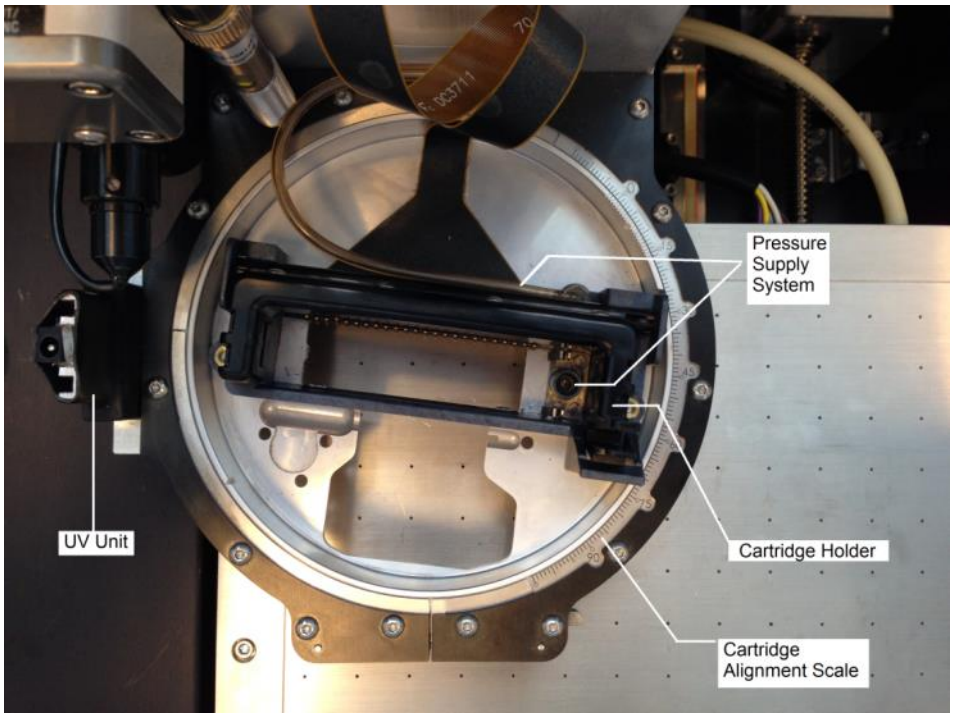

Figure 3.4: Structure of the Dimatix printing unit

The disposable printhead is supplied in two separate parts: a fluid module and a jetting module. The ink is filled into the fluid bag inside the fluid module through a fill port. The fluid bag is made from Polypropylene film which can resist most of the chemicals and it is surrounded by a hard fluid case. The cavity between the case and the inner bag was directly connected to the pressure supply system through a pressure port. The pressure system can provide positive or negative pressure to achieve ink purging or holding.

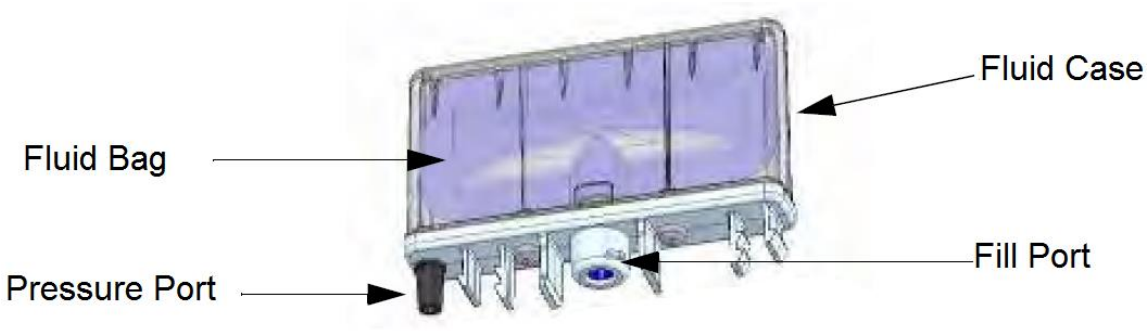

Figure 3.5: Structure of the disposable printhead's fluid module (Modified from Dimatix user's guild, Dimatix, 2010)

The jetting module consists of a jetting unit and an electrical connector. There are 16 square shape nozzles on the jetting unit, each with 21 µm edge length. Each nozzle has its own pumping chamber and can eject ink individually. Figure 3.7 is a schematic of the jetting unit cross section. Before printing, the ink needs to be purged through the pumping chamber to allow it to be fully filled. Any air remaining in the chamber will cause unstable droplet formation or even nozzle failure. When a positive voltage is applied, the piezo element will push down on the pumping chamber and eject a droplet. When the voltage is removed, the piezo element will resume which creates negative pressure inside the chamber and pulls ink to refill the chamber. Sometimes, a slight negative pressure will be applied to help refilling and also prevent the nozzle surface from flowing out of the cartridge nozzles.

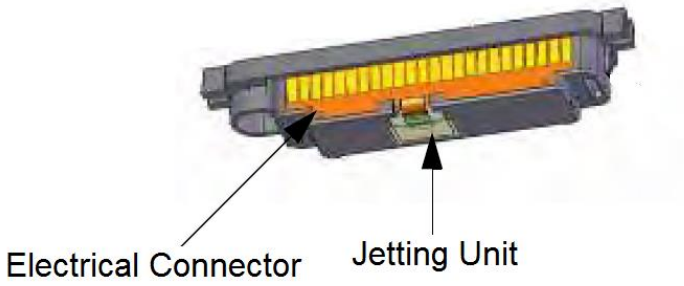

Figure 3.6: Structure of the disposable printhead's jetting module (Modified from Dimatix user's guild, Dimatix, 2010)

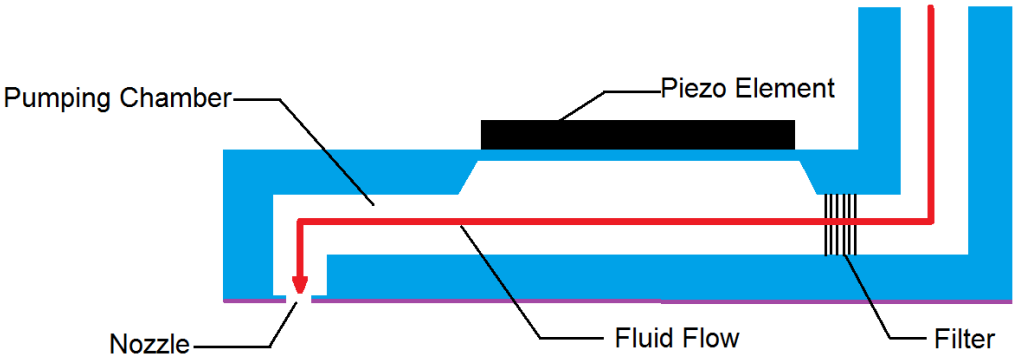

Figure 3.7: Schematic of jetting unit's cross-section structure

Figure 3.8 shows a disassembled printhead nozzle part. On the nozzle plate, each nozzle is 254 µm away from each other. The length of the pumping chamber is 3mm and the width is about 175 µm with a 100 µm wall between each pumping chamber.

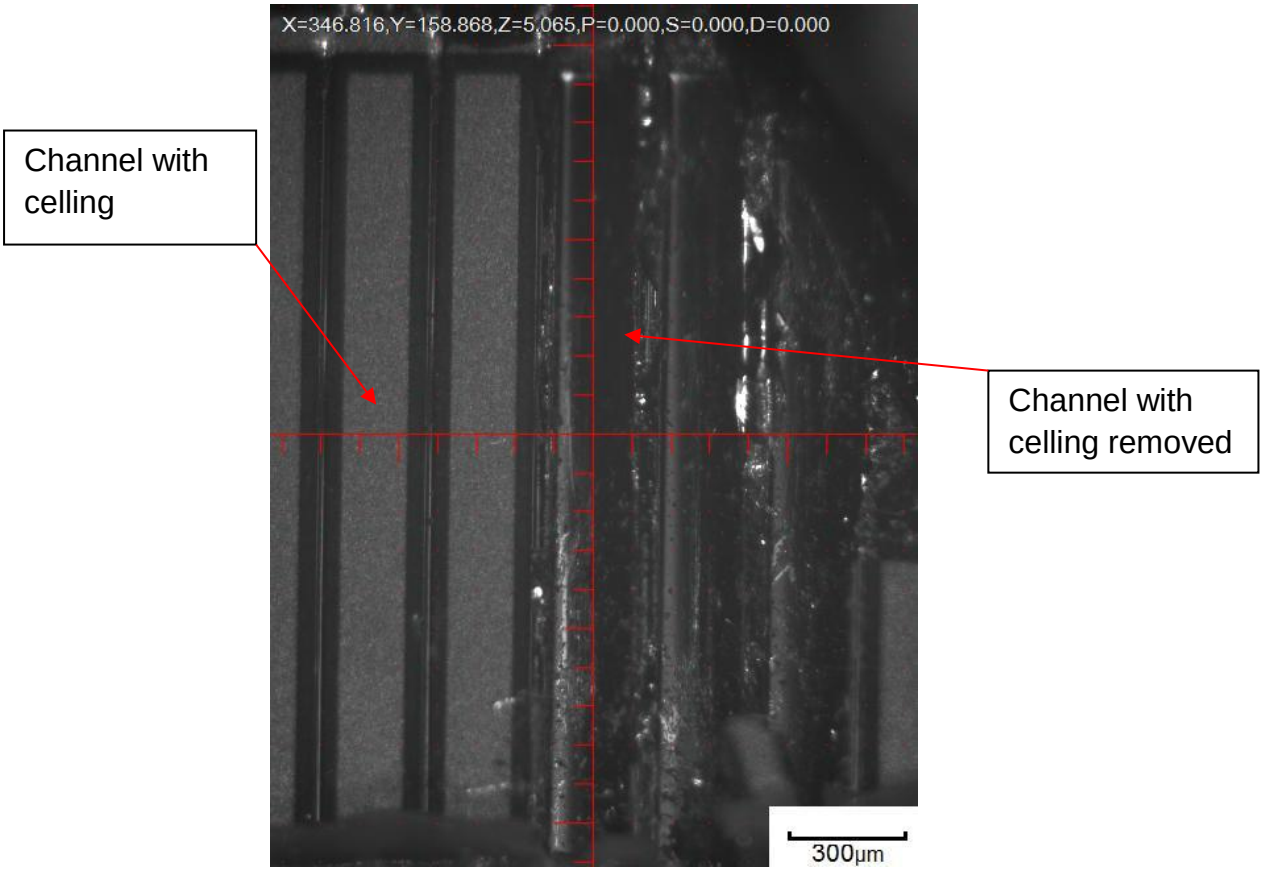

Figure 3.8: Optical microscope images of the rows of printhead channels

The cartridge alignment scale is used to adjust the angle between the printhead and printing direction. This angle is the key to control droplet spacing as well as the printing resolution. Figure 3.9 shows the mechanism of print resolution adjustment. The droplet spacing in the printing direction can be controlled by the printhead moving speed and jetting frequency. However the droplet spacing in the *y* axis is directly related to the interval between two nozzles in the *y* direction. This distance is set when the printhead was manufactured, but their interval in the *y* axis can be reduced by turning the printhead toward the printing direction. By adjusting the printing angle, the interval (droplet spacing) can be changed between 5 µm (1.1 degree) and 254 µm (90 degree) corresponding to a resolution of 5080 dpi (1.1 degree) and 100 dpi (90 degree).

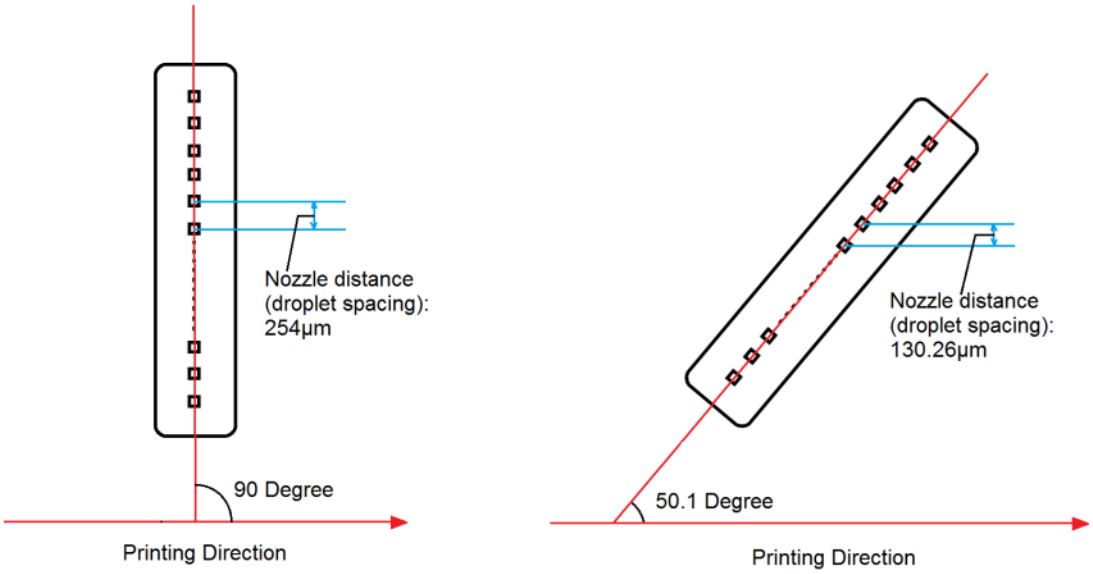

(a) (b)

Figure 3.9: Droplet spacing (resolution) adjustment by changing printing angle: (a) designed in resolution without adjustment (@100 dpi), (b) Printhead oriented for higher resolution (@130.26 dpi)

3.3 Reaction Unit

Two kinds of reaction units have been established for use with the Dimatix printer: substrate heating and UV reaction unit, for evaporation based solvent ink and reaction based UV curable inks respectively. The substrate heating function is provided by the printer's platform with a temperature up to 60°C attainable.

An independent UV reaction unit was attached to the left-hand end of the printing unit. During printing, the UV reaction unit moves with the printing unit, providing a real-time UV illumination after an ink is printed. The disadvantage of this design is that the UV reaction unit is moving with the printing unit and therefore the illumination time as well as energy deposited within a certain area is quite limited during a single scan, and therefore there is a higher

requirement on the ink's reactivity to achieve real-time curing. The UV reaction units consist of a mounting with UV LED (365 nm wavelength) and a control box (Figure 3.10). The energy output of the UV reaction unit with a 1 mm illumination distance is 264 mW/cm^2.

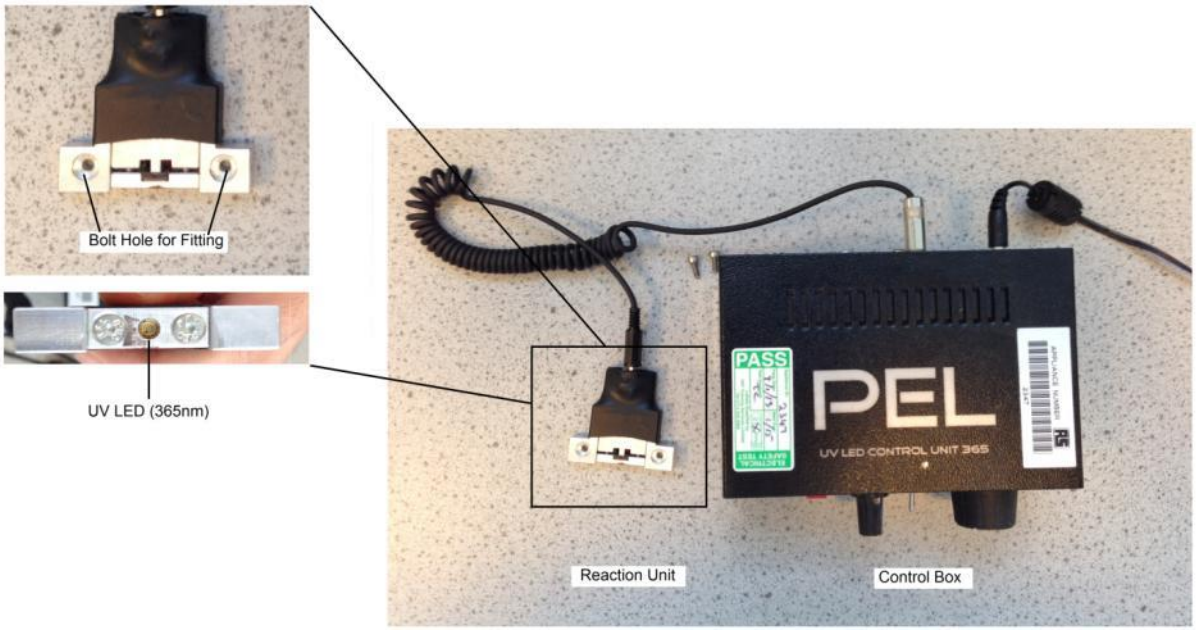

Figure 3.10: UV illumination reaction unit and control box

3.4 Droplet Formation Monitoring

Droplet formation is monitored using a drop watching camera system assembly within the printer. When the drop watcher is active, the printing unit will move to the observing area, placing the nozzles at the observing position. The drop watcher camera system provides direct viewing of the jetting nozzles. All the ink droplets jetted during monitoring are collected by a container positioned below the nozzles.

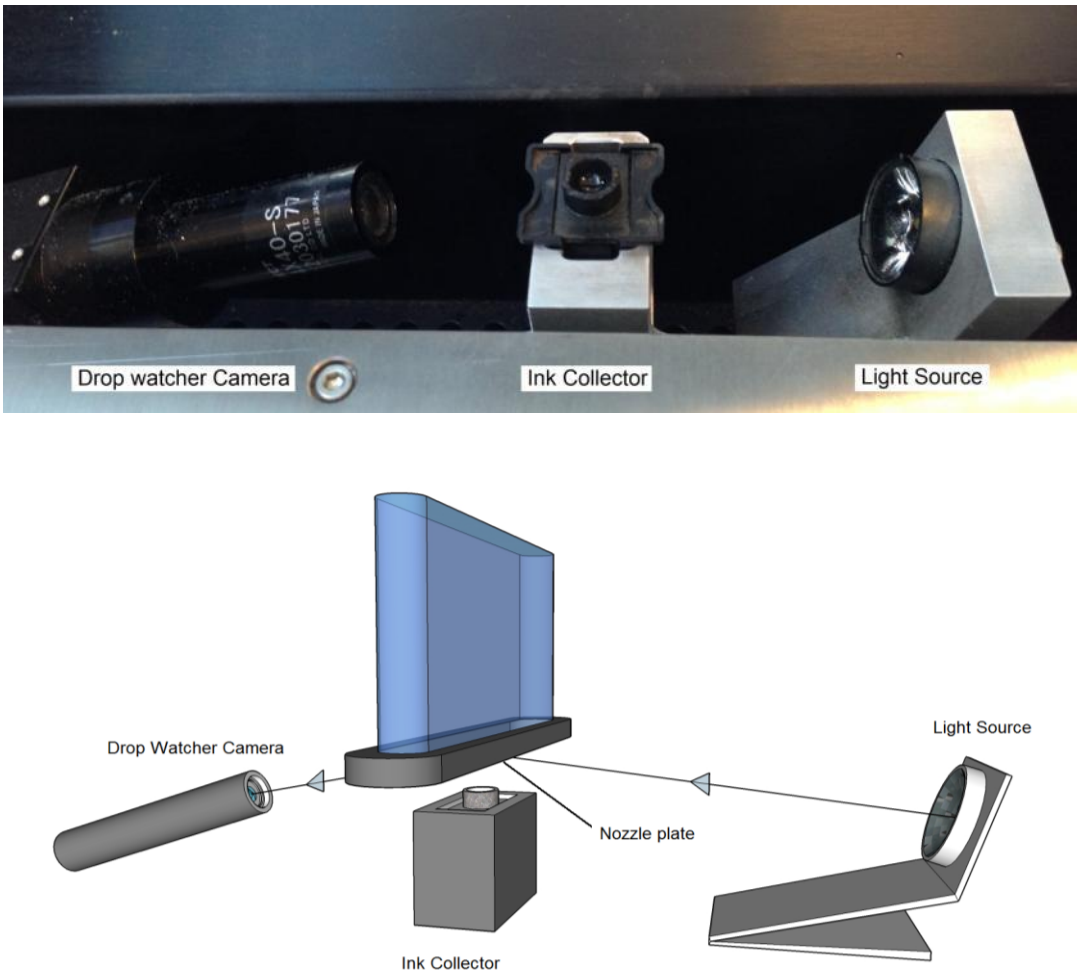

Figure 3.11: Droplet formation monitoring system

The images taken by the camera are presented on the drop watcher screen in movie mode or frame mode. The drop watcher screen also provides a scale on the images to help locate droplet position and measure the droplet velocity.

Each nozzle can be opened individually to check their stability, the printing parameters of the current nozzle are shown at the bottom of the drop watcher screen including printing temperature, printing voltage and waveform file.

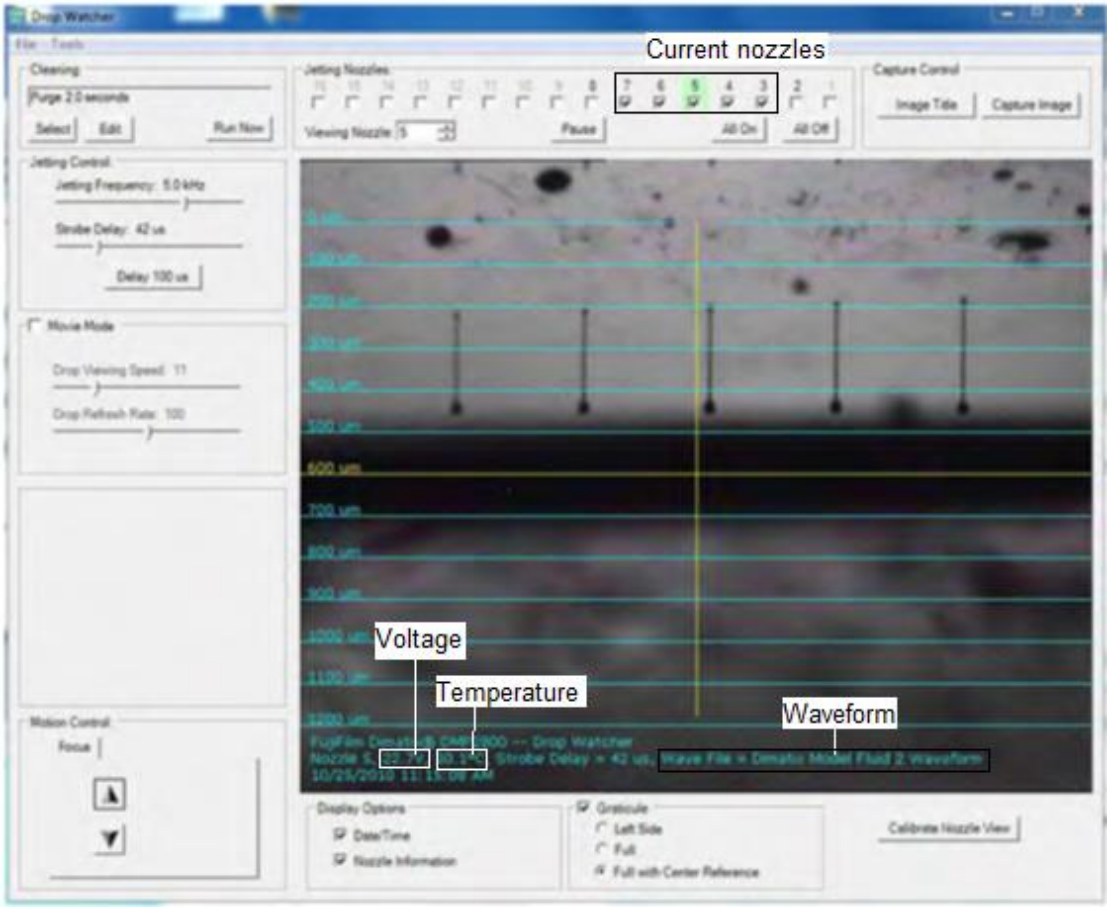

Figure 3.12: Droplet monitoring screen

3.5 Cartridge Setting Adjustment

As different inks have different properties, in order to achieve stable jetting, optimized cartridge settings need to be developed at the droplet formation monitoring stage for a specific ink. The cartridge setting window is shown in Figure 3.13. Several important printing parameters can be adjusted through this window including printing voltage, printhead temperature, jetting waveform and so on. An optimized cartridge setting should be able to provide a single droplet in each jetting cycle with minimal satellite effect.

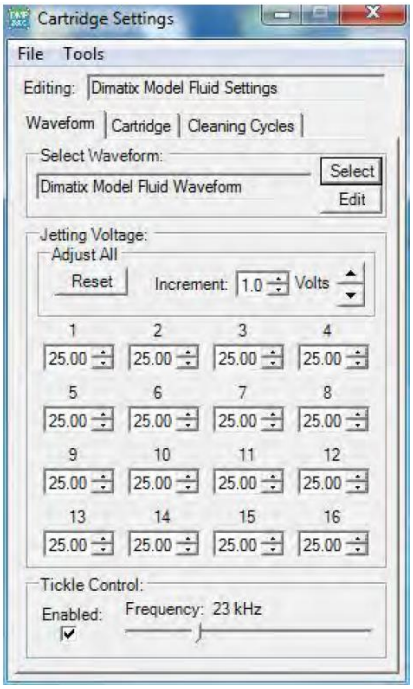

Figure 3.13: Cartridge setting parameters

Printing voltage directly influences the imparted energy to form a droplet and is normally used to adjust the droplet velocity, and is able to be adjusted to between 16 and 40 volt. As mentioned before (Equation 2.2), imparted energy will provide the energy of forming new droplet surface ($E_{surface}$), the energy loss caused by ink viscosity (E_{loss}) and the kinetic energy to eject a droplet ($E_{kinetic}$).

Printhead temperature has an impact on the ink's viscosity as well as surface tension. Increasing printhead temperature will lead to both viscosity and surface tension reduction and therefore cause E_{loss} and $E_{surface}$ to reduce. This can be used to help control droplet velocity as well as a method to reduce an ink's viscosity to bring it into the ejectable range.

The Dimatix printer allows the programming of the jetting waveform and therefore controls the pressure inside the pumping chamber as well as the droplet formation state.

A typical single peak waveform contains three phases: Phase 1-standby, Phase 2-eject, Phase 3-refill (as shown in Figure 3.14).

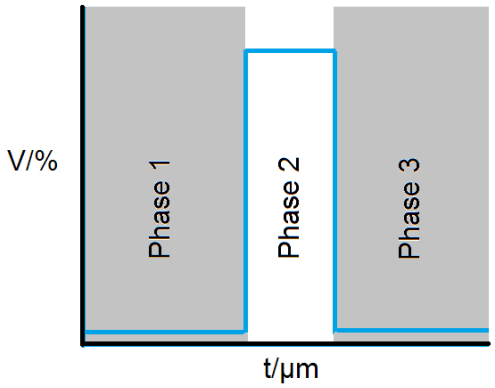

Figure 3.14: An example of a basic waveform used for a piezo actuator based DoD printhead

Phase 1-standby:

Before jetting, the printhead is in standby mode and no voltage is applied. Therefore the piezo element does not deform and no internal pressure is created in the pumping chamber. Phase 1 is the period during which the ink inside the pumping chamber can stabilize and be ready for the next jetting event.

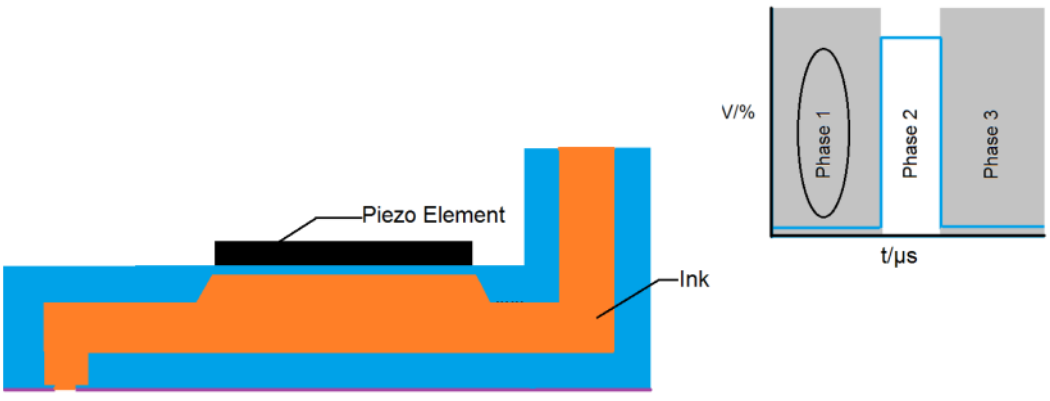

Figure 3.15: A schematic of the printhead's internal state at Phase 1: standby.

Phase 2- eject:

At this stage, the voltage is applied and the piezo element deforms to compress the chamber. The pressure generated inside the chamber will then eject an ink droplet. The level of piezo element deformation is positively correlated with the applied voltage and therefore determines the internal pressure amplitude as well as the energy input.

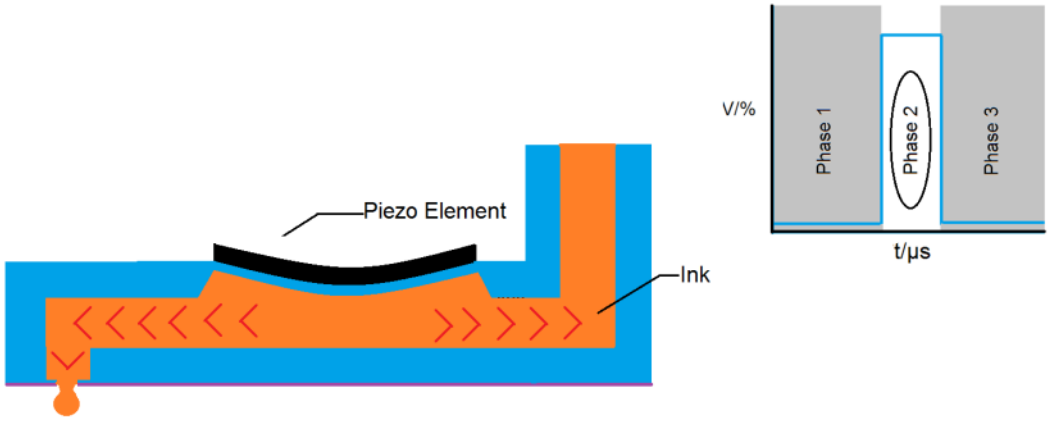

Figure 3.16: A schematic of the printhead's internal state at Phase 2: eject

Phase 3-refill and standby:

At refill and standby phase, the applied printing voltage is removed and piezo element will return to standby mode. The chamber will decompress and generate negative pressure inside to help ink refill the pumping chamber for the next jetting cycle. Meanwhile, the internal pressure will also work as a pull back force at the nozzle which will benefit the ink droplet's pinch off.

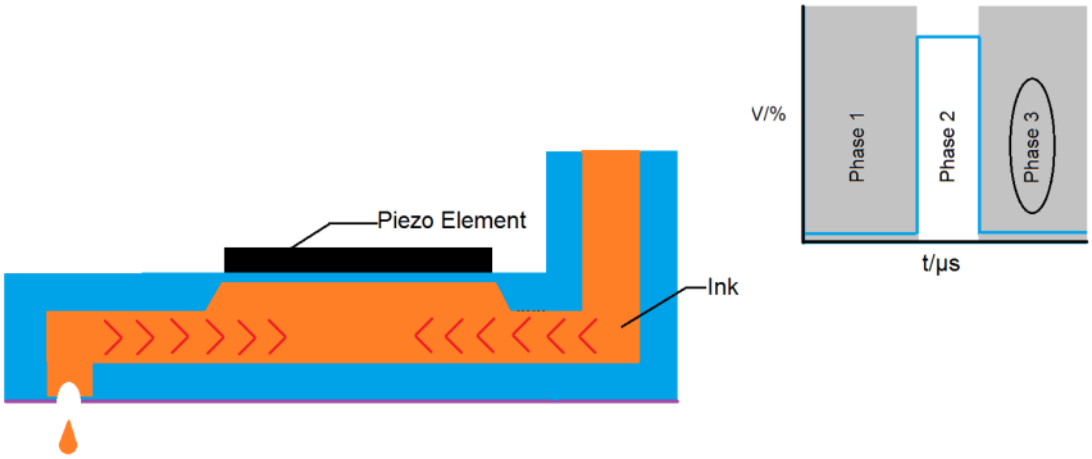

Figure 3.17: A schematic of the printhead's internal state at Phase 3: refill and standby

3.6 Cartridge Maintenance

For piezo based DoD printheads, nozzle failure is very normal over a long printing period. Therefore, cartridge maintenance before and during printing is necessary. When running cartridge maintenance; the printing unit will move to the cleaning pad and go through a preset cleaning program. The cleaning program normally consists of three functions with their own running period:

Purging: pressurising of the cavity inside the fluid module and pushing the ink out through the nozzle. This procedure can help remove trapped air inside the chamber or fix clogging caused by small contaminants or precipitation.

Blotting: Lowering of the printhead to the cleaning pad to allow excess ink on the nozzle plate to be absorbed.

Spitting: The jetting of droplets to perform some initial jetting and help the printing to stabilize.

For different inks, the cause of nozzle failure might be different. Therefore, the cleaning programme will be varied and Figure 3.18 is an example used for UV curable ink.

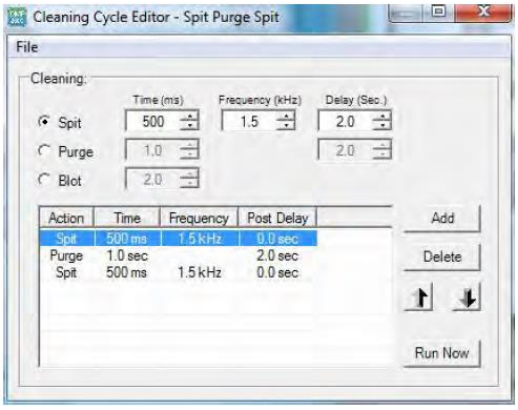

Figure 3.18: An example of a cartridge cleaning programme

3.7 Environment Control

Some solidification methods have specific requirements on the environment such as Oxygen or moisture concentration. The front cover of the DMP-2830 is only designed to ensure a relatively stable air motion in the jetting area and protect the user from being injured by the machine during printing. It is not able to provide an enclosed jetting spacing with Oxygen or moisture controlling. Therefore, a glove box was fabricated to enclose the whole printer. The glove box is made of 10mm thick acrylate sheets with detachable front and top cover. A window on the top provides access. Inert gas is supplied from a valve on the right and a sensor was attached on the left side of the box to monitor the Oxygen concentration in the box. This glove box can support an inert environment with Oxygen levels as low as 1% with around a 0.8% loss after 3 hours after stopping the inert gas supply.

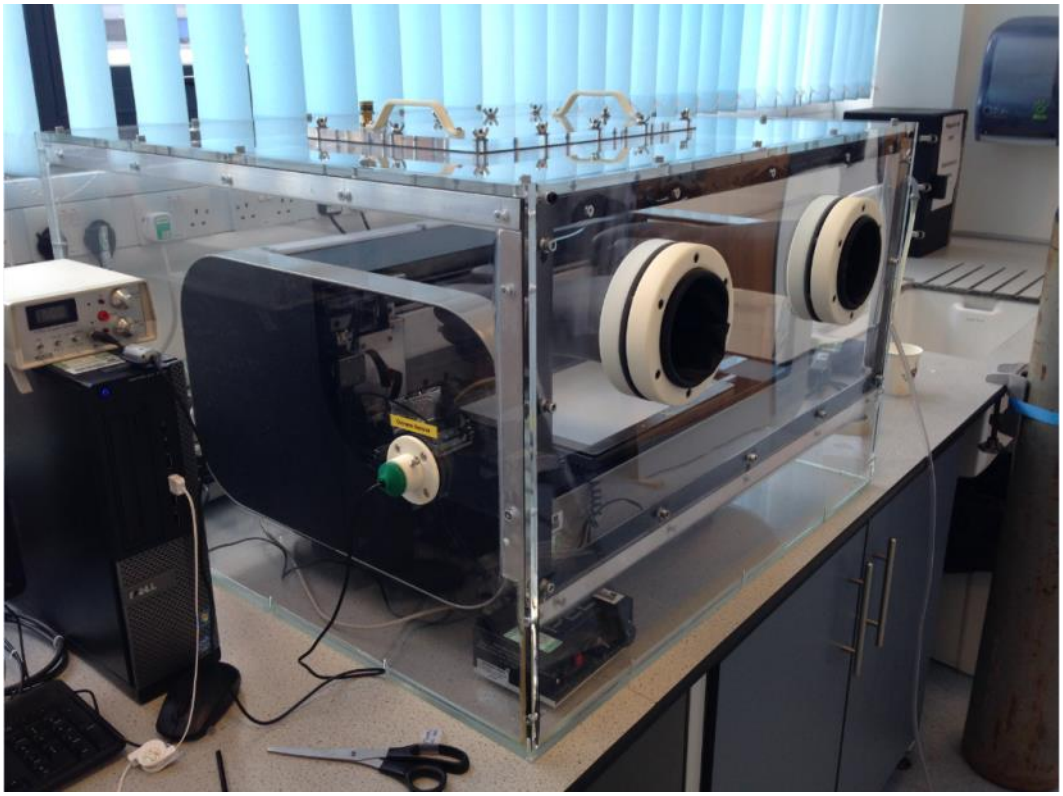

Figure 3.19: The glovebox designed to create inner atmosphere to overcome Oxygen inhibition.

3.8 Ink Preparation

This project has investigated inks based on two different solidification methods respectively: evaporation and UV curing. Evaporation based inks are also described as solvent based ink in the following sections. These inks were prepared by dissolving the polymer into a suitable solvent to obtain a printable ink. Solidification was achieved by precipitation of the dissolved polymer during evaporation of the solvent. For UV curing based ink, the printed ink was prepared with a low viscosity acrylated oligomer of the target polymer, which can then solidify by UV induced crosslinking reaction with the presence of photoinitiator.

3.8.1 Solvent Based Inks

The first step of PCL solvent based ink preparation is choosing a suitable solvent. The solvents chosen in this project include acetone, 1,4-dioxane, ethyl acetate, ethanol and chloroform (Tang et al., 2004)..

Polycaprolactone (PCL, Mn~10000g/mol), 1,4-dioxane (Anhydrous ≥99.8%), acetone (for HPLC ≥ 99.9%), ethyl acetate (anhydrous ≥99.9%), Chloroform (for HPLC, ≥ 99.9%), and ethanol (anhydrous) were purchased from Sigma-Aldrich in order to perform solubility checks. For each solvent, 10 ml was taken and placed in a glass vial. Both 5 wt% and 10wt% of PCL granules were added and the mixtures were left at room temperature for 24 hours. These mixtures were then stirred using an IKA RCT Basic IKAMAG Magnetic Stirrer (with temperature controller) at 800 rpm at room temperature for 5 minutes to improve the dispersion of the dissolved PCL and then settled for another 24 hours to allow bubbles to release naturally. Microscope glass slides 75 mm (L) x 25 mm (W) x 1 mm (H) were used as a printing substrate. Before printing, the slides were soaked into 2-propanol (99.9% min, Fisher Scientific) and ultrasonicated (A Branson Ultrasonic Bath Model 1210) for 5 minutes. Then they were rinsed by 2-propanol and dried in air. The inks were passed through a nylon syringe filter 5.0 µm in diameter (Cole-Parmer) during injection into the cartridge to remove any particulates that might block the nozzle.

3.8.2 UV Curing Ink

As pure Polycaprolactone is not UV curable, chemical modifications were required to graft UV functional groups onto the Polycaprolatone's main chain. Several different methods have been developed to prepare Polycaprolactone with a UV curing function (Feng et al. 2003; Park et al., 2007; Ferreira et al., 2008). Both Feng et al. and Park et al. used a method based on condenstation polymerization and used acrylol chloride as a reactant to provide a UV curable functional group. The main differences between the two studies were the solvent system and the reaction temperature; where Ferreira et al. used 2-isocyanatoethyl methacrylate instead of methacryloyl, which will not generate small molecules during the reaction and the preparation procedures are simpler. However 2-isocyanatoethyl methacrylate is sensitive to water and has a more critical requirement for the reaction environment.

The synthesis sequences used in this project are designed based on a condensation polymerization reaction mentioned above with some modifications. This part of the synthesis was carried out by Sam Kilsby, a PhD student and collaborator at Loughborough University. The synthesis procedures was as follows:

A round bottomed flask was flame dried and filled with anhydrous Tetrahydrofuran, 100 ml (anhydrous, ≥99.9%, inhibitor-free, Sigma-Aldrich), PCL-dio 110 ml, 20.2 mmol (average Mn~530, Sigma-Aldrich) and dried triethylamine, 8.46 ml, 60.7 mmol (≥99%, Sigma-Aldrich) in a nitrogen environment. The flask was then wrapped with foil and cooled down to 0ºC. Methacryloyl chloride 5.92 ml, 60.7 mmol (≥97.0% (GC), contains ~0.02% 2,6-

di-tert-butyl-4-methylphenol as stabilizer) was then added within a one hour period using an automatic syringe pump. The syringe was also wrapped in foil to protect the chemical from direct light.

The reaction was left for 17 hours and then the temperature raised back to room temperature. The residual solvent was removed using a rotary evaporator, after which diethyl ether 100ml (laboratory, Fisher Scientific) and distilled water 100ml were added in and stirred for 15 minutes. Then the mixture was settled down and separated. The organic layer was extracted by a separator funnel and washed by 100ml distilled water inside the funnel 5 times. The organic layer was dried by adding magnesium sulphate and then placed in a vacuum oven to remove volatiles. The final yield of the synthesized UV curable Polycaprolactone (Polycaprolactone di-methylacrylated, PCLDMA) was 13.187 g and the appearance was pale yellow (Figure 3.21). The FTIR spectra of PCLDMA showed absorption band at 1637 and 810 cm^{-1}, which represents the C=C due to methyl acrylation of the PCL diol. The formation of PCLDMA was also confirmed by using ^{1}H-NMR spectrometer and the C=C groups appeared in the δ 5.5-6.2 ppm range. Both results are comparable to the characterization results of photocrosslinkable PCLDA synthesised by Kweon et al. (2003).

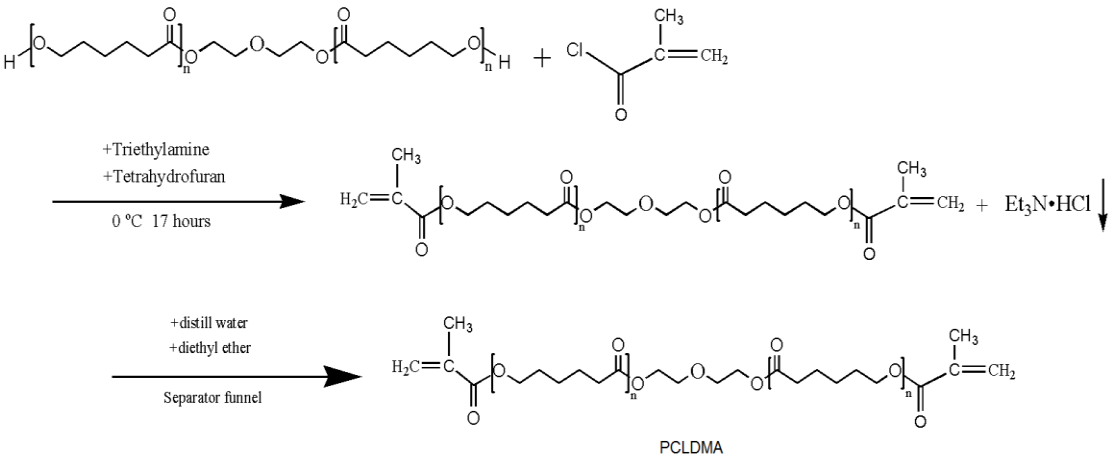

Figure 3.20: Synthesis and separation procedures of PCLDMA

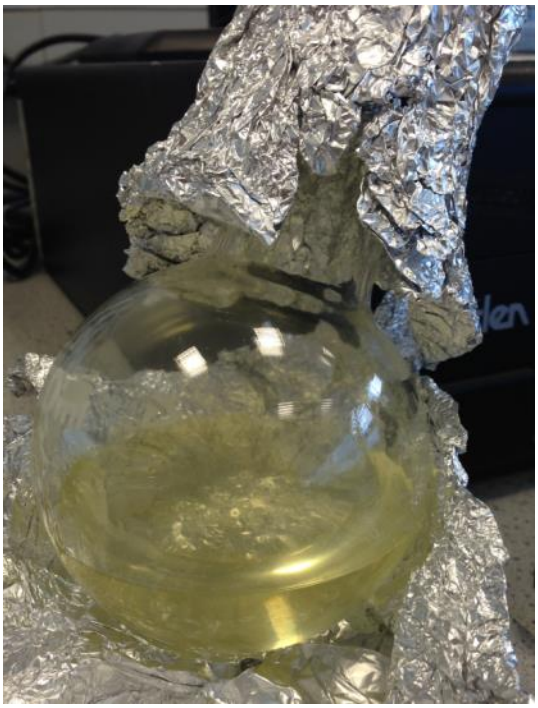

Figure 3.21: Appearance of synthesised PCLDMA

PCLDMA (synthesized) and PEGDA (Sigma-Aldrich average Mn~250) were added to an amber vial and stirred at room temperature for 15 minutes at 800 rpm using an IKA RCT Basic IKAMAG Magnetic Stirrer (with Temperature Controller). Photo-initiator and accelerator were added into the PCLDMA: PEGDA mixture and stirred at 80ºC for 5 minutes until all the solutes were

fully dissolved. Before printing, the prepared ink required a deoxygenized procedure to remove dissolved Oxygen and to help minimize the 'Oxygen inhibition' effect. The degassing procedure was carried out by purging nitrogen gas through the ink for 15 minutes. However, this procedure created lots of bubbles within the ink which seriously reduces the stability of the ink and increases the chance of nozzle failure. Therefore the ink needed to be prepared 24 hours prior to printing and then settled to allow the bubbles to release. The inks were passed through a 5.0 µm nylon syringe filter (Cole-Parmer) during injection into the cartridge to remove any solid contaminants. This procedure needed to be carried out carefully to avoid creating additional bubbles.

3.9 Characterization

3.9.1 Printability Assessment

As mentioned in section 2.5.2, the key parameters for determining ‘’printability’’ are viscosity and surface tension. The optimum printing viscosity and surface tension range slightly varies on the type of printheads being used.

The viscosity of each ink candidates were measured by a rheometer (Malvern Kinexus Pro) with a cone plate configuration (40mm plate diameter with 3 degrees angle). The minimum measuring gap at the centre of the plate was set to 150 µm. A protocol of waiting 300 seconds after reaching the test temperature was set to ensure the ink was in a steady state condition. At each temperature point and shear rate, the viscosity was recorded at 5s intervals within a 180s test time.

Surface tension was measured at different temperatures using a Kruss DSA100S. The surface tensions of each PCL solvent ink were measured within a small environment box which can be heated up by circulating water. Droplet profiles were captured at the equilibrium state and the surface tensions of each ink was given by the software directly.

As mentioned in section 2.5.1, the printing indicator *Z* can be used as an indicator to predict an ink's printability. The printing indicator *Z* was then calculated by following equation to help predict an ink's printability:

$$Z = \frac{\sqrt{\rho r \gamma}}{\mu} \qquad \text{Equation 3.1}$$

where ρ is the density, r is the characteristic length (or the nozzle diameter), γ is the surface tension of the fluid and μ is the viscosity of ink. Generally if *Z* falls between 1 and 10, printing is considered possible (Gibson, 2010).

3.9.2 Printed Sample Characterization

Based on the thickness of the printed sample, different characterization methods were used to characterize the printed specimens.

PCL Solvent Based Ink

As each layer of the printed and solidified PCL solvent ink was less than 1 μm, the chosen characterization techniques were mainly focused on the printed sample's morphology. Printed PCL samples were initially studied with optical microscopy (Reichert-Jung MEF3). Both Bruker Contour GT-I and Talysurf 2000 were then used to acquire the surface profile data of the solidified PCL films.

PCL UV Curing Based Ink

PCL inks were printed in both air and nitrogen environments. The mechanical properties of printed samples were characterized and compared by nano-indentation at room temperature (Micro Materials, NanoTest NTX with hot stage and inert gas cabinet). The peak force was set to 5 mN with a 0.25 mN/s loading and unloading rate and a spherical indenter with 50 µm radius was used. FT-IR measurement in attenuated total reflectance (ATR) mode (Bruker Tensor-27) with 2 cm^{-1} interval was used to help comparing the curing level of PCL UV based ink with different formulations. Printed mesh structures were also sputter coated with Platinum and examined by SEM (XL30 ESEM Philips). The absorbance spectrum of the printed ink was measured by printing different layers of ink onto quartz slides and which were then characterized for their spectral response by a UV-vis spectrophotometer (Varian UV-Visble Spectrophotometer).

Chapter 4. Polycaprolactone Solvent-based ink

Dissolving a target material into a suitable solvent and allowing it to precipitate through evaporation after jetting is one method to convert a solid polymer into a printable ink. Polycaprolactone solvent-based inks were prepared by dissolving 5 and 10 wt% of polycaprolactone flakes into different solvents following the procedures outlined in Section 3.8.1. These inks were then used to perform a series of printability assessment experiments. The influences of printing voltage, droplet velocity, substrate temperature and droplet spacing on polycaprolactone solvent-based ink droplet formation as well as final deposition quality were investigated. Multi-layer polycaprolactone structures were printed and the morphology of deposited polycaprolactone was characterized with the Talysurf 2000 and Bruker ContourGT-I.

4.2 Results and Discussion

4.2.1 Solvent selection

The used solvents and concentrations were determined based on the studies carried out by Tang et al. (2004), which studied the surface properties and biocompatibility of solvent-cast poly[epsilon-caprolactone] films. As mentioned in section 2.8, residual solvent will induce toxic components to the final product, which will influence the biocompatibility. The safety of the suggested

solvents was investigated based on the guidelines from International Council for Harmonisation (ICH) (Table 4.1).

Table 4.1: Residual solvent guidelines (Grodowska and Parczewski, 2010)

Solvent	Permissible daily exposure limit (mg)	Concentration limit (ppm)
1,4-dioxane	3.8mg	380
Chloroform	0.6	60
Ethyl acetate	>50	>5000
Acetone	>50	>5000
Ethanol	>50	>5000

Ethyl acetate, Acetone and Ethanol are classified as safe solvents by the ICH. 1,4-dioxane and chloroform were classified as Class 2 (less toxic solvent). None of these solvents are included in Class 1 (toxic solvent which should be avoided). Therefore all the solvents could be used to prepare a potentially biocompatible PCL solvent ink.

The PCL granules in 1, 4-dioxane and Chloroform were fully dissolved after 24 hours. For the samples in acetone and ethyl acetate, debris was observed to peel from the granules' outer surface but no significant dissolution was observed. Nothing happened to the granules in ethanol. Tang et al. (2004) suggested that heating is required to help accelerate the dissolution for both acetone and ethyl acetate. Therefore, the vials with undissolved PCL granules were placed in a water bath at 40°C for 10 minutes, after which PCL granules inside acetone and ethyl acetate were fully dissolved. However, white

precipitates of PCL were found within the acetone and ethyl acetate based mixtures after cooling and settling. As inks for jetting need to stay in a stable state inside the cartridge, the precipitation of the solute inside the cartridge may cause nozzle blockage or even printhead damage. Therefore, both ethyl acetate and acetone cannot be used for PCL solvent ink preparation. 1, 4-dioxane and chloroform were chosen as potential solvents for preparing PCL solvent based inks.

For ink preparation, another important factor is the stability of the base liquid. During the whole printing period, the ink will be exposed to the atmosphere at the exit of each nozzle. The solvent in the ink can evaporate at the nozzle surface causing a localized concentration increase or even form a precipitate in and around the nozzles, especially during the stand-by stage. This will influence droplet formation quality, causing nozzle faults (Figure 4.1) or even failure.

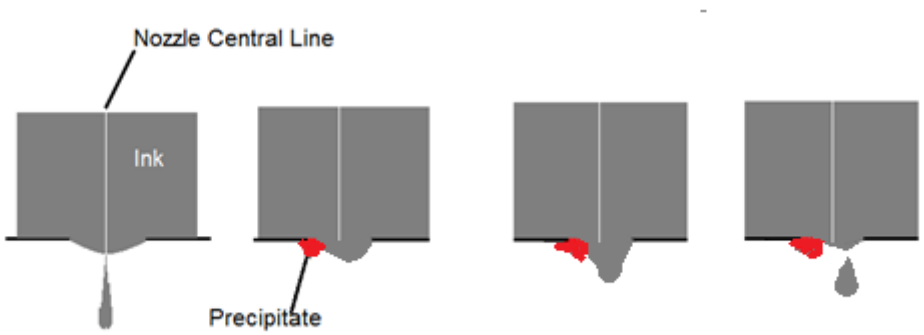

Figure 4.1: Nozzle fault or failure caused by precipitation.

Therefore, the boiling points of these solvents (as shown below) were also taken into consideration during solvent selection. The suggested boiling temperature for inkjet inks is at least 100°C and solvents with higher boiling point are preferred to provide the best printing stability. Meanwhile 1,4-

dioxane has a higher residual concentration limit which means less difficulties in sample purification during post-process, therefore 1, 4-dioxane was chosen as the solvent which is going to be used to prepare PCL solvent based inks.

Table 4.2: Boiling point of the solvents used for PCL solubility test.

Solvent	Boiling point
1,4-dioxane	101°C
Chloroform	61.15°C
Ethyl acetate	77.1°C
Acetone	56°C
Ethanol	78.37 °C

4.2.1 Rheology and Surface Tension

The viscosity of the ink was measured between 25°C and 40°C to identify the processing temperature and ink composition that would give an optimum viscosity for inkjet printing.

Surface tension was measured by the pendant drop method at 25°C, 30°C, 35°C and 40°C respectively, using a Kruss DSA100S. The surface tensions of each PCL solvent ink were measured within a small environment box which can be heated by circulating water.

The results of the viscosity versus shear rate sweep are shown in Figure 4.2. For the 5 wt% ink it can be observed that the viscosity is within the range of 3 to 6 cp. The viscosity was observed to decrease with increasing temperature. For the 10 wt% ink, the same trends were observed, but with a shift upwards

in viscosity such that it lays in the range 8 to 12 cp. The small peaks in viscosity results around the shear rate of 50 s^{-1} were due to sensor switching. The increment of viscosity after 200s^{-1} was due to the formation of Taylor-vortex flow which generated extra resistance to the spinning plate (Bohlin, 1994). As the viscosity is defined under laminar flow, the real viscosity of the ink should equal the flat section between 80s^{-1} and 200s^{-1}.

The surface tension of the inks was measured as a function of temperature (Figure 4.3). It was found that the surface tension was around 34 mN/m at 25ºC and then reduced with increasing temperature. The surface tension at 40ºC was found to be 32 mN/m. This trend is consistent with the relationship determined by Eötvös (Palit, 1956) who predicted that a liquid's surface tension will be linearly related to the environmental temperature through:

$$\gamma(MV_{sp})^{\frac{2}{3}} = K_E(T_C - T) \qquad \text{Equation 4.1}$$

where γ is surface tension, M is molecular weight, V_{SP} is specific volume, T_C is the critical temperature of a selected liquid, K_E is a constant for all liquids and T is environmental temperature.

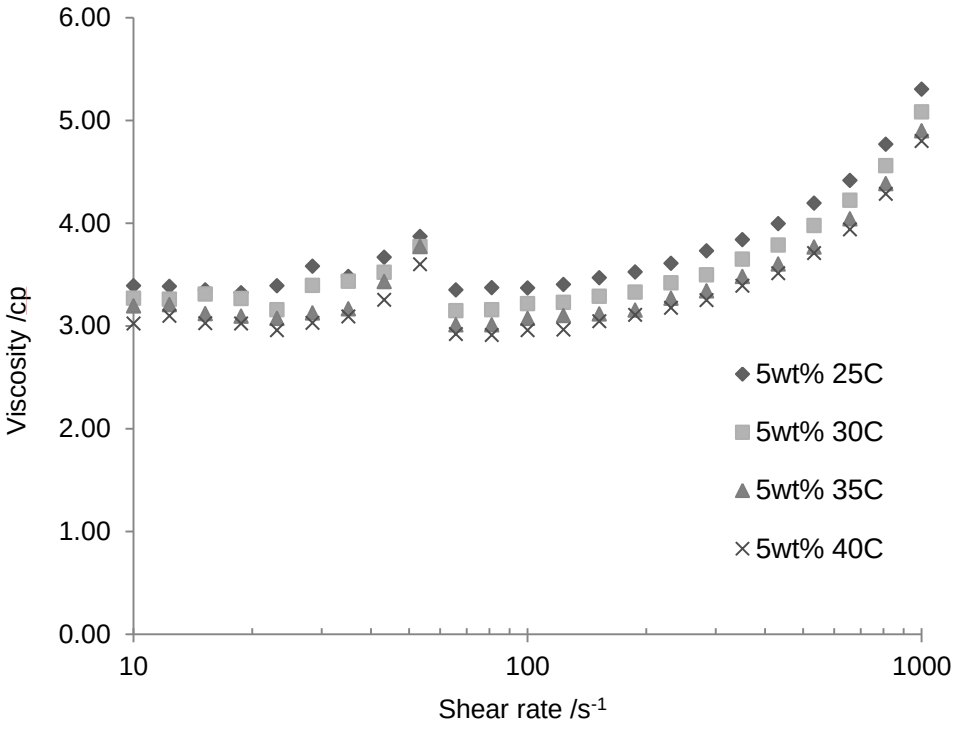

(a)

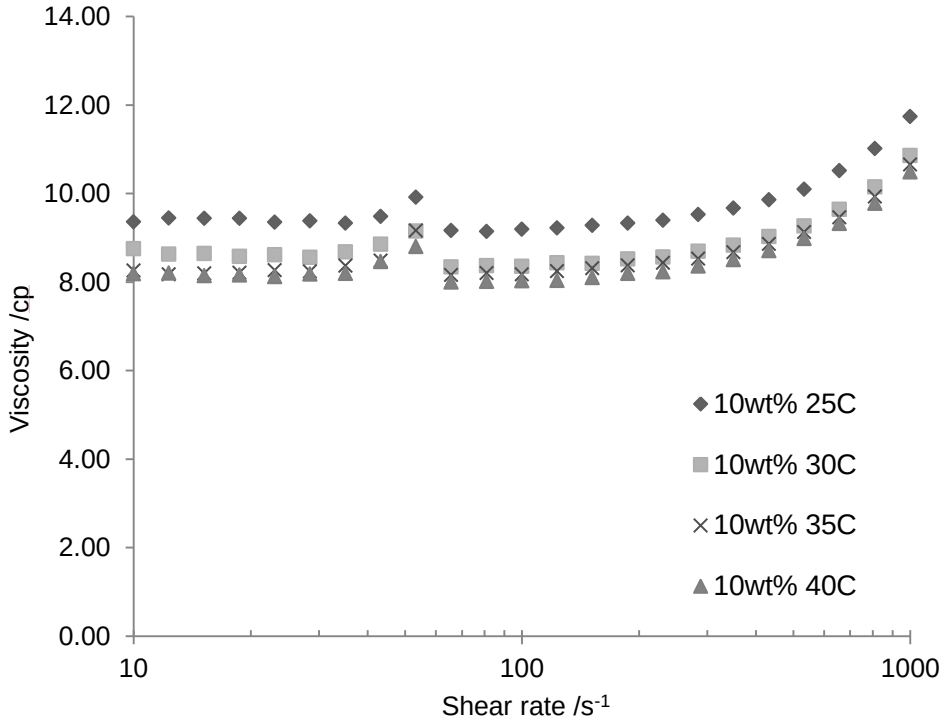

(b)

Figure 4.2: Viscosity of (a) 5wt% and (b) 10wt% PCL solvent ink, tested from 25 ºC to 40 ºC with shear rate range between 10 s^{-1} and 1000 s^{-1}.

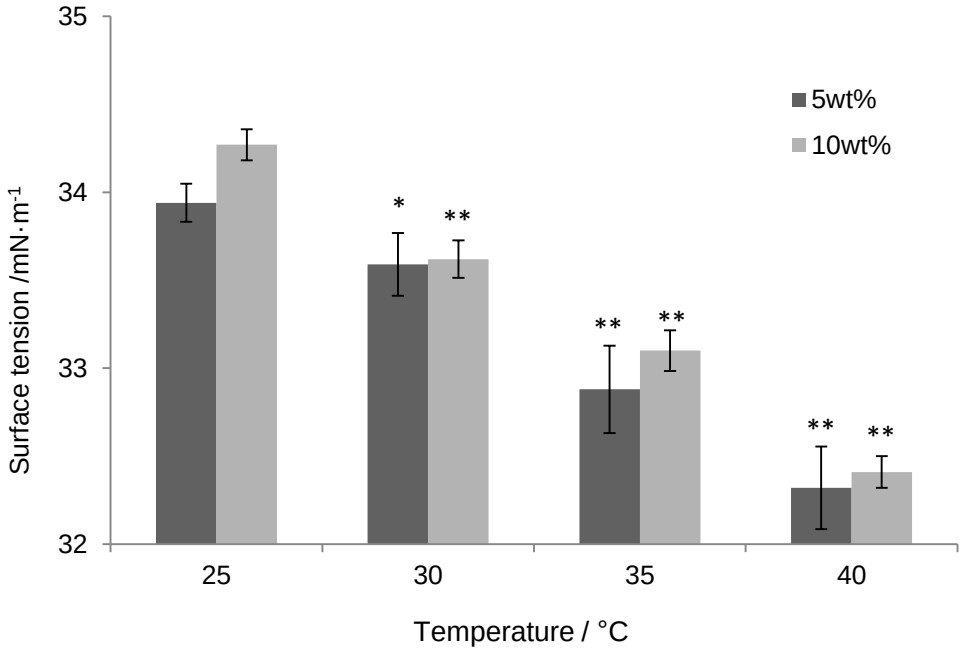

*Figure 4.3: Surface tension of 5wt% and 10wt% PCL solvent ink tested from 25 ºC to 40 ºC compared to 25°C (Mean ± Standard Deviation, n=5, *p<0.01, **p<0.001)*

The remaining relevant properties to determine printability were also determined and are shown in Table 4.3. The printing indicators *Z* for each PCL solvent were calculated and shown.

Table 4.3: Physical properties and printing indicator value of PCL solvent ink at a temperature of 25ºC.

Sample	Nozzle Diameter (µm)	Density (g/cm^3)	Viscosity (at 1000 s^{-1}) (mPa s)	Surface Tension (mN/m)	*Z* (Oh^{-1})
PCL 5wt%	21	1.03	3.5	31.9	7.52
PCL 10wt%	21	1.05	9.2	33.6	3.02

It has been reported that an ink can be considered printable when Z falls between 1 and 10 (Ainsley, 2002). Since Z is 3.02 for 10 wt% and 7.52 for 5 wt% it can be assumed that these inks are printable. It was found, however, that only the 5 wt% solvent ink samples were printable and the 10wt% ink blocked the nozzle directly. Observation of the ink behaviour during jetting showed that the solvent evaporate at the nozzle leading to PCL precipitating on the nozzle plate, which blocked the nozzles directly.

4.2.2 Droplet Formation Assessment

The droplet formation of the 5 wt% ink was examined and optimized. The effects of different printing parameters were investigated through the Dimatix drop watcher camera system to study their influences on the droplet formation quality. As mentioned in section 2.5.2, both Shin et al. and Dong et al suggested a double pulse waveform for jetting low viscosity inks (Shin, 2011; Dong, 2006). Therefore a double pulse waveform was chosen as the starting printing waveform for printing quality assessment. The aim of this stage was to optimize the printing parameters and achieve single regular ink droplet formation and minimize the ‘satellite effect’ (as mentioned in Section 2.5.2).

In this study the time gap between pulses was varied between 1 and 8 μs, whilst the width of the peaks was fixed at 3 μs. The printing voltage was an additional variable that would affect the pulse height. Three kinds of droplet formation states were observed when changing the printing parameters. (Figure 4.5)

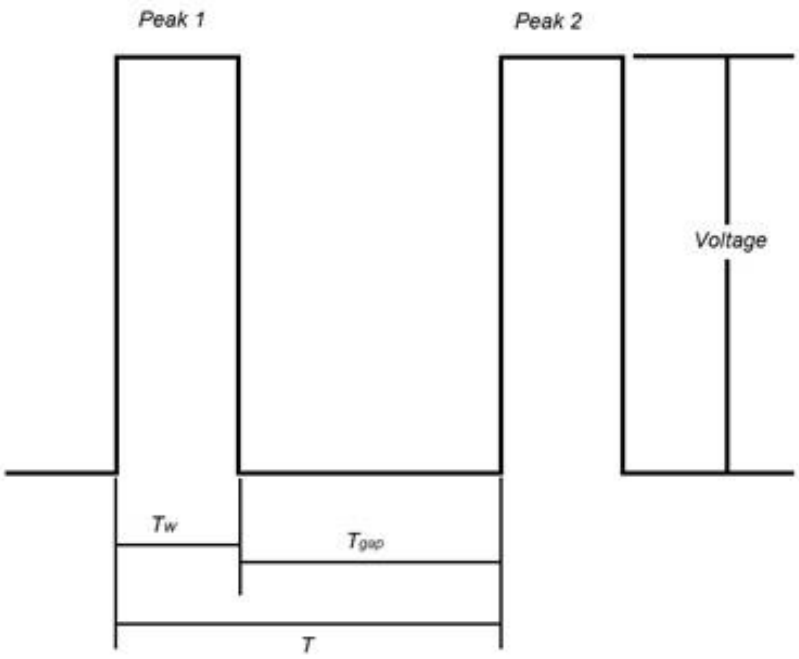

Figure 4.4: Printing waveform used in this research.

The situations in Figure 4.5 (a) and (b) were defined as acceptable in this study as only one primary droplet was formed before reaching the substrate. Dong et al.(2006) studied these effects in detail and they concluded that whether satellite without recombination happened or not depended on the thread length and primary droplet speed when the thread broke up. They demonstrated that the retreating speed of the thread tail is almost constant for an ink while the primary droplet speed was related to printing voltage and waveform. When the retreating speed is lower than the primary droplet speed, satellites without recombination occur. Therefore, the satellite effect can be minimized by adjusting the front droplet speed. Figure 4.6 shows how the time gap *T* between the starting points of two peaks and printing voltage affected the droplet velocity, which reached a maximum at a time gap of around 7 μs.

Increasing the printing voltage increased the velocity of the primary droplet for any given time gap.

The primary droplet speed variation by time gap can be explained, in some cases, by investigating the pressure waves being transmitted and reflected within the ejection chamber. For example, Kwon et al. (2007) indicated that the pressure waves will superimpose and act to dissipate the pressure wave when the time gap (T) between the start of the second peak and that of the first peak, is either $2L/c$ or $6L/c$ (where L is the channel length and c is the speed of sound inside the ink). This can be expressed in terms of the peak gap, T_{gap}, and peak width, T_w, such that $T = T_{gap} + T_w$ This gives some indication of the bounds on the separation of the two peaks. The channel length in the case of Dimatix cartridge is 3 mm and the speed of sound in the ink can be estimated from the speed of sound in 1,4-dioxane with 5 wt\% polystyrene, which is 1360 m/s (Toti and Kariduraganavar., 2000). By plotting the velocity of the drop versus T, it was found that the minimum velocities occurred at approximately 4 µs and 12 µs (Figure 4.6), matching closely the predictions from Kwon et al. Going beyond these values for T, one would see that the two voltage peaks will join together if we reduced its value.

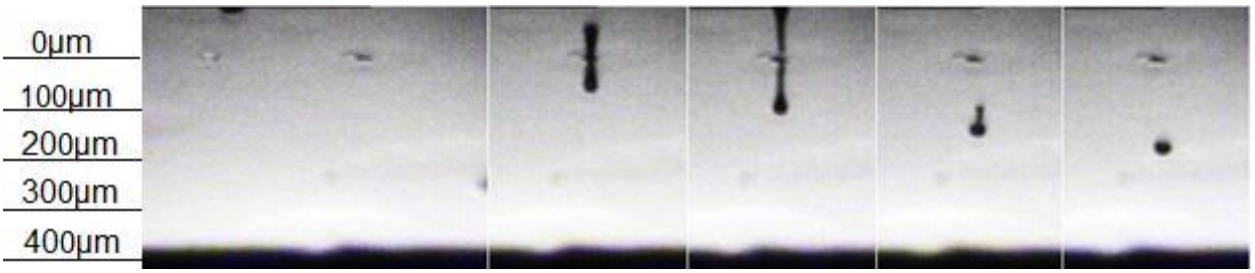

0 µs 10µs 20 µs 30 µs 40 µs

(a)

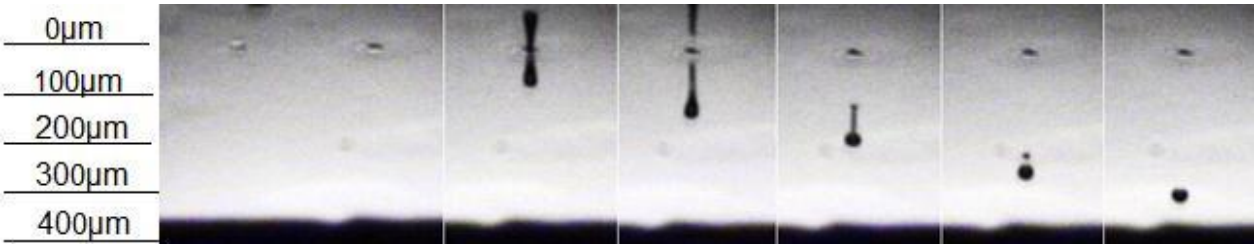

0 µs 10 µs 20 µs 30 µs 40 µs 50 µs

(b)

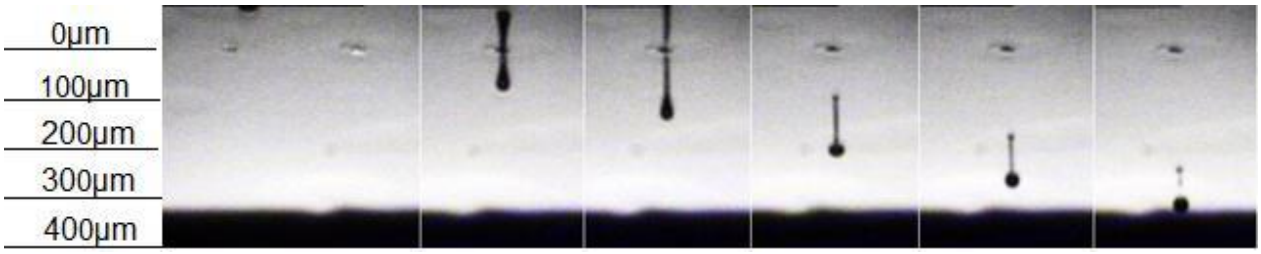

0 µs 10 µs 20 µs 30 µs 40 µs 50 µs

(c)

Figure 4.5: Three types of different droplet formation: (a) single droplet without satellite, (b) satellite with recombination and (c) satellite without recombination.

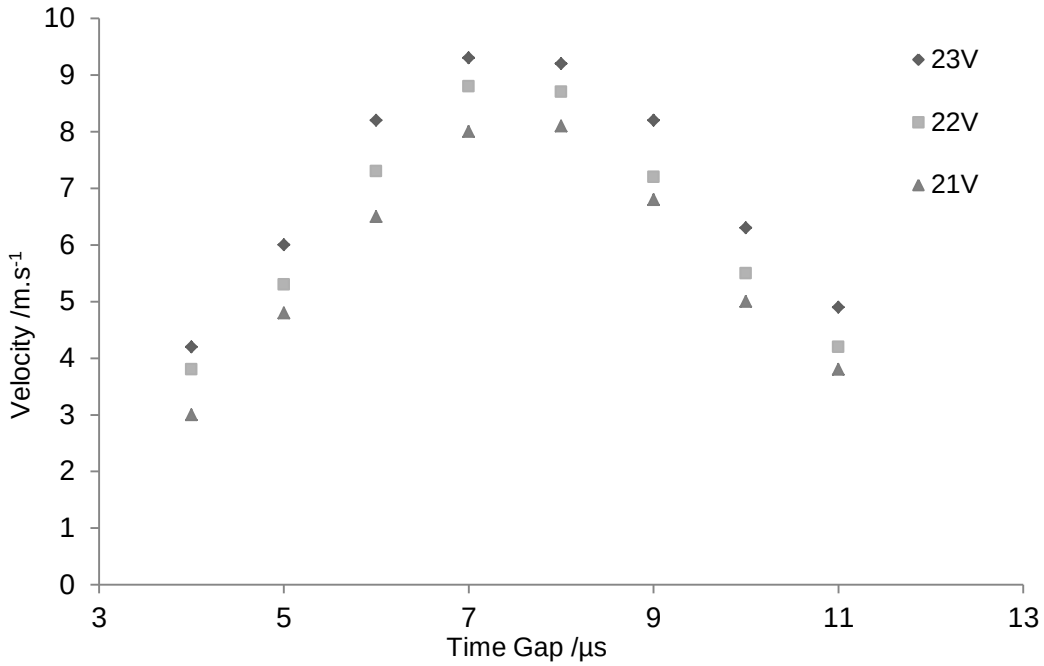

Figure 4.6: Droplet Velocity change under different time gap and printing voltage.

4.2.3 Inkjet Deposition Assessments

Following printing quality assessment, different patterns were printed using a Dimatix DMP-2830 (FujiFilm) to investigate the deposition of the ink. An array of dots with 100 µm droplet spacing was firstly printed to study the deposited and solidified ink droplet morphology. PCL solvent ink was printed with different jetting speeds and substrate temperatures. Then, a line pattern and a square pattern were printed with 20, 40 and 60 µm droplet spacing under different substrate temperatures to inspect deposited droplet interaction. Optical microscope pictures of printed samples were taken and surface profiling data was collected.

Droplet Deposition

The effects of changing droplet velocities on the deposited and solidified droplet morphology were investigated. The experiments were carried out by

printing individual droplet arrays with different droplet speeds at room temperature. The solidified droplets were then observed by optical microscope.

Optical microscope images of the solidified PCL ink are shown in Figure 4.7. It can be seen that solidified PCL tended to concentrate near the outer perimeter of the droplet under all printing conditions. This phenomenon is known as the 'Coffee Ring' effect (as mentioned in section 2.5.3) and often occurs with suspension based inks.

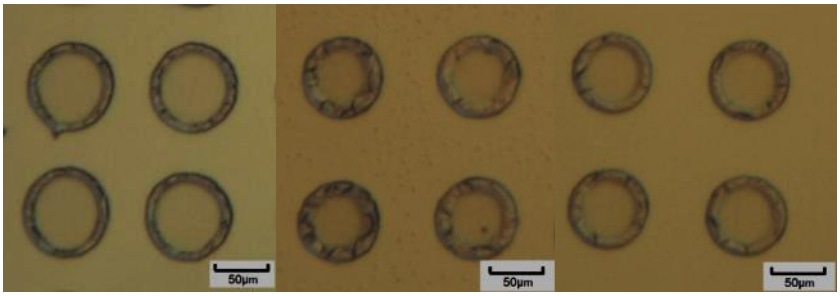

(a) (b) (c)

	(a)	(b)	(c)
Droplet velocity	5m/s	6m/s	7m/s
Droplet diameter	83.9±1.7µm	78.7±0.8µm	77.1±1.2µm

Figure 4.7: Optical microscopy images and the diameter of of solidified 5 wt% PCL solvent ink printed at different droplet velocity (a) 5 m/s (b) 6 m/s (c) 7 m/s (Droplet spacing was 100 µm, substrate temperature was 25°C, mean ± standard deviation, n=4).

As the solidification procedure of PCL solvent ink is dependent upon the evaporation of the solvent, the substrate temperature is also a key variable to decide the solidified structure's morphology. Therefore, further experiments were carried out to investigate the effect of the temperature on the

morphology of the solidified deposits. Droplet arrays were printed under various droplet speeds (5 m/s, 6 m/s and 7 m/s) and substrate temperatures (25ºC, 30°C and 35ºC).

Figure 4.8 shows optical microscope images of printed and solidified droplets with different combinations of velocities and substrate temperatures. The diameters of the solidified droplets were measured (Table 4.4 and Figure 4.9) and it was found that droplet sizes tended to reduce as the substrate temperatures increased. The cause of this behaviour could be due to a number of effects. The surface tension will be affected by the substrate temperature and since the surface tension reduces with temperature for 1,4-dioxane, this may result in an increase in contact angle and a reduction in observed deposition diameter. Alternatively, the reduced deposition diameter may be a function of the increased evaporation rate of the solvent. Meanwhile, as higher substrate temperature will also accelerate solvent evaporation, it is quite advantageous for reducing the residual solvent in each printed layer. Therefore samples prepared at higher temperature may show improved biocompatibility as well as require less post-processing to remove any residual solvent.

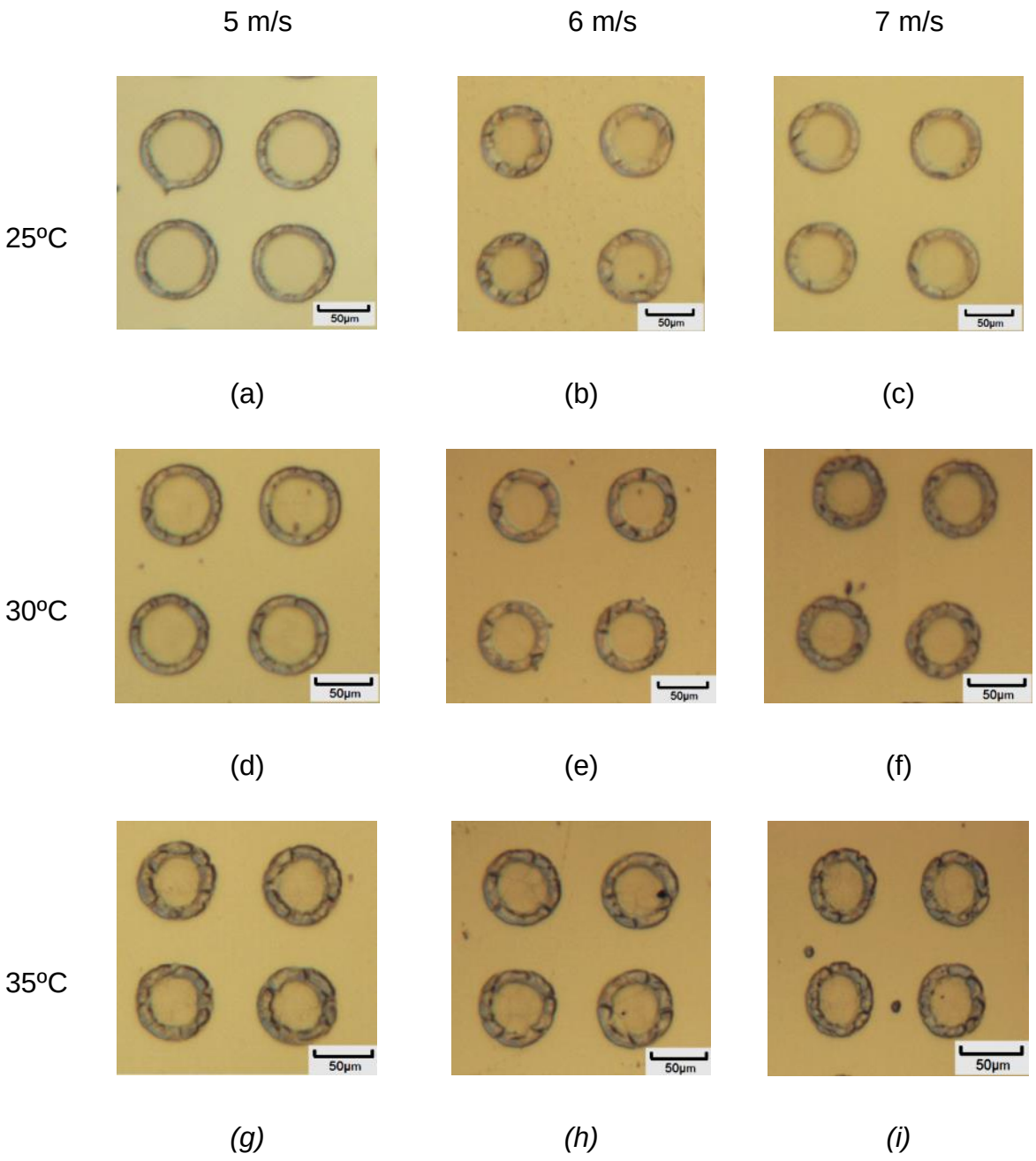

Figure 4.8: Optical microscope images of deposited and solidified PCL printed with different droplet velocities (horizontal row) and substrate temperatures (vertical column).

Table 4.4: Solidified droplet diameter of PCL solvent ink printing under velocity of 5 m/s, 6 m/s and 7 m/s with substrate temperature equals to 25 ºC, 30 ºC and 35 ºC respectively. (mean ± standard deviation, n=4)

Droplet Diameter (µm)			
Substrate Temperature	Velocity		
	5 m/s	6 m/s	7 m/s
25ºC	83.9±1.7	78.7±0.8	77.1±1.2
30ºC	76.1±1.5	75.0±0.9	69.1±1.3
35ºC	68.6±1.2	67.6±0.7	64.4±1.2

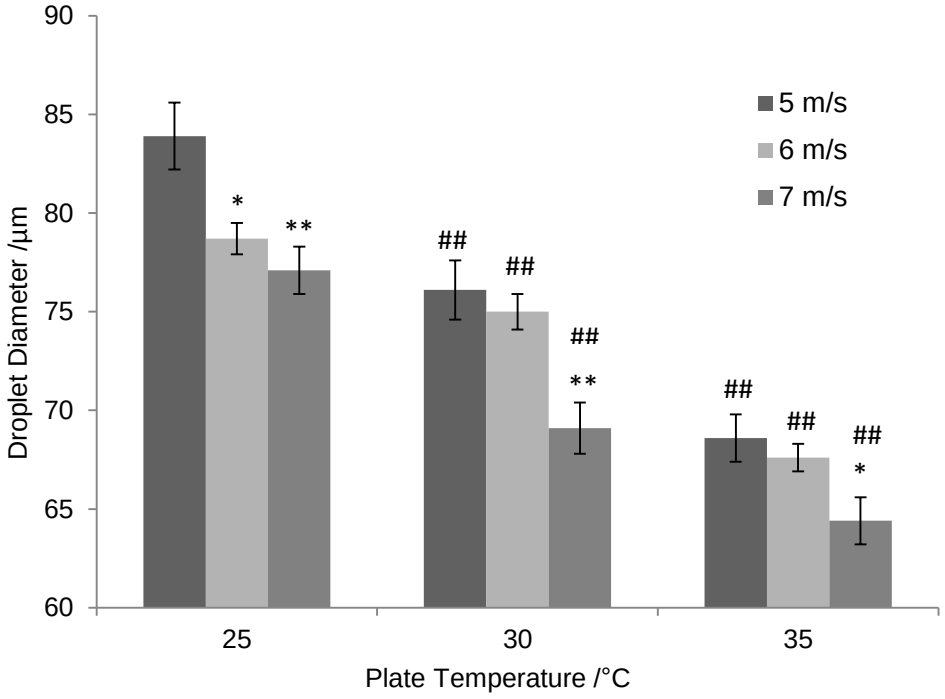

*Figure 4.9: Plot of droplet diameter against plate temperature with droplet velocity equal to 5, 6 and 7 m/s. (Mean ± Standard Deviation, n=4, compared to droplet diameter at 5m/s under the same temperature *p<0.01, **p<0.001, compared to droplet diameter at 25°C at under the same droplet speed #p<0.01, ##p<0.001)*

Solidified droplet structures were also examined using white light surface profiling to determine the spatial variation in height. An example of the white light profiling data in Figure 4.10 showed that after solidification, precipitated PCL concentrated at the outer edge which verified the observations made via optical microscopy. Table 4.5 shows average edge and central thickness which showed that the average thickness tends to increase as plate temperature increased and deposited droplet diameter decreased. Assuming each ejected droplet has a similar volume size, less wetting means higher solute concentration in a unit area which led to the height increment for solidified droplet.

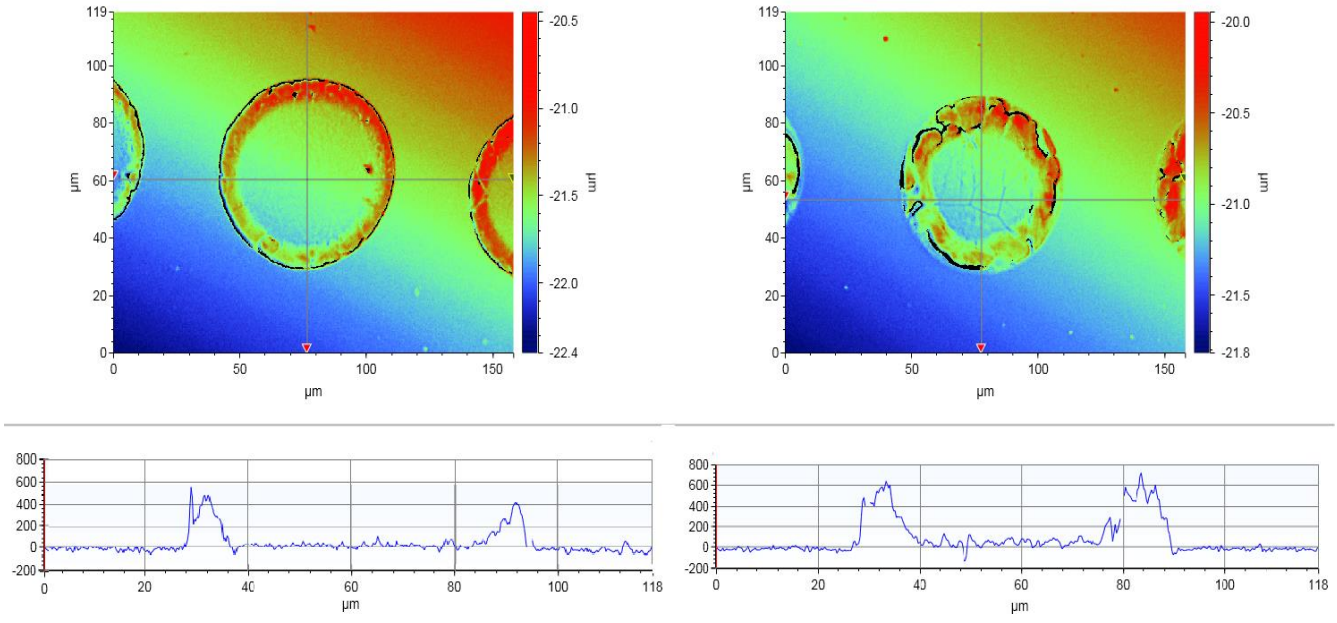

(a) (b)

Figure 4.10: An example of white light surface profiling of printed PCL solvent based ink with different substrate temperature: (a) 25ºC (b) 35ºC.

Table 4.5: Solidified droplets edge and central thickness of PCL droplets printed with different printing parameters.

Plate Temperature	Droplet Velocity	Average Edge Thickness (nm)	Average Central Thickness (nm)
25 ºC	5 m/s	284	34
	6 m/s	304	33
	7 m/s	303	36
30 ºC	5 m/s	321	52
	6 m/s	365	51
	7 m/s	342	50
35 ºC	5 m/s	373	58
	6 m/s	385	55
	7 m/s	390	68

Line Formation

In this section, the effects of different droplet spacings on PCL line formation are reported. Jetting droplet velocity was chosen to be 6 m/s due to the greater observed consistency of droplet size at this velocity. In order to make every single droplet combine and form a continuous line, the droplet spacing needs to be smaller than the deposited droplet size. Three different droplet spacings (20 μm, 40 μm and 60 μm) were chosen to investigate how droplet overlap influences the morphology of printed lines. The effect of different substrate temperatures was also examined since it has already been

observed that variation in temperature can lead to changes in deposit diameter, and which should have a knock on effect on the line formation too.

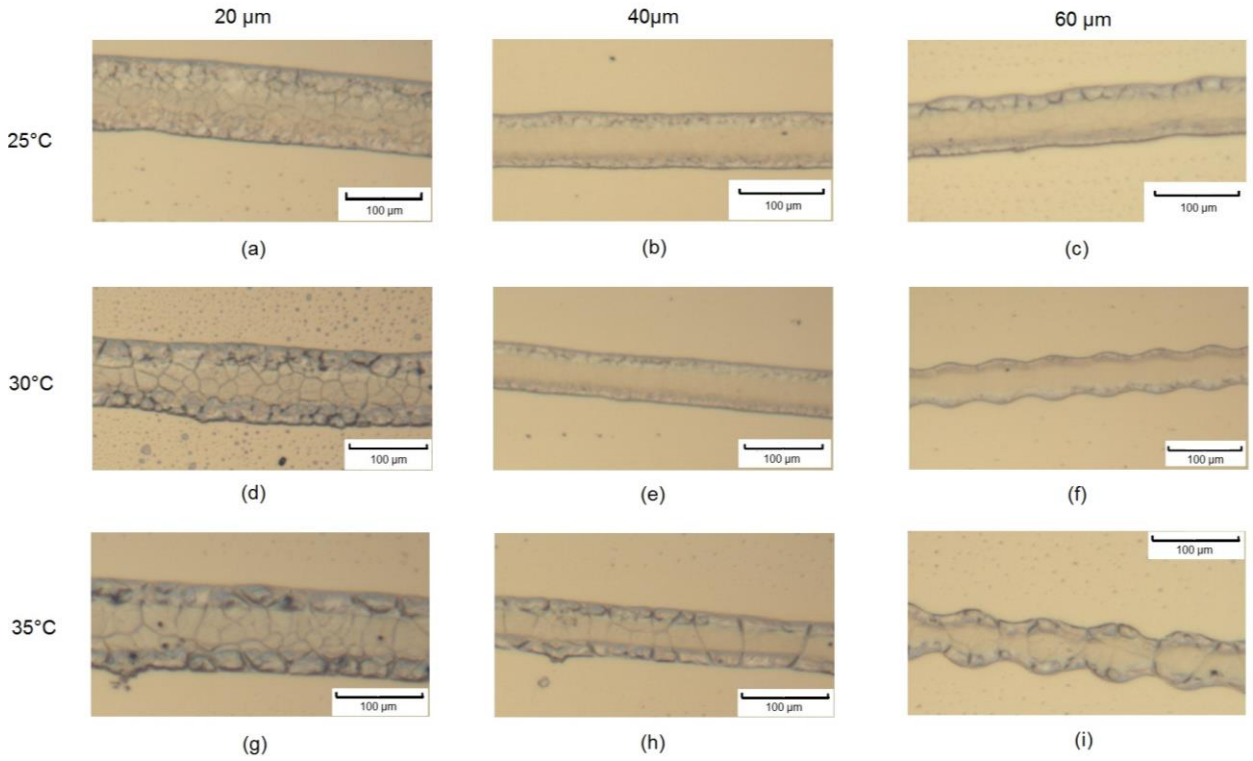

Figure 4.11: Optical microscopy result of line formation test for PCL solvent ink printed with different droplet spacing (horizontal row) and substrate temperature (vertical column) with droplet velocity equal to 6m/s

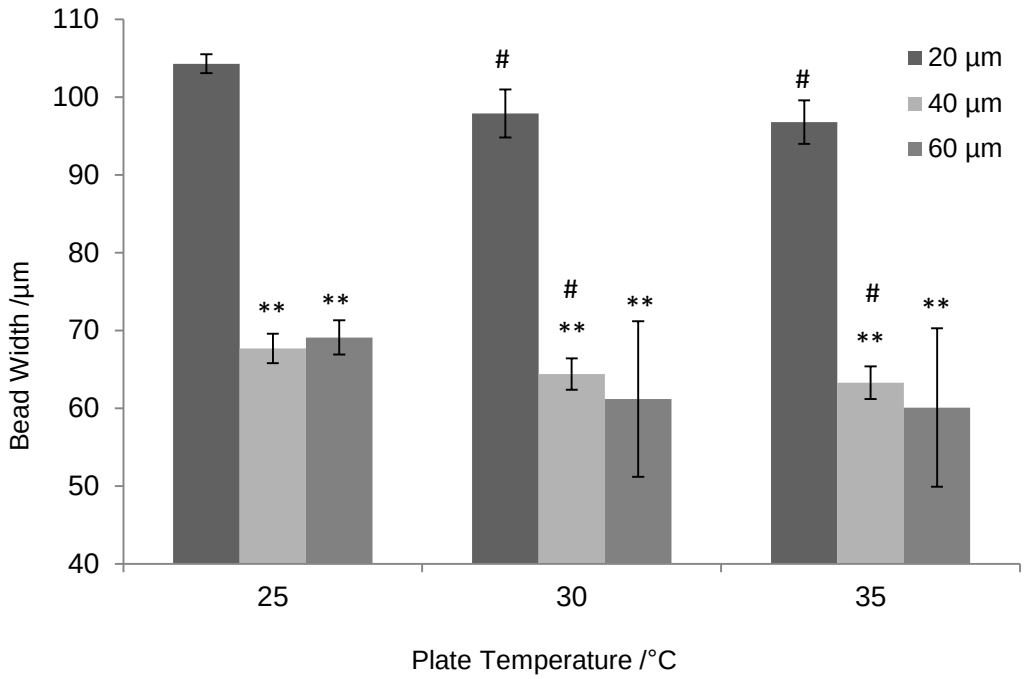

*Figure 4.12: A plot of solidified PCL line width against plate temperature with different printing droplet spacing: 20 µm, 30 µm and 40 µm. (Mean ± Standard Deviation, n=4, compared to line with at 20 µm under the same temperature *p<0.01, **p<0.001, compared to line width at 25°C at under the same droplet spacing #p<0.01, ##p<0.001)*

Microscope images of the lines are shown in Figure 4.11 with the average line widths shown in Figure 4.12. It can be observed that when droplet spacing was 20 µm, considerably wider tracks appeared compared with that seen with 40 µm and 60 µm droplet spacing. The low droplet spacing resulted in highly overlapped droplets and a large volume of ink per unit area. It is likely that the triple line of the deposited droplets was unable to support such a large amount of ink and moved outwards in response. Additionally, the printed track widths were seen to be dependent upon the substrate temperature as well (Figure 4.12).

Stringer J. and Derby B. suggested an equation to help predict the printed bead width as follow (Stringer, J., Derby B., 2010):

$$w = \sqrt{\frac{2\pi d_0^3}{3p(\frac{\theta}{Sin^2\theta} - \frac{\mathrm{Cos}\,\theta}{Sin\theta})}} \qquad \text{Equation 4.2}$$

where w is the bead width, p is droplet spacing, d_0 is droplet diameter, θ is the contact angle. From this equation, it can be concluded that the bead width has a negative correlation with droplet spacing p. The contact angle θ is calculated from the deposited droplet pattern size

As in equation 4.2, Stringer and Derby assumed that the deposited droplet can be treated as a spherical cap (Stringer, J., Derby B., 2010). Based on this assumption and also Deegan R.D. et al.'s (Deegan, R. et al., 1997 and Deegan R. et al., 2000) assumption in investigating coffee ring effects, that the contact line is pinned during evaporation, the contact angle of the deposited droplet can be calculated by determining the droplet volume and radius of the deposited spherical cap (radius of the dried droplet). The volume of spherical cap V can be calculated by the following equation:

$$V = \frac{\pi h(3r^2+h^2)}{6} = \frac{\pi h^2}{3}(3R - h) \qquad \text{Equation 4.3}$$

where V is the volume of the sphere cap, h is the height of the cap, R is the radius of the sphere and r is the radius of the cap (Figure 4.13).

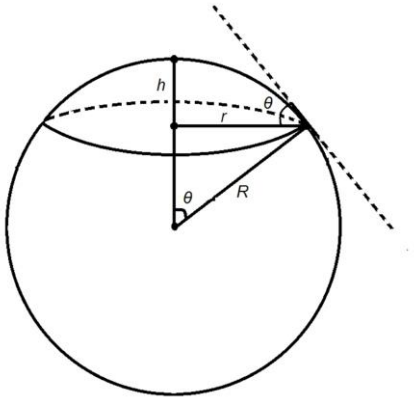

Figure 4.13: Schematic of calculating the contact angle through deposited droplet diameter and droplet volume.

The diameter d_0 of a single droplet can be measured which was about 27µm and the volume of a droplet V equals to:

$$V = \frac{\pi {d_0}^3}{6} \qquad \text{Equation 4.4}$$

The height of the sphere cap h can then be calculating using the following equation:

$$\pi h^3 + 3\pi r^2 h - \pi {d_0}^3 = 0 \qquad \text{Equation 4.5}$$

After which the radius of the sphere can also be calculated as follow:

$$R = \frac{{d_0}^3}{6h^2} + \frac{h}{3} \qquad \text{Equation 4.6}$$

The contact angle θ then equals to:

$$sin\theta = \frac{r}{R} = \frac{r}{\left(\frac{{d_0}^3}{6h^2} + \frac{h}{3}\right)} \qquad \text{Equation 4.7}$$

Table 4.6 shows measurements of measured line widths as a function of temperature and droplet spacing. This was compared with the predictions

based on Stringer J. and Derby B.'s equation. It can be concluded that the 'bead width' has an inverse relationship with droplet spacing *p*. The comparison is reasonable, with differences typically less than 10%. This suggests that this can be a useful guide for manufacturing, allowing the user to predict the line spacing required to achieve reasonable coverage of the substrate, at least within the constraint that the deposited drops are within the range of separate that allow them to merge and form a cylindrical cap.

Table 4.6: Comparison of theoretical printing bead width and actual bead width with different droplet spacing and plateform temperature. (mean ± standard deviation, n=4)

	Average Line Width (μm)					
Substrate Temperature	Droplet spacing (μm)					
	20 μm		40 μm		60 μm	
	Theoretical	Actual	Theoretical	Actual	Theoretical	Actual
25ºC	107.06	104.3±1.2	75.70	69.7±1.9	61.81	69.1±2.2
30ºC	99.58	97.9±3.1	70.41	64.4±2.0	57.49	61.2±10.0
35ºC	85.16	96.8±2.8	60.22	63.3±2.1	49.17	60.1±10.2

Film Formation

PCL films (using 5 wt% PCL solvent based ink) were jetted with 20, 40 and 60 μm droplet spacing while substrate temperatures were set at 25, 30 and 35ºC respectively to investigate the effect of droplet spacing as well as the substrate temperature on PCL film formation. Figure 4.14 shows the optical images observed for films printed under a range of parameters. Regular

structures appear corresponding to the regularity of the tracks. Surface roughness data were collected using white light surface profiling.

It can be seen that for films printed with 20μm droplet spacing, no significant waviness on the surface was observed until the substrate temperature reached 35ºC. This is likely caused by the competition between ink evaporation and merging. When the ink was printed with a 20 μm droplet spacing (~70% overlapping) at 25ºC, the printed ink merged with previously unsolidified ink to form a uniform flat surface. As the substrate temperature increased, the solidification speed also increased. When the printed ink can finish solidification before the next row of ink was jetted, the boundary interface between two rows will appear. (Figure 4.14(g)).

When the droplet spacing was fixed to 40 μm and 60 μm, waviness and boundary interfaces were seen regardless of the temperature. This was because when film samples were printed with 40 μm and 60 μm droplet spacing, the ink volume per area reduced to 26% and 13.5% of the volume at 20 μm droplet spacing respectively. This implies that less volume of solvent per unit needed to be evaporated for solidification, which subsequently reduced solidification time. Therefore the printed PCL tended to form boundaries at the interfaces as the printed ink cannot merge with previously solidified PCL precipitation.

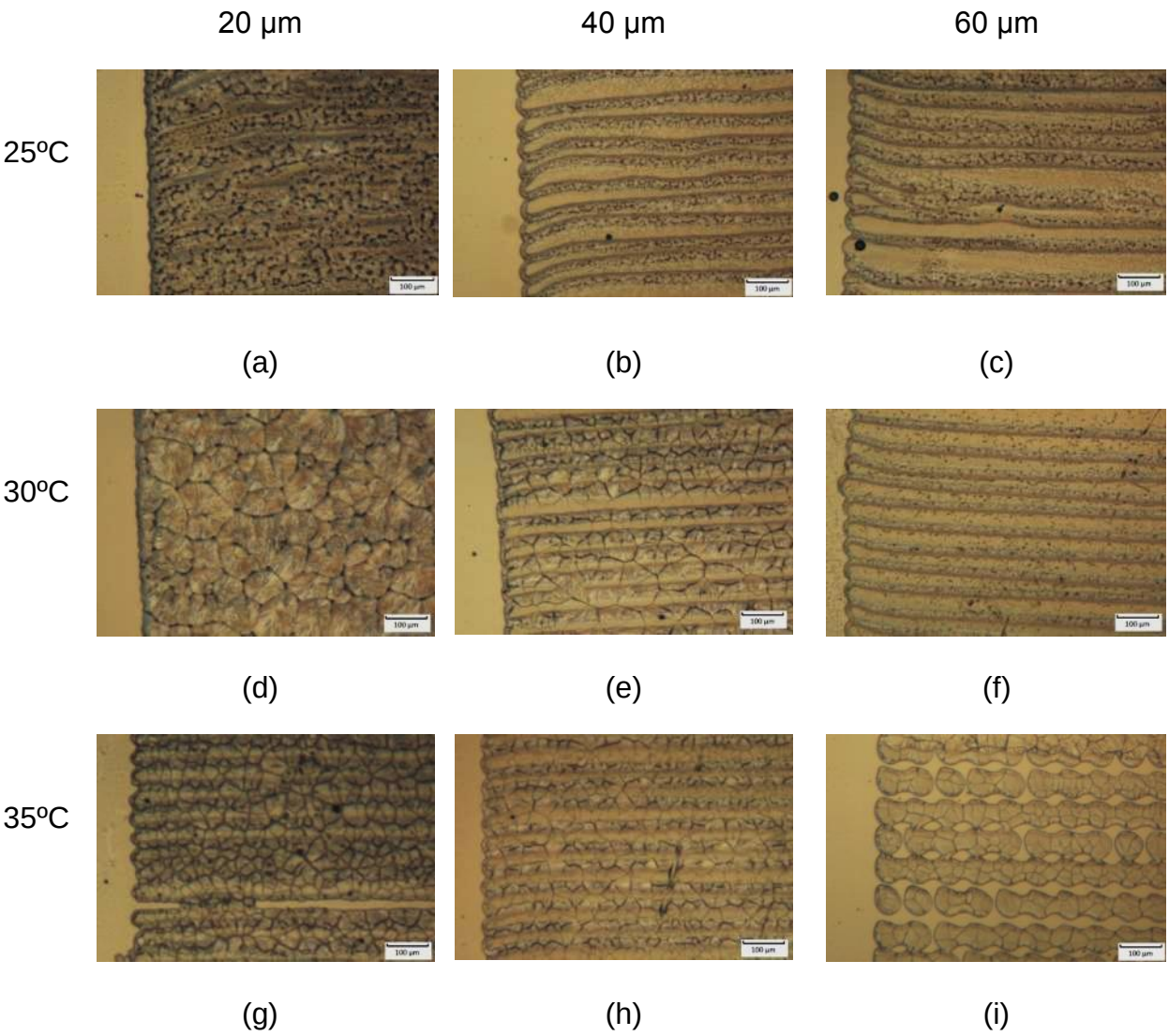

Figure 4.14: Microscopy picture of printed PCL solvent film with different droplet spacings (horizontal row) and substrate temperatures (vertical rows).

These boundaries were observed by both Teichler et al. (Teichler et al., 2011) and Lee et al. (Lee et al., 2011) as mentioned, while they showed different opinions about whether this effect is preferred or not for film printing based on the surface appearance only. Therefore, a quantitative parameter will be helpful to judge the surface quality and in this project, surface roughness was used.

Meanwhile, when the substrate temperature reached 35ºC, nozzle failure started to occur and the droplet became unstable. This is because the nozzles were close to the substrate (1 mm) in order to minimize the air flow influences during droplet flight. This, however, led to the nozzles being heated by the hot substrate, causing the PCL to precipitate around the nozzles and blocking the nozzles. Even though higher substrate temperature is beneficial for solvent removal as well as reducing the chemical residual, with the consideration of printing stability, the substrate temperature needs to be limited. The removal of chemical residuals can also be carried out during post processing in a vacuum oven.

The quality of jetted films under different printing parameters were characterized by measuring ten-point mean roughness value (R_z) through Bruker Contour GT-I. From Table 4.7, it can be noticed that 40 μm droplet spacing with a 30ºC substrate gave the best film quality (both low Rz value and standard deviation). For films printed at 35 ºC with 60 μm, as it did not cover the whole substrate, the R_z value cannot show the real state of the sample's surface roughness, and therefore, it was not included. It can also be noticed that as droplet spacing decreases, the film tends to be less uniform as the standard deviation value of R_z increased significantly.

Table 4.7: Ten-point mean roughness of printed film for 5wt% PCL solvent ink. (mean ± standard deviation, n=4)

Ten-point Mean Roughness value (Rz)			
Substrate Temperature	Droplet Spacing		
	20 µm	40 µm	60 µm
25ºC	0.56±0.25 µm	0.41±0.03 µm	0.39±0.04 µm
30ºC	0.38±0.15 µm	0.27±0.04 µm	0.38±0.03 µm
35ºC	0.46±0.20 µm	0.37±0.07 µm	N/A

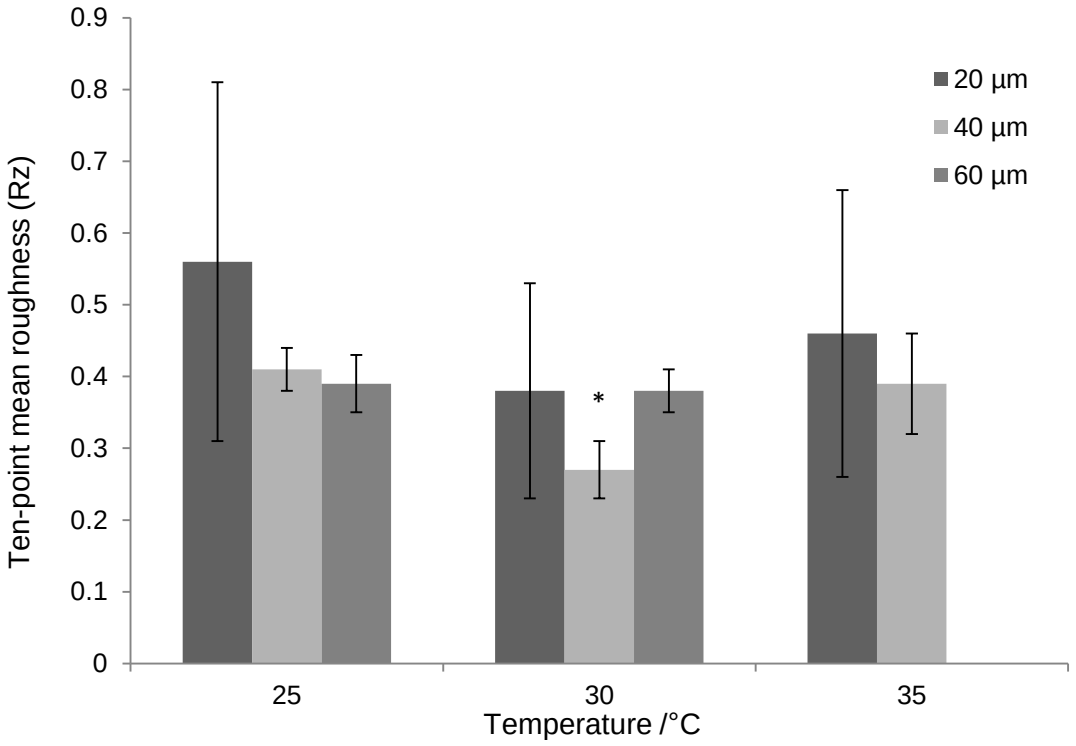

*Figure 4.15: A plot of solidified PCL film surface roughness against plate temperature with different printing droplet spacing: 20 µm, 30 µm and 40 µm. (Mean ± Standard Deviation, n=4, compared to Rz at 25°C, *p<0.01)*

Multi-Layer Printing

Multilayered samples of PCL 5 wt% solvent ink were jetted with 6 m/s droplet velocity (1 mm printing gap), 40 µm droplet spacing as well as 30ºC substrate temperature.

The multilayer samples were characterized using a Talysurf 2000. Figure 4.16 shows the surface profiling result of a printed PCL sample with three different sizes of squares (6×6 mm; 4×4 mm; 2×2 mm). The layer thickness was around 0.6 µm.

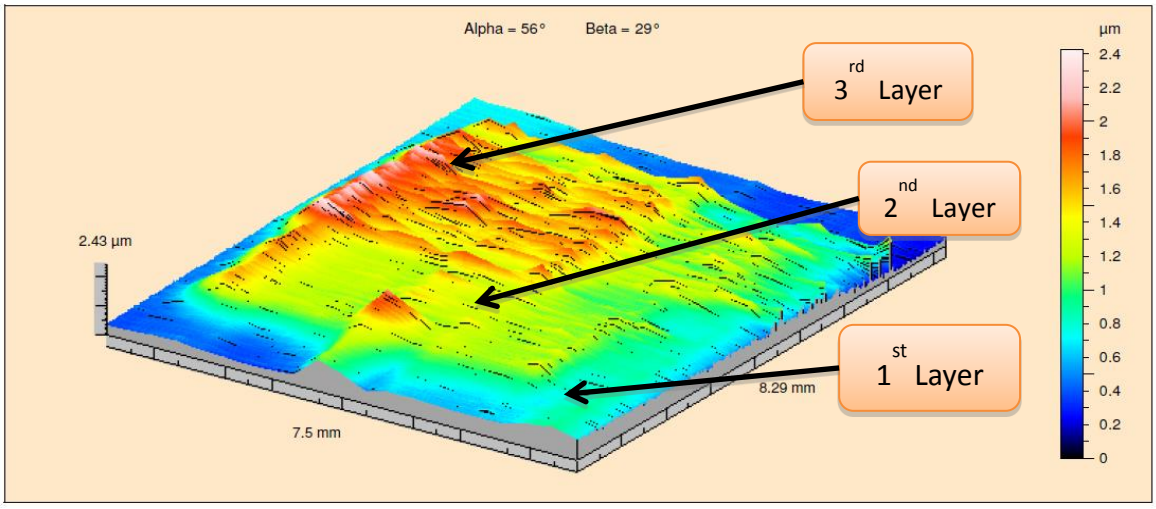

Figure 4.16: Surface profile of a PCL square sample printed at 30ºC substrate with 40 µm droplet spacing.

4.3 Summary

In this study, material jetting was used as a processing method to produce biodegradable Polycaprolactone. It was found that higher Polycaprolactone concentration (10 wt%) can easily cause nozzle blockage due to easier precipitation of PCL at the nozzle plate.

The printing waveform influences the droplet formation. As the time gap of the waveform increases, this showed good correlation with the prediction equation from the work in Kwon et al., (2007). As printing voltage increases, the velocity of droplet will increase.

At droplet deposition stage, it was found that PCL tended to concentrate at the outer rim after solidification due to the coffee ring effect described by Deegan R.D. et al.'s (Deegan, R. et al.,1997 and Deegan R. et al., 2000). Higher substrate temperatures reduced the size of solidified PCL droplet and increased the thickness of solidified PCL deposites. When the droplet velocity was 6m/s, the droplet diameter showed minimum deviation.

During line formation tests, it was found that higher substrate temperature and larger droplet spacing will both cause the printed PCL track width to reduce. The width of the printed track follows the prediction equation given by Stringer, J and Derby B (2010). During film formation tests, films formed at 40 μm and 60 μm droplet spacing manifested wavy patterns on the surface. Higher substrate temperatures made the waviness become more significant. When the substrate temperature reached 35ºC, the ejection from the nozzle started to become unstable. PCL was found to have the best film formation when the droplet speed was 6 m/s with a substrate temperature of 30ºC and a droplet spacing of 40 μm.

It was also found that the printing efficiency of PCL solvent based ink is a potential problem which may restrict its application. Meanwhile as chemical solvents were used, there is a potential of residual solvent, which may influence the biocompatibility and required further study.

Chapter 5: Polycaprolactone UV curing based ink

In Chapter 4, it was shown that a solvent based Polycaprolactone (PCL) ink can be printed through material jetting process. However, there are still obstacles preventing it being used for 3D material jetting. The first challenge is printing stability; solvent inks rely on solvent evaporation to generate solid structures. Therefore, the boiling point of the solvent needs to be sufficiently low to allow solidification to complete within a time frame to support another layer printed on top. This could be accelerated by using a more volatile solvent, but this can be disadvantageous since it may then evaporate at the nozzle, leading to solute precipitation and nozzle clogging. Substrate heating is one of the methods which can be used to help accelerate the evaporation, allowing a less volatile solvent to be used without sacrificing the solidification time. In practice, however, as the printhead is positioned close to the substrate during printing (0.5mm to 1mm), the nozzle surface will be gradually heated up by the hot substrate, which increases the risk of precipitation and of causing nozzle blockage.

The second obstacle for solvent based ink is printing efficiency. Due to viscosity constraints, the volume concentration of the solute is normally restricted to a relatively low level. As shown in the previous chapter, the thickness of each polycaprolactone precipitation layer after evaporation was

around 0.8μm (measured by probe based surface profiling). This might be helpful when making relatively delicate structures with sample height in micrometres or when producing a defined surface coating, but in practice the low concentration prevents it from being used to make 3D objects on the centimetre level or above.

When compared with a solvent-based ink, an ink cured through UV light after being jetted presents more potentials as it can overcome the problems faced when jetting solvent-based inks. UV cured inks mainly consist of acrylated monomers or oligomers, most of which are not volatile and show good stability during jetting. Meanwhile, UV light provides better controllability and creates fewer influences on the printing environment in comparison to heat initiation, which may result in an increase in the environmental temperature, which in turn may deleteriously affect the physical properties that are important for printing.

The main limitations for UV curable inks are that the materials are generally restricted to UV reactive oligomers and the viscosity of some oligomers may be too high to be used for piezo-based jetting. The use of acrylate based polymers and photoinitiators may also increase the chemical residuals, particularly if the reaction is not fully completed, which may affect the product's biocompatibility (section 2.7.2). Therefore, a post-process is usually required to help remove the residual reactant.

UV curable PCL is not a commercially available material, however as mentioned in section 2.7.2, it has been shown that UV curable PCL can be synthesized. Therefore, UV curable polycaprolactone: Polycaprolactone di-

methylacrylated (PCLDMA) was prepared following a similar procedure to that described in literature and the steps were described in detail in section 3.8.2.

5.2 Result and Discussion

5.2.1 Viscosity Assessment and Modification

The viscosity of the pure PCLDMA was measured at two shear rates (100 s^{-1} and 1000 s^{-1}) respectively within a temperature range starting at 25ºC with 5ºC increments up to 60ºC.(Table 5.1 and Figure 5.1). It shows the viscosity for pure PCLDMA is not within the suggested optimum printing range (12 to 18 cp). Therefore, further modification was required to reduce its viscosity down to a printable range.

Table 5.1: Viscosity dependency on temperature of pure PCLDMA in the range 25°C to 60°C.

Temperature (°C)	Viscosity (cp) Shear rate	
	100 s^{-1}	1000 s^{-1}
25	109.77	122.64
30	85.96	96.14
35	68.85	76.96
40	56.15	62.64
45	46.54	51.78
50	38.98	43.28
55	33.06	36.62
60	28.4	31.48

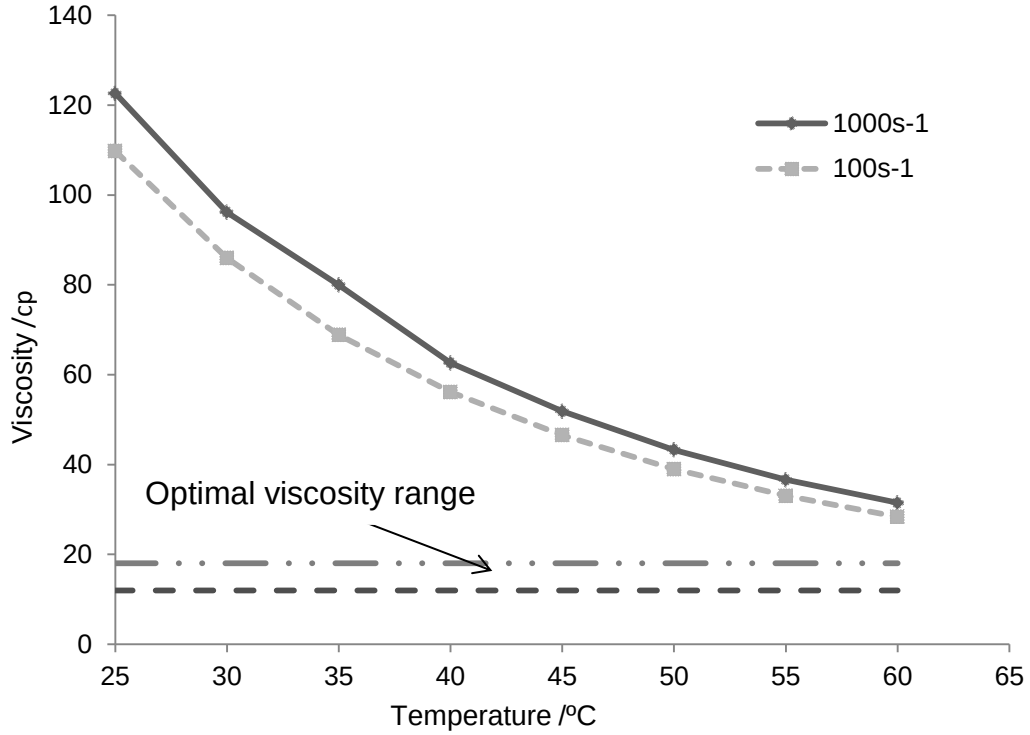

Figure 5.1: The plot of pure PCLDMA viscosity as temperature increased from 25°C to 60°C.

Diluent can be used to reduce an ink's viscosity. This project aims to prepare samples for potential bio-engineering applications; therefore the toxicity should be taken into consideration when choosing materials. Polyethylene glycol diacrylated (PEGDA) can be used as such a diluent. As mentioned in the literature review PEGDA has been widely used for preparing UV curable biocompatible materials (Cuchiara et al., 2010; Hahn et al., 2005; Hahn et al., 2006) which can also modify drug release profiles as PCL is hydrophobic and PEG is hydrophilic (Jette et al., 2004). The viscosity of PCLDMA:PEGDA mixtures with different proportions were measured under the same conditions as pure PCLDMA to look for a suitable composition for printing. As mentioned previously, printing with the DMP-2830 usually requires inks within the viscosity range 12 cp and 18 cp. Meanwhile as PEGDA is a diluent that is bio-

compatible but not degradable, it is necessary to minimize the proportion of PEGDA to maintain the bio-degradability. As a result of these considerations the proportions of PCLDMA:PEGDA were chosen as 70:30 and 80:20. This was further reduced to 70:30 to accommodate viscosity increases when photoinitiator is added.

Table 5.2: Viscosity of varying proportions of PCLDMA: PEGDA mixture in the temperature range 25°C to 60°C. Shear rate was fixed to 100 s^{-1}. (Mean ± Standard Deviation, n=3)

Temperature	PCLDMA:PEGDA					
	50:50	60:40	70:30	80:20	90:10	100:0
25 ºC	33.21±1.01	39.85±1.02	46.58±1.03	58.35±0.97	80.64±1.00	109.77±0.98
30 ºC	26.91±1.00	32.19±0.98	37.47±1.00	46.75±0.96	63.84±0.94	85.96±0.92
35 ºC	22.18±1.02	26.56±0.99	30.80±1.00	38.16±0.97	51.69±0.96	68.85±0.93
40 ºC	18.59±1.00	22.14±1.00	25.67±0.99	31.59±0.98	42.51±0.97	56.15±0.95
45 ºC	15.86±1.02	18.76±1.01	21.63±1.02	26.54±0.99	35.44±0.99	46.54±0.95
50 ºC	13.62±1.02	16.05±1.02	18.50±1.00	22.48±1.00	29.98±0.99	38.98±0.97
55 ºC	11.83±1.02	13.86±1.01	15.98±1.02	19.25±1.02	25.59±0.99	33.06±0.99
60 ºC	10.40±1.01	12.12±1.03	13.98±1.03	16.70±1.01	22.06±1.00	28.40±0.97

Table 5.3: Viscosity of varying proportions of PCLDMA: PEGDA mixture as the temperature is increased from 25°C to 60°C, shear rate was fixed to 1000 s^{-1}. (Mean ± Standard Deviation, n=3)

Temperature	PCLDMA:PEGDA Proportion					
	50:50	60:40	70:30	80:20	90:10	100:0
25 ºC	35.85±1.03	43.14±1.02	49.71±1.02	63.09±1.04	87.81±1.00	122.64±0.98
30 ºC	29.22±1.00	34.97±1.00	40.07±0.97	50.45±0.98	69.68±0.95	96.14±0.92
35 ºC	24.44±1.01	29.00±0.98	33.00±0.99	41.25±0.96	56.47±1.00	76.96±0.93
40 ºC	20.90±1.00	24.44±1.00	27.58±1.00	34.21±0.99	46.45±0.99	62.64±0.94
45 ºC	18.24±1.02	20.99±1.00	23.41±1.01	28.81±0.98	39.15±0.98	51.78±0.97
50 ºC	16.18±1.02	18.33±1.03	20.15±1.03	24.51±1.00	33.05±0.99	43.28±1.00
55 ºC	14.56±1.02	16.25±1.02	17.60±1.03	21.14±0.99	28.24±1.01	36.62±1.00
60 ºC	13.30±1.02	14.65±1.02	15.63±1.03	18.84±0.99	24.48±1.00	31.48±1.00

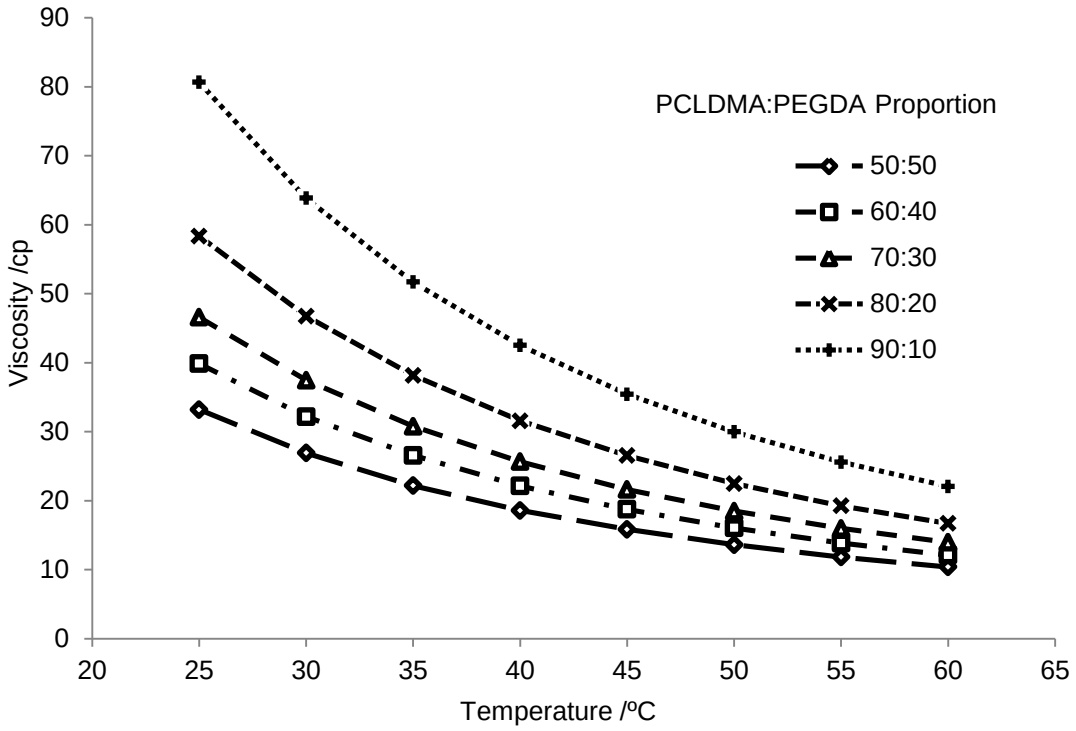

Figure 5.2: Viscosity of varying proportions of PCLDMA:PEGDA mixtures as the temperature increased from 25°C to 60°C, shear rate was fixed at 100s^{-1}.

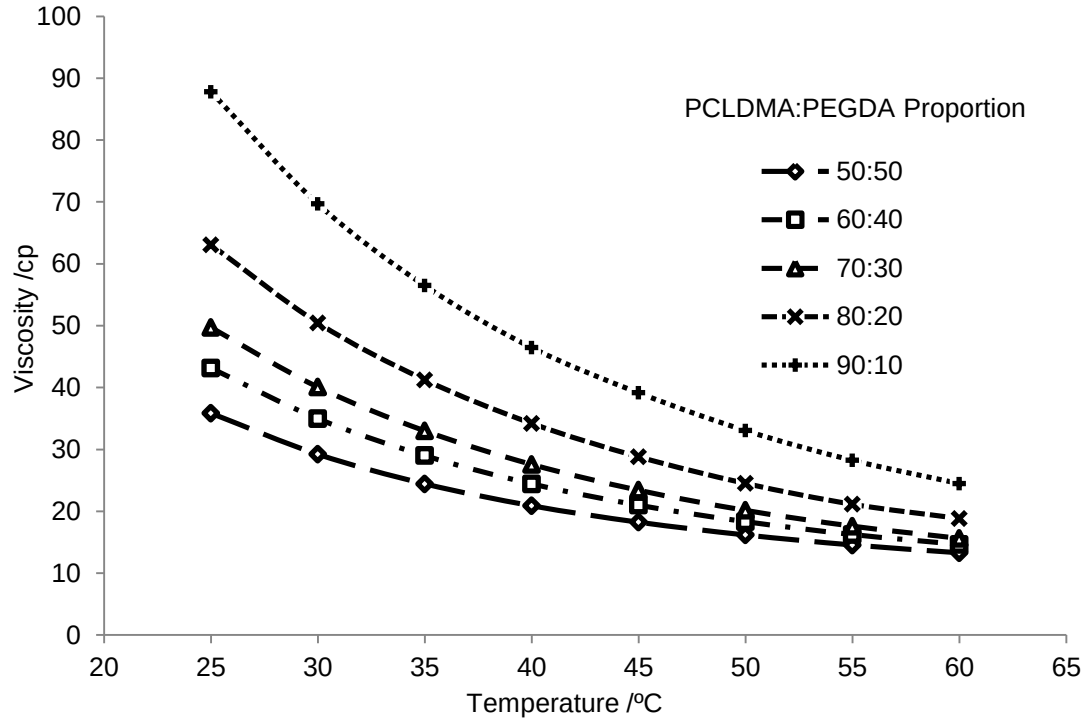

Figure 5.3: Viscosity of varying proportions of PCLDMA: PEGDA mixtures as the temperature increased from 25°C to 60°C, shear rate was fixed at 1000s^{-1}.

5.2.2 UV Curing Assessment and Modification

The photoinitiator is another key component for UV curable ink preparation. Irgacure 2959 (a type I photoinitiator, BASF) is a relatively bio-safe UV initiator that has been widely used in bio-engineering fields to prepare photo-crosslinked structures (Nicodemus and Bryant, 2007; Albrecht et al., 2005; Leach and Schmidt, 2005; Ovsianikov et al., 2011; Fedorovich et al., 2009). In order to perform a preliminary curing check, PCLDMA and PEGDA were mixed with a predefined composition and with different initiator concentrations (1 wt%, 2 wt%, 3 wt%). 10 µL of the prepared reactants was deposited onto pre-cleaned glass slides and illuminated with the Dimatix UV curing unit (λ=365 nm) for 1 minutes. The initial curing check showed that no solid was formed and the droplets were maintaining a liquid state after UV illumination.

Oxygen inhibition was considered as a possible effect that could prevent curing. It has previously been found that inhibition normally happens on a sample's top surface and the inhibited depth was usually limited to 10 µm to 15 µm when curing reaction was carried out in an ambient air environment (Gauthier et al., 2005; Schwalm, 2006). The skin depth is much smaller than the droplet diameter deposited by pipette, therefore, the oxygen in the environment should only inhibit the reaction on the deposited droplet surface and the inner part should be able to cure. However, as the deposited droplet was not cured at all, the inhibition may be introduced by pre-dissolved oxygen in the ink. A protocol to purge nitrogen through the ink was adopted to remove pre-dissolved Oxygen (Zhang et al., 2001; Juszczak and Friedman, 1999). The nitrogen was purged through prepared inks for 15 minutes to help expel

dissolved Oxygen and then curing trials were repeated. It was found that all these deoxygenated inks were fully solidified.

Following confirmation that the solidification reaction can proceed under UV illumination, the ink (with 3 wt% of Irgacure 2959) was placed into a Dimatix 10pl cartridge to run a jetting trial. One layer of ink was printed onto a pre-cleaned glass slide and illuminated with the Dimatix's UV unit. However, it was found that the deoxygenated ink with Irgacure 2959 did not cure after jetting. The printed layer was illuminated by the same UV curing unit for another 1 and 2 minutes, but the printed ink layer still remained liquid.

With the consideration of droplet size and film thickness formed during jetting, oxygen inhibition was identified as a possible reason for this failure. Although the ink cured after being deposited by a pipette, the jetted droplet the size is around 10 pl (Figure 5.4(a)). The printed droplet therefore has a very high surface area to volume ratio, and it is likely that Oxygen can penetrate throughout the droplet. Further, after a droplet was deposited on to a substrate, it spreads into a thin film (as depicted in Figure 5.4(b)), the thickness of which was typically 8 μm. Therefore, a large surface area was exposed to the Oxygen in the environment and it could diffuse into almost the whole printed ink again, inhibiting the reaction.

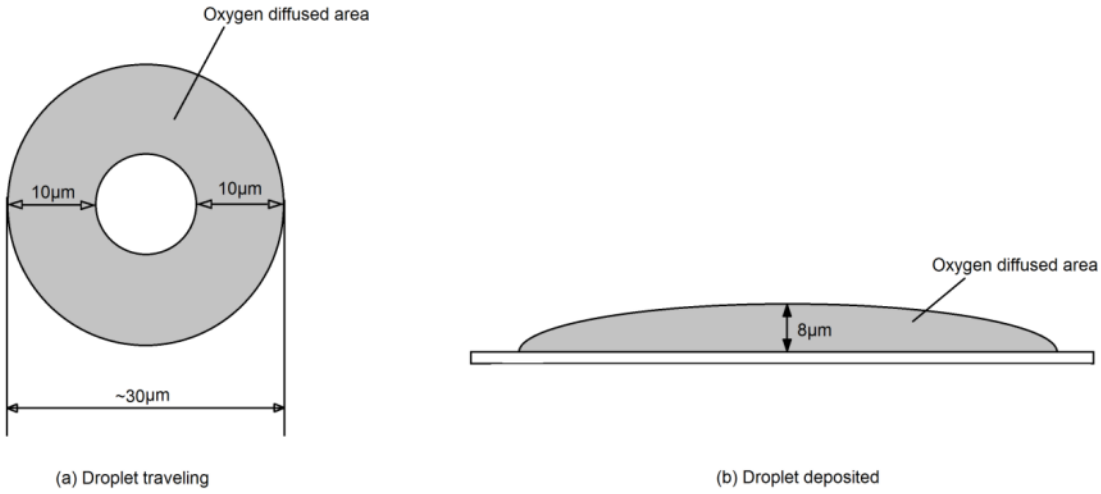

Figure 5.4: Schematic of Oxygen diffused area for droplet (a) travelling through the printing gap and (b) deposited onto the substrate.

Proposed methods to overcome the Oxygen inhibition (as mentioned in Section 2.6.3) includes:

- Increase of photoinitiator concentration
- Increase UV intensity
- Use of an inert atmosphere for printing
- Use Type II photoinitiator

Increasing the photoinitiator concentration aims to increase the concentration of excited free radicals per unit time. As Oxygen inhibits the curing reaction by reacting with the excited photoinitiator free radicals, a rise in the excited free radical concentration would theoretically provide more survivors after oxidation and then initiate the curing reaction. Therefore, 5 wt% of Irgacure 2959 was dissolved into PCLDMA: PEGDA mixture and deoxygenated with nitrogen. However, no solidification was observed after jetting. Meanwhile, Irgacure 2959 precipitation was found after the ink was settled overnight.

Therefore, increasing the photoinitiator concentration was not likely to overcome the inhibition for jetting.

Similarly, increasing UV intensity was another way to increase the concentration of excited free radicals per unit time, but in this case the intensity of the UV LED unit was already maximal. As a result, increased UV intensity was also not a way forward.

As a consequence, the two remaining methods; use of inert atmosphere and changing to a Type II initiator, were developed in parallel. .

As mentioned in Section 2.6.2, type I photoinitiators are cleavage type photoinitiators whereas type II photoinitiators (PI) are H-abstraction initiators. Due to this, type II PIs need to be coupled with accelerators (synergists), which work as hydrogen donators. Accelerators can also act as Oxygen scavengers after excitation to protect photoinitiators from being oxidized. Benzophenone (ReagentPlus, 99%, Sigma-aldrich), is one of the most typical type II photoinitiator and was purchased together with an amine based accelerator. 3 wt% of both Benzophenone and amine based accelerator was added into a PCLDMA: PEGDA mixture and deoxygenated with nitrogen. The ink droplet deposited by the pipette fully solidified after UV illumination. Following jetting and UV illumination trials, it was observed that the printed film partially cured and a soft gel was formed in an air environment. These trials showed that a type II photoinitiator can help overcome Oxygen inhibition when jetting in air environment, but since only a soft gel could be formed it was concluded that the UV unit attached on the printing unit cannot provide enough energy for a printed sample to be fully cured. As a consequence a

more efficient photoinitiator with better absorbance at the available UV unit wavelength (365 nm) was sought.

4-(Dimethylamino) Benzophenone (98%, Sigma-Aldrich), was selected as an alternative photoinitiator since its absorbance wavelength sits in a range between 320 nm and 420 nm, and the UV light absorbance at 365 nm is at least 18 times higher than that for Benzophenone (as shown in Figure 5.5). PCLDMA:PEGDA ink with 3 wt% of both 4-(Dimethylamino) Benzophenone and an amine based accelerator were prepared and solidification trials were conducted using both pipette and printer. It was found that an ink with 3 wt% of both 4-(Dimethylamino) Benzophenone and accelerator were able to be successfully solidified.

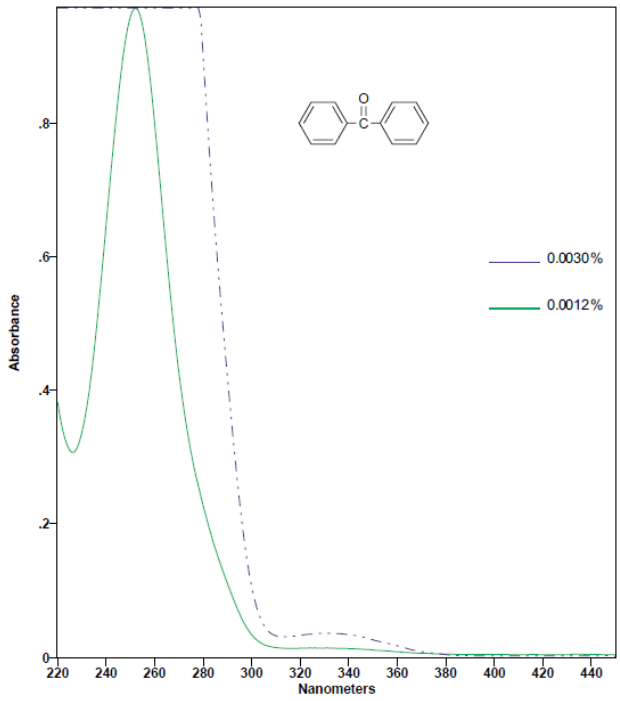

(a)

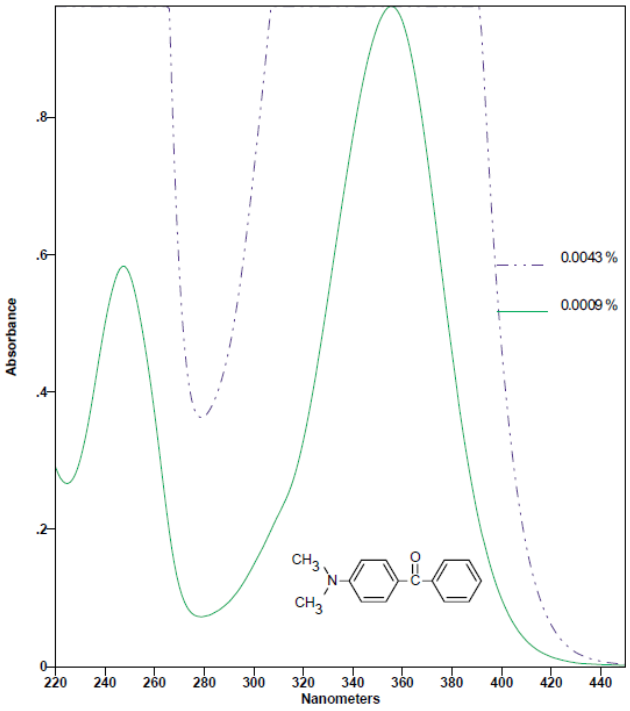

(b)

Figure 5.5 Absorbance spectrum of (a) Benzophenone and (b) 4-(Dimethylamino) Benzophenone (Aldrich, 2014)

Through a range of trials with different type I and type II photoinitiators, it was confirmed that type II initiators were more effective and enabled curing during jetting in an air environment. In the meantime, when the UV intensity of the curing unit was limited, choosing a photoinitiator with higher absorbance at 365nm could be used as an alternative way of increasing UV intensity.

Although the combination of 4-(Dimethylamino) Benzophenone and amine seems to be an effective photoinitiator system for jetting in an air environment, the safety of using 4-(Dimethylamino) Benzophenone and amine became another issue for final application. 2,4-diethylthioxanthone (DETX) and Ethyl 4-(dimethylamino) benzoate (EDB) (≥99%, Sigma-Aldridch) were located as a safer type II photoinitiator system, both of which were not recognized as

hazardous from the safety datasheet. Meanwhile, DETX shows suitable absorbance (Figure 5.6) at 365nm.

3 wt% of both photoinitiator (DETX) and accelerator (EDB) were used to prepare a PCLDMA:PEGDA trial batch, which fully solidified in both pipette deposition and jetting trials.

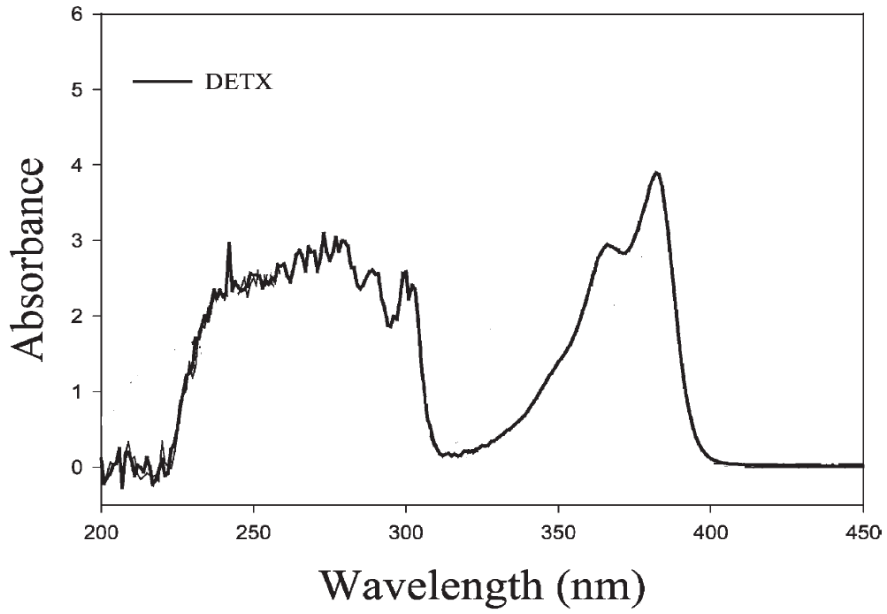

Figure 5.6: Absorbance spectrum of DETX (modified from Cho et al., 2003)

After a range of photoinitiator assessments with different kinds of type I and type II initiators, DETX and EDB were chosen for future experiments. Oxygen removal was also recognized as an indispensable procedure for maximising the effect of UV ink reactivity.

5.2.3 Printability Assessment

In section 5.2.1, PCLDMA: PEGDA with a ratio of to 70:30 was chosen as the composition to be used for jetting between 50°C and 60°C. Measurements

were made with the reformulated inks (Table 5.4 and Table 5.5) to confirm that they remained within the optimum printing viscosity range.

Table 5.4: Viscosity monitoring of PCLDMA: PEGDA=70:30 sample with 3 wt% of both DETX and EDB in the temperature range of 50 ºC to 60 ºC. Shear rate was fixed at 100s^{-1}. (Mean ± Standard Deviation, n=3)

Temperature	PCLDMA:PEGDA=70:30	
	Without PI and AC	With PI and AC
50 ºC	18.50±1.00	19.61±0.78
55 ºC	15.98±1.02	17.80±0.98
60 ºC	13.98±1.03	15.95±1.05

Table 5.5: Viscosity monitoring of PCLDMA: PEGDA=70:30 sample with 3 wt% of both DETX and EDB in the temperature range 50 ºC to 60 ºC. Shear rate was fixed to 1000s^{-1}. (Mean ± Standard Deviation, n=3)

Temperature	PCLDMA:PEGDA=70:30	
	Without PI and AC	With PI and AC
50 ºC	20.15±1.03	20.44±1.02
55 ºC	17.60±1.03	18.35±1.01
60 ºC	15.63±1.03	16.57±1.02

The surface tension of the chosen ink was then measured at both room and printing temperature (60°C). and the printing indicator was calculated through equation 2.1 (Ainsley, 2002). It was found that the printing indicator of the ink at 60 ºC was 1.56, which was within the theoretical printing range (Table 5.6).

Table 5.6: Physical properties and printing indicator value of PCLDMA: PEGDA (70:30) mixture at temperature of 25ºC and 60 ºC

Temperature	Nozzle Diameter (µm)	Density (g/cm^3)	Viscosity (cp)	Surface Tension (mN/m)	PI (Oh^{-1})
25 ºC	21	1.08	51.61	37.26	0.56
60 ºC	21	1.08	17.55	32.31	1.56

As the ink's viscosity and surface tension were both within the suggested range, a standard waveform suggested by Fujifilm Dimatix was used (shown in Figure 5.7). A stable single droplet formation was achieved with the standard waveform at 60°C with 24 V jetting voltage.

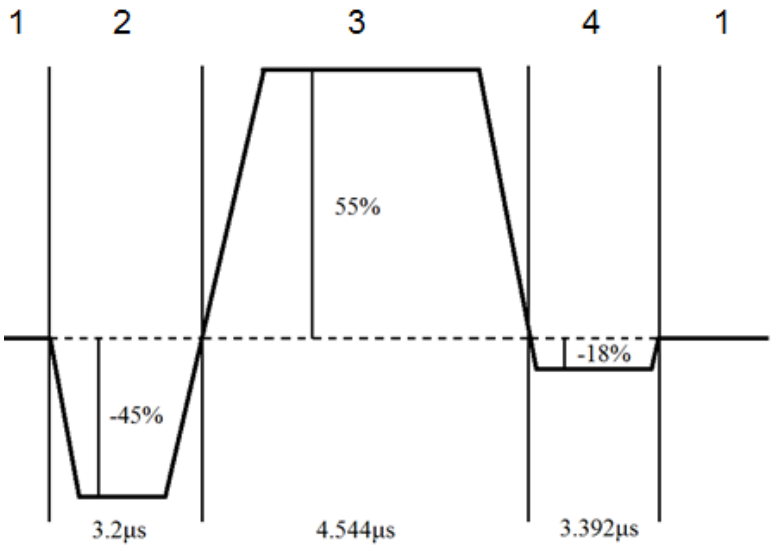

Figure 5.7: Preformed waveform used for PCLDMA: PEGDA ink printing.

5.2.4 3D Structure Printing Trials

Mesh structures were printed with PCLDMA:PEGDA ink (3 wt% photoinitiator and accelerator respectively); a schematic figure of the printing pattern is shown in Figure 5.8(a). Meshes with three different wall thicknesses (150 µm, 300 µm and 500 µm) were printed onto glass slides for further SEM examination. The distance between each wall was set to 1 mm to allow each printed vertical or horizontal wall to be seperated from each other. Ten layers of PCLDMA:PEGDA (70:30) were printed and the sample appearance is shown in Figure 5.8(b).

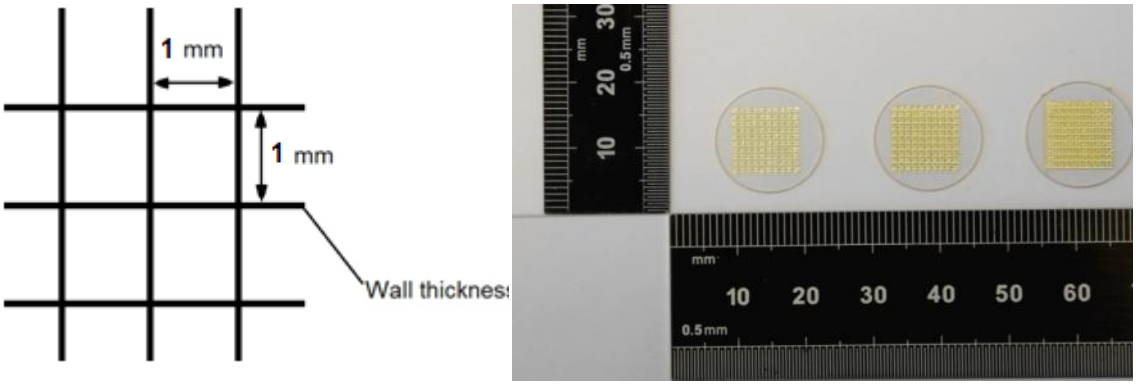

(a) (b)

Figure 5.8: Printed mesh samples for checking processing accurancy (a) Schematic digram of printing pattern design (b) printed sample.

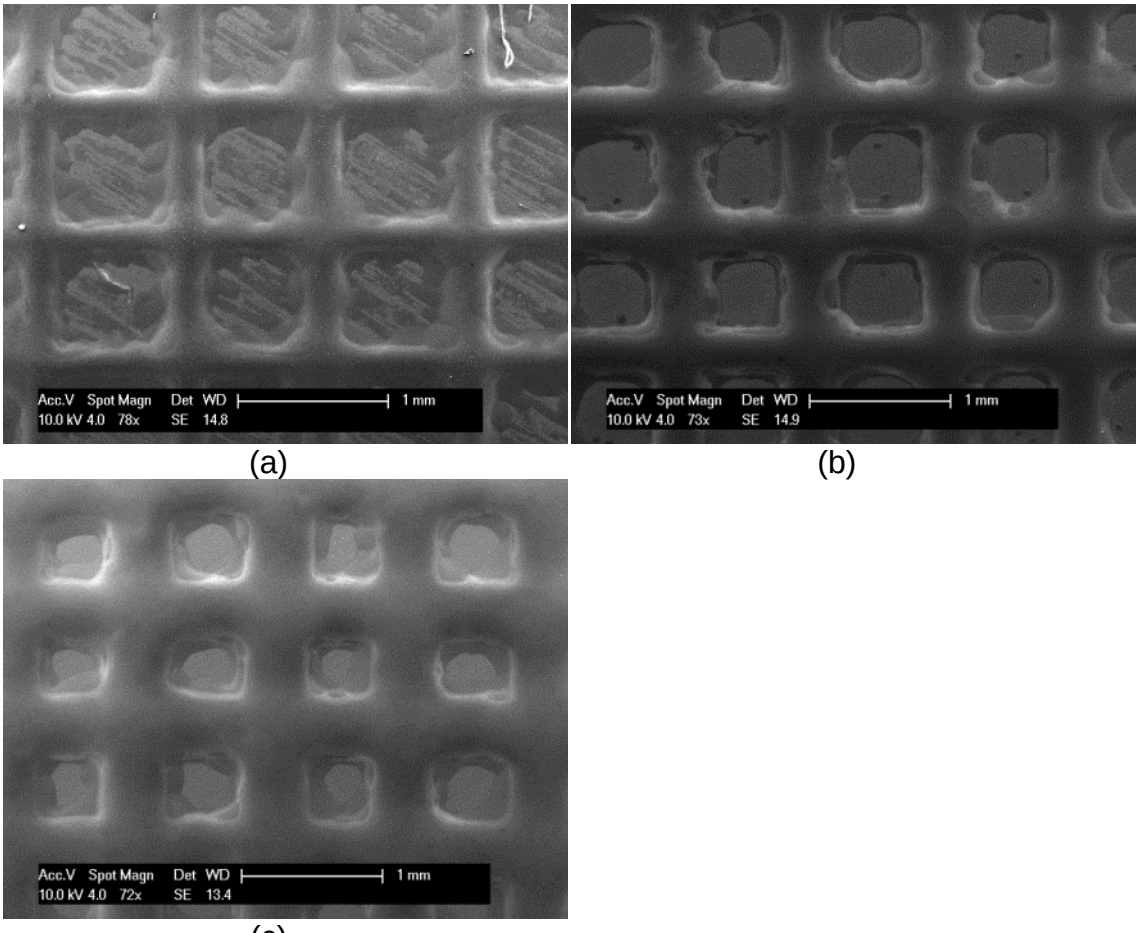

(a) (b)

(c)

Figure 5.9: SEM pictures of printed mesh structure with different wall thickness: (a) 150 μm, (b) 300 μm, (c) 500 μm.

Figure 5.9 showed that the PCLDMA:PEGDA (70:30) ink could not form a precise shape during printing. Rectangular gaps were designed inside the mesh structure. However in the actual printed structure, the gaps became rounded rectangular shapes. Meanwhile, curving walls were also observed in the SEM pictures. These may be due to the slow curing speed of the printed ink. Although, the ink was illuminated by UV light immediately after being printed, the illumination time was still limited due to the UV unit being attached and moving with the printhead. So the exposure time or the energy received by the printed ink in a single swipe was limited to the duration of the pass and may not be sufficient to allow freshly deposited ink to become fully cured. Therefore, merging and dislocation of the uncured ink could happen due to gravity, movement of the platform and merging with the ink deposited in subsequent printing cycles. All these can lead to rounding of the walls.

The printed ink can receive extra swipes UV illumination during the printing of a subsequent ink layers. So the printed ink can receive additional UV illumination and eventually cure if it obtains enough energy, though likely with a longer curing time than constant UV illumination.

Increasing the curing speed could help printed ink solidify in a shorter period of time, hence reducing the chance of ink dislocation and improving the sample quality. This could be achieved by increasing the intensity of UV illumination or printing in an oxygen free environment, both of which can accelerate the curing speed.

Figure 5.10 is a printed curving mesh structure with PCLDMA:PEGDA (70:30) ink. Fifty layers were printed and surface profiling data Figure 5.10(d) showed

the total height of the structure was around 250μm. Figure 5.11 shows optical microscope images of this structure. Similar effects were also observed as the ink droplets, which were supposed to be deposited onto the pattern's edge, slipped down to the substrate forming coarse structures at the base. This problem could be solved by increasing curing speed or printing support material around the pattern to restrict the movement of uncured ink, and therefore increase the sample quality. However, this will require printers with multiple printheads, to print different materials respectively.

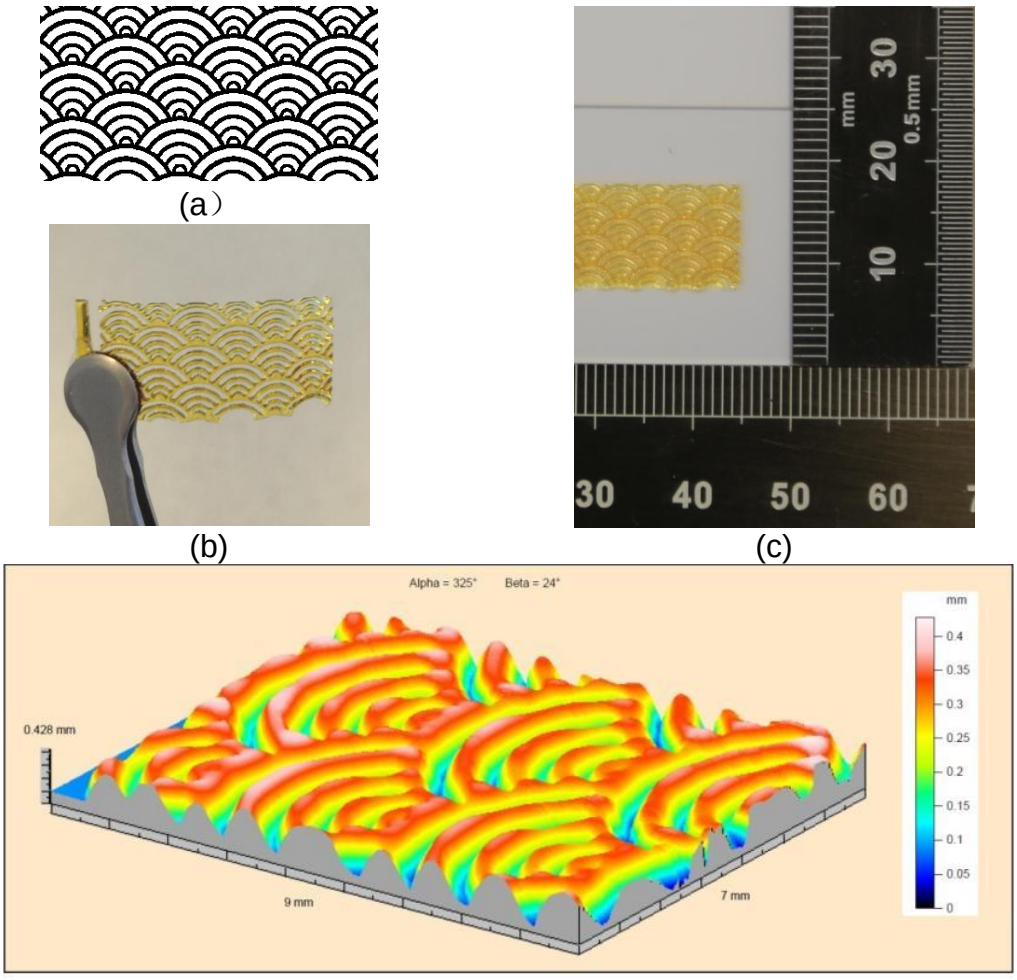

Figure 5.10: Curving mesh structure printing: (a) Printing pattern, (b) Sample appearance after taking off from glass slide, (c) Top view of printed sample, (d) Surface profiling of printed curving mesh structure.

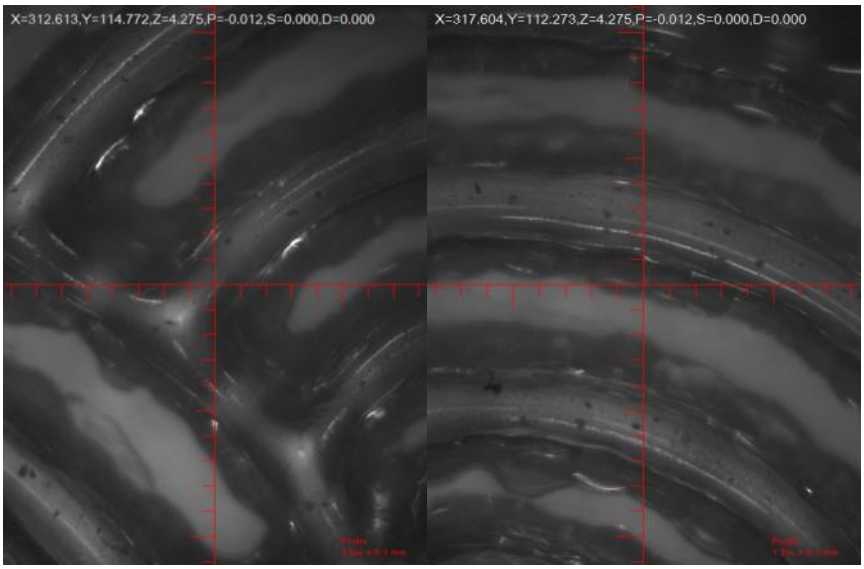

Figure 5.11: Microscopy pictures of printed curving mesh (1 division=100μm)

5.2.5 Real-time Curing and Post-Curing in Different Printing Environment

The effect of different processing strategies were investigated by comparing the mechanical properties of samples using nano-indentation. Square specimens, 5 mm × 5 mm, were prepared for nano-indentation. The intended pattern and the appearance of samples printed to 100 layers in an air environment are shown in Figure 5.12. The final thicknesses of these square samples were ~700 μm.

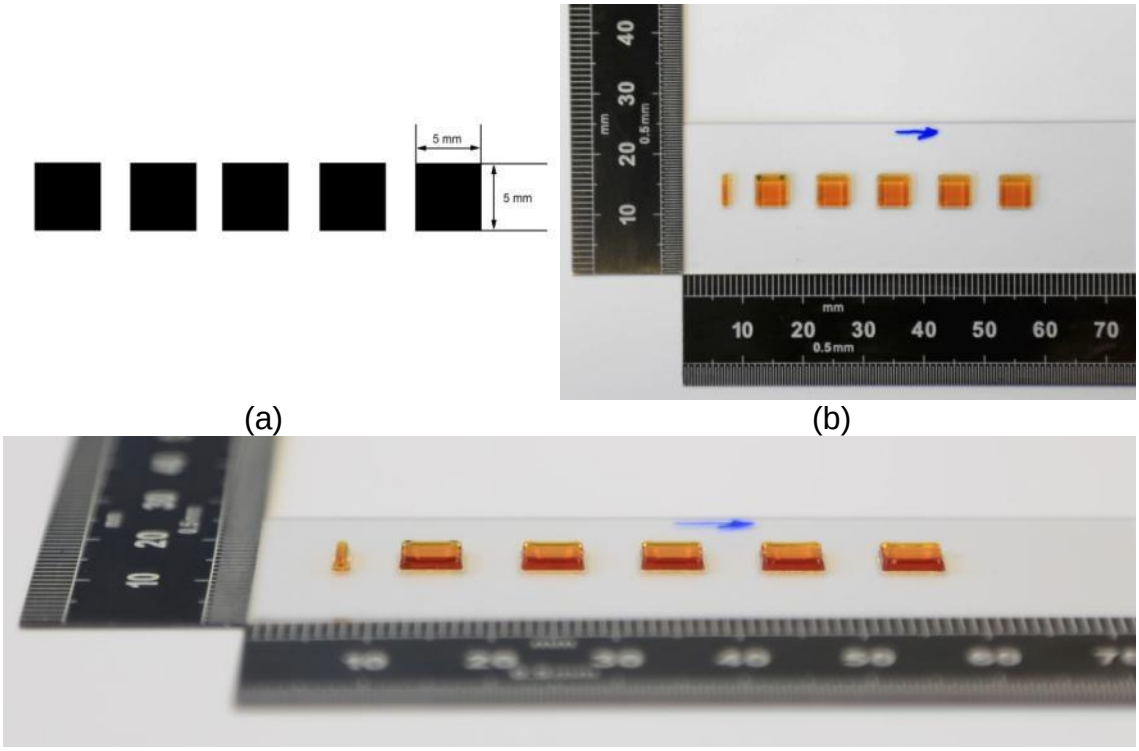

Figure 5.12: Printed square samples for nano-indentation test: (a) Printing pattern, (b) Top view of printed square samples, (c) Side view of printed square samples.

The printed samples were also illuminated by UV light (100 mW/cm^2, 365 nm) from above to provide extra curing after the solid samples were produced. Post-curing (via extra UV illumination) is a procedure to help eliminate the unreacted acrylate and photoinitiators inside the fabricated sample, and can therefore reduce the concentration of residual chemicals and potentially improve the biocompatibility of the sample. In addition, further curing can also help increase the mechanical properties.

Samples were illuminated with UV light for 0, 30, 60 and 90 minutes respectively in order to investigate if post-curing promote further crosslinking in the printed samples. These samples were then vertically mounted in epoxy and polished to expose their cross-section for nano-indentation (as shown in

Figure 5.13). The reason for carrying out mechanical property characterization through the cross-section is that curing variation potentially exists through the cross-section due to the processing sequences (Chen et al., 2015). As the square samples were printed layer by layer from the bottom to the top, previously printed layers will still be exposed to UV when the subsequent layers are printed. This will lead to the materials at the bottom having longer cumulative UV exposure compared with those in the uppermost layers. As the curing is directly related to the amount of UV exposure, it is supposed that bottom layers have more complete curing than top layers, which normally manifests itself in a variance in the mechanical properties (Clay et al., 1995).

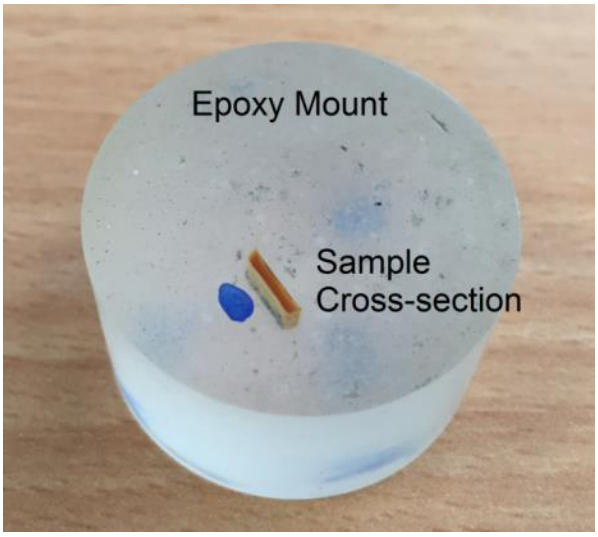

Figure 5.13: Example of printed square sample mounted into epoxy and polished for cross-sectional property characterization.

Nano-indentation was carried out as shown in Figure 5.14. The max loading and unloading force was set to 5 mN with a rate of 0.25 mN/s. Each indentation point was set 50 μm away from the others. For each column, 13 points were set for each column of indentation to cover the whole cross-

section. This indentation was repeated and each testing column was 50 μm away from the previous one.

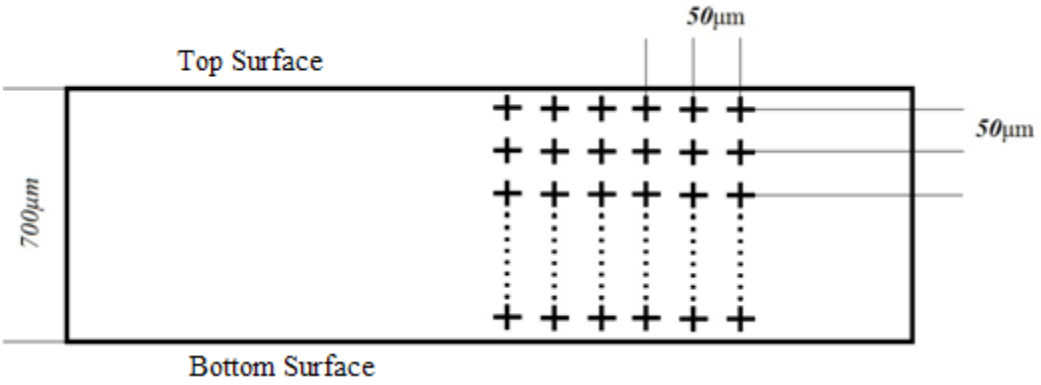

Figure 5.14: Schematic diagram of nano-indentation test method.

Both hardness and indentation modulus were measured and shown in Figure 5.15 and 5.16. The observed differences in hardness did not show a specific trend with post-curing time. Another observation was that the measurements close to the edge consistently showed a higher value than the other points in the middle of the sample. As the sample with no post-curing shows the same trend as well, this suggest that post-curing did not introduce any further crosslinking, which is conflict with previous hypothesis that bottom layers could show more curing due to longer UV exposure time.

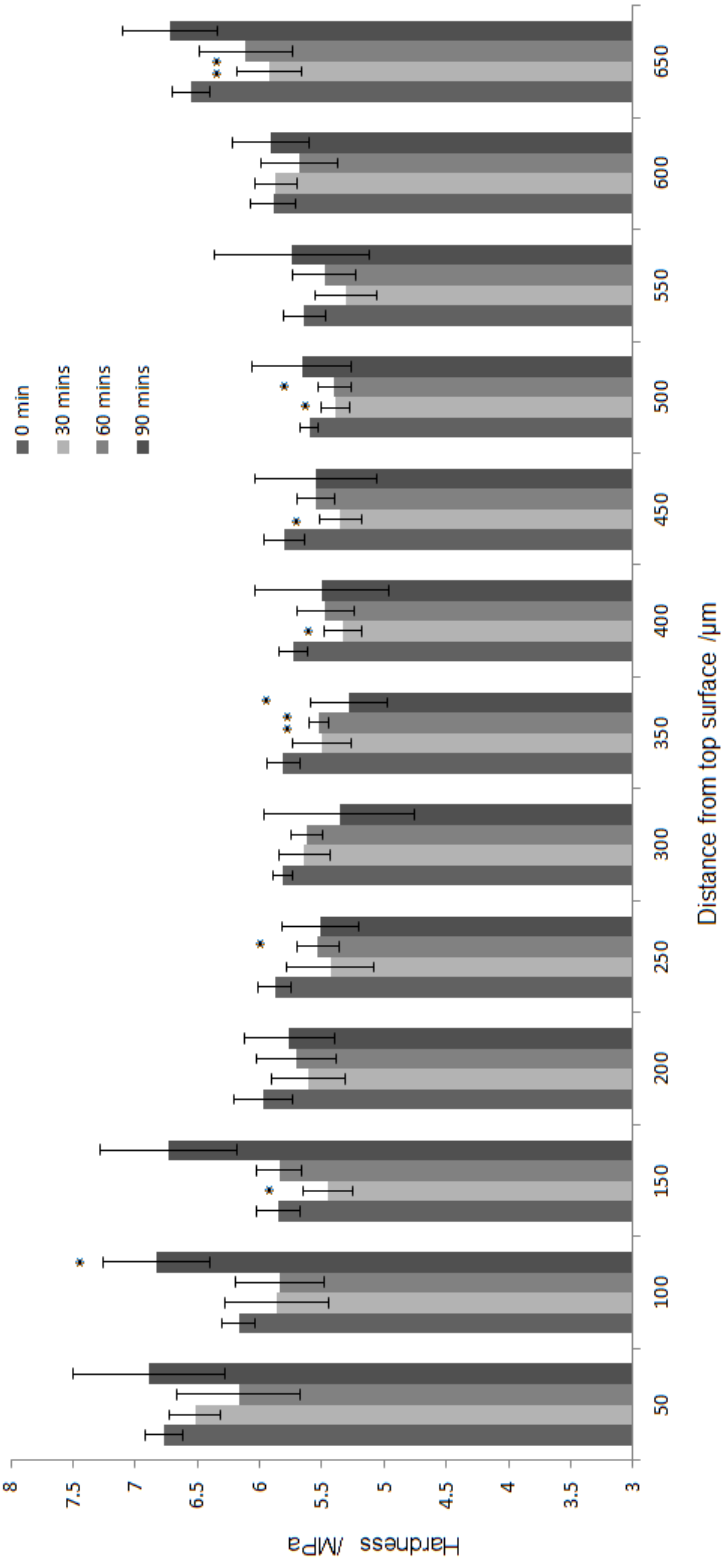

*Figure 5.15: Hardness distribution through the cross-section of printed square sample with different post-curing time. (Mean ± Standard Deviation n=6, compared with no post curing *p<0.01, **p<0.001)*

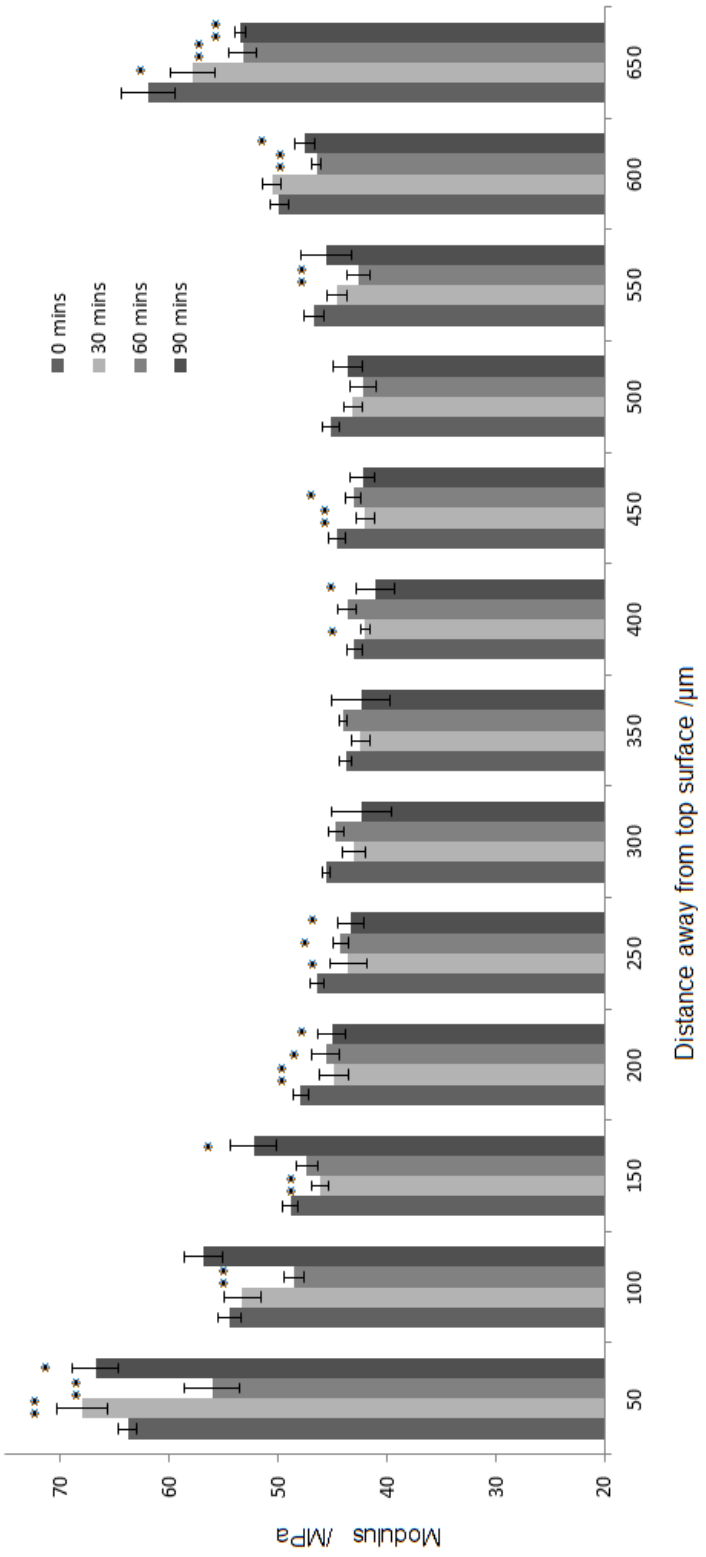

*Figure 5.16: Modulus distribution through the cross-section of printed square sample with different post-curing time. (Mean ± Standard Deviation n=6 compared with no post curing, *p<0.01, **p<0.001)*

An explanation of this conflict is that the measured results at top and bottom surfaces (which were also the interface between printed sample and mounting epoxy as shown in Figure 5.13) were influenced by the mounting epoxy materials. As epoxy has higher hardness comparing with printed samples, the measurement near the interface may manifest higher values. Chen et al. (Chen et al. 2014) investigated this effect. The stress field under the testing point at interface was simulated, which shows that the stress field created by the indenter will go across the interface and enter the mounting material region, which will then influence the measurement.

As the measured properties near the upper and lower surfaces were supposed to be affected by the much stiffer surrounding epoxy used to mount the sample, the indentation was, instead, performed only on the printed samples' top and bottom surfaces without mounting it into epoxy. Indentation tests were carried out on both surfaces on a 5×5 grid with indentations 100μm apart from each other following the sample protocol used before. The hardness and indentation modulus were measured and shown in Table 5.7.

Table 5.7: Hardness and indentation modulus for printed PCLDMA:PEGDA (70:30) with 3wt% of both photoinitiator and accelerator before and after post-curing in an air environment. (Mean ± Standard Deviation n=50)

Curing Time		Hardness (MPa)	Indentation Modulus (MPa)
Top Surface	0min	5.01±0.42	32.28±3.99
	10mins	6.13±0.08	71.97±1.47
	20mins	6.27±0.09	72.17±1.04
	30mins	6.01±0.14	70.2±1.78
Bottom Surface	0mins	4.84±0.44	28.44±1.87
	10mins	5.07±0.20	34.90±1.27
	20mins	5.09±0.19	35.01±1.84
	30mins	5.75±0.08	39.88±2.01

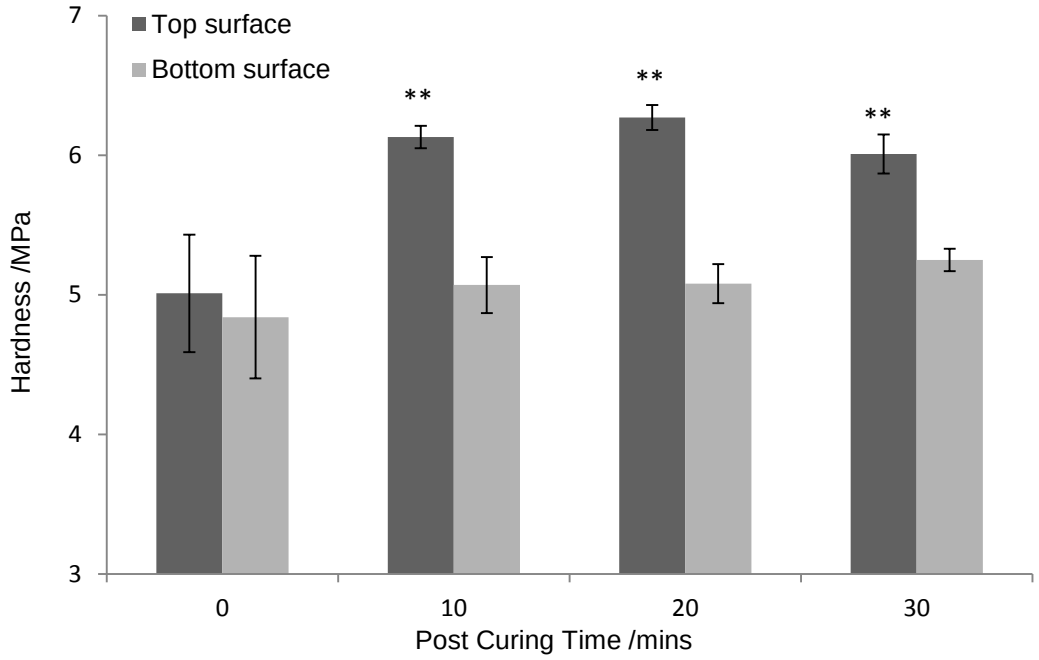

*Figure 5.17: Hardness of the top and bottom surface of the square samples printed in an air environment after different period of post-curing using PCLDMA:PEGDA (70:30) (3wt% of both photoinitiator and accelerator, Mean ± Standard Deviation n=50, compared with no post curing, *p<0.01, **p<0.001).*

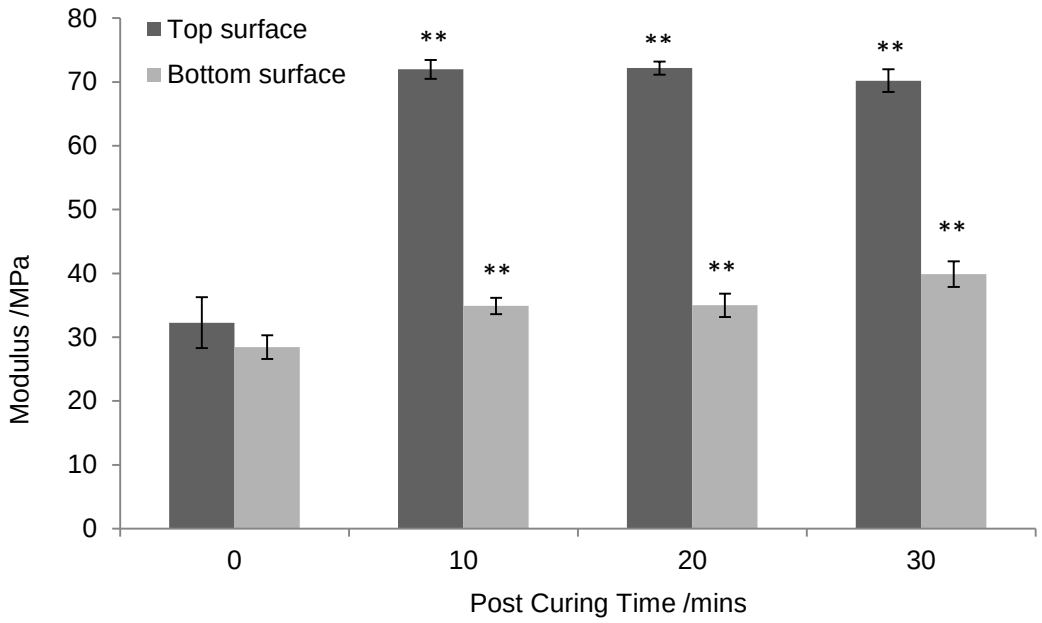

*Figure 5.18: Modulus of the top and bottom surface of the square samples printed in an air environment after different period of post-curing using PCLDMA:PEGDA (70:30) (3wt% of both photoinitiator and accelerator, Mean ± Standard Deviation n=50, compared with no post curing, *p<0.01, **p<0.001).*

The results in Figure 5.18 did not show firm evidence to support the previous hypothesis that property deviations exist on printed sample's top and bottom surface before post-curing (0 minutes). This also showed that post-curing can introduce further crosslinking and increase both modulus and hardness on the samples, but that UV illumination from the top surface may not penetrate deep into the sample and as a consequence less extra curing occurs at the bottom compared to the top.

The mechanical properties of the sample's top surface, which was directly illuminated by UV light, had a significant increase after 10 minutes of post-curing. However additional post-curing for 20 and 30 minutes did not further increase these properties.

The rise of hardness and modulus on the top surface after post-curing was mainly due to the increase in cross-link density. Studies have shown that the hardness and modulus of a crosslinked material is positive in relation to its crosslink density (Gardel et al., 2004; Coran, 1978). At low crosslink density, polymer chains are less restricted, which can therefore easily deform with an applied force, manifesting as a low hardness and modulus. As crosslink density increases, those free segments are connected with each other building an increasingly dense network. The mobility of the polymer chain segments becomes restricted and the specimen will then show stronger resistance to an applied force. When a specimen was printed, the conversion of the C=C group into the covalent crosslink normally cannot reach 100%. During the post-curing stage, UV illumination will provide extra energy to help the residual C=C group form new crosslinking and therefore, further increase the crosslink density and hence its hardness and modulus.

Meanwhile, the properties of the sample's bottom surface did not show as much change as top surface. This could be because during the post-curing procedure, samples were illuminated from the top surface and the UV light needs to penetrate the whole sample before reaching the bottom surface. During the penetration procedure, the intensity of the UV light would be reduced by absorption of the printed material and result in only a small quantity of radiation reaching the bottom surface.

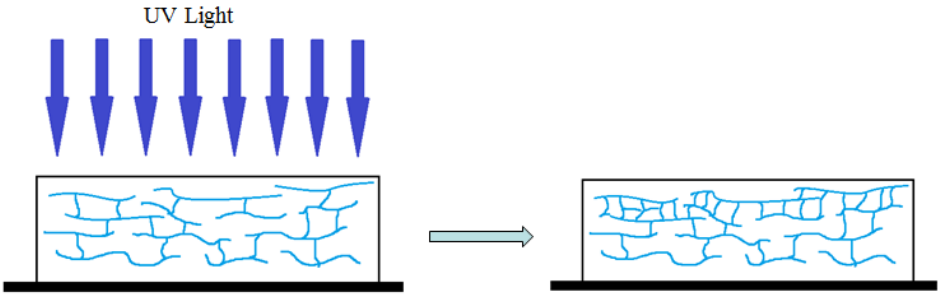

Figure 5.19: Schematic of the crosslinking of the internal polymer chains during post-curing.

In order to prove that the UV light attenuation through the sample during post-curing caused the hardness and modulus of the bottom layer to remain the same before and after post-curing, a single layer of PCLDMA:PEGDA ink with 3 wt% photoinitiator and accelerator was printed on to a quartz slide to characterize the absorbance spectrum of the printed sample. A clean quartz slide was used as a reference sample. The results are shown in Figure 5.20 which indicates that the sample has a moderate absorbance around 365 nm, which is the UV wavelength used for post-curing.

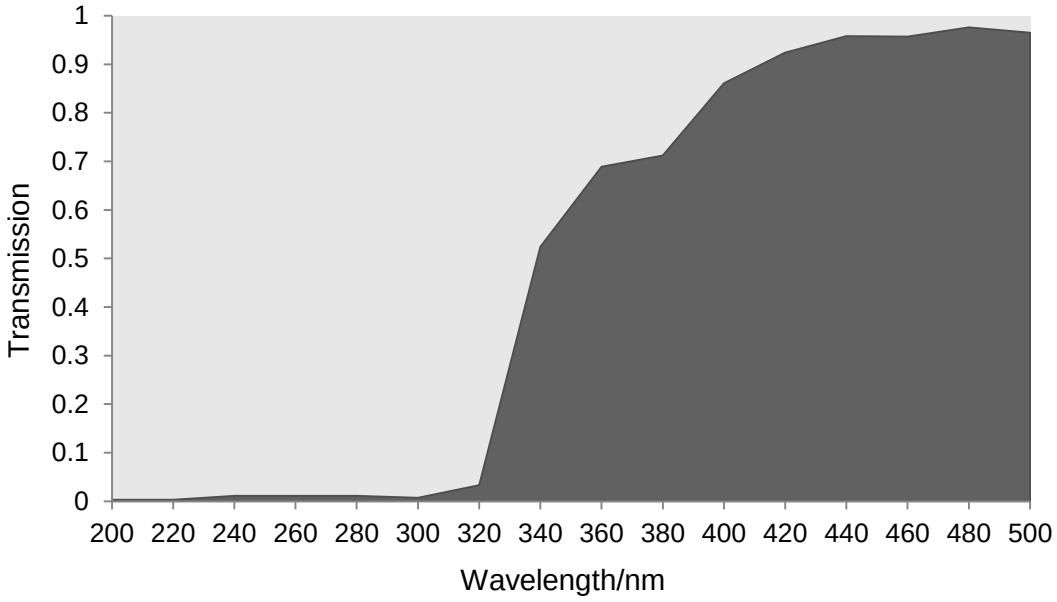

Figure 5.20: Transmission spectrum for one layer of printed PCLDMA: PEGDA ink with 3 wt% photoinitiator and accelerator in air environment.

Further experiments were carried out to investigate how the absorbance vary as the number of printed layers was increased. Three layers, five layers, seven layers and nine layers of the ink with 3 wt% photoinitiator and accelerator were printed on quartz slides and the absorbance spectrum between 300 nm and 400 nm was measured with a 5 nm interval. Figure 5.21 shows that the light between 300 nm and 325 nm are almost absorbed by only one layer of sample. As wavelength increases, the material shows less absorbance. Meanwhile, as the number of layers increased, the transmission of the UV light significantly reduced (Figure 5.21).

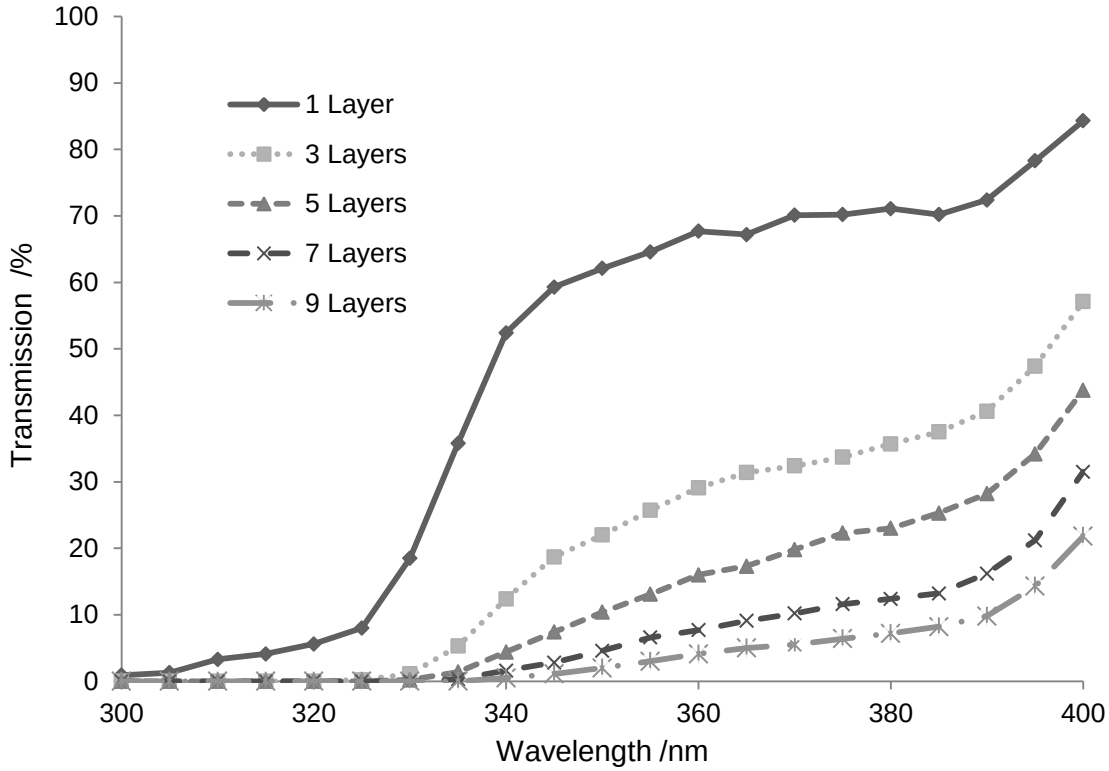

Figure 5.21: Transmission spectrum of PCLDMA: PEGDA ink with 3 wt% photoinitiator and accelerator printed with 1, 3, 5, 7, 9 layers printed in air environment.

Each square sample printed for previous indentation test consisted 100 layers, so the bottom layer may only receive negligible amount of UV light when post-

curing was carried out from the top surface. This can then explain why the hardness and modulus on bottom layer did not show much variation after post curing while the top surface has a significant growth. From Figure 5.22, it can be seen that the transmission of the sample with 9 printed layers was around 5%; for 1 layer it was around 67%. Based on Beer-Lambert law, the transmission of the light follows:

$$T = \frac{I}{I_0} = e^{-\varepsilon l} = e^{-\sigma N t} \quad 5.1$$

where T is the transmissivity, I_0 is the incident radiation, I is the transmitted radiation, ε is the attenuation coefficient, σ is the attenuation cross section, l is the distance the light travelled, N is the number of sample layers and t is the single layer thickness. Therefore an exponential form to full absorption was fitted resulting in (Figure 5.22):

$$T = e^{-0.342N} \quad 5.2$$

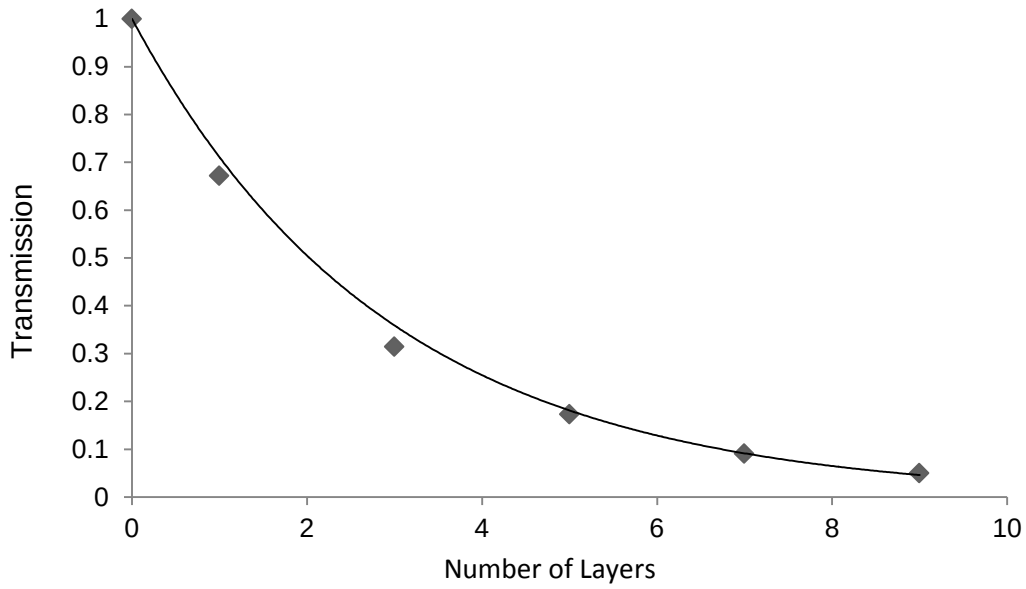

Figure 5.22: Plot of transmission change at 365nm with increasing layers for PCLDMA: PEGDA ink with 3wt% photoinitiator and accelerator printed in air environment.

This experiment showed that post-curing is a method that may have limited results, since it may only create a hard thin shell of full curing around the object. However for general applications, a uniform distribution of properties for both the outer and inner structure is required. Increasing of the post-curing time may help the inner structure receive more UV light, but meanwhile, it also increases the risk of polymer aging. As a result, it is identified that more thorough curing during processing is desirable, since post-curing cannot achieve our aims.

Table 5.8: Hardness and indentation modulus for printed PCLDMA: PEGDA (70:30) with 3wt% of both photoinitiator and accelerator before and after post-curing in nitrogen environment (Mean ± Standard Deviation n=50)

	Curing Time	Hardness (MPa)	Indentation Modulus (MPa)
Top Surface	0 mins	5.28±0.02	41.44±0.23
	10 mins	6.77±0.03	86.33±0.34
	20 mins	6.95±0.07	87.13±0.40
	30 mins	6.88±0.04	85.83±0.34
Bottom Surface	0 mins	6.25±0.04	69.03±0.23
	10 mins	6.44±0.05	73.85±0.14
	20 mins	6.60±0.32	77.93±0.22
	30 mins	6.70±1.65	82.35±1.48

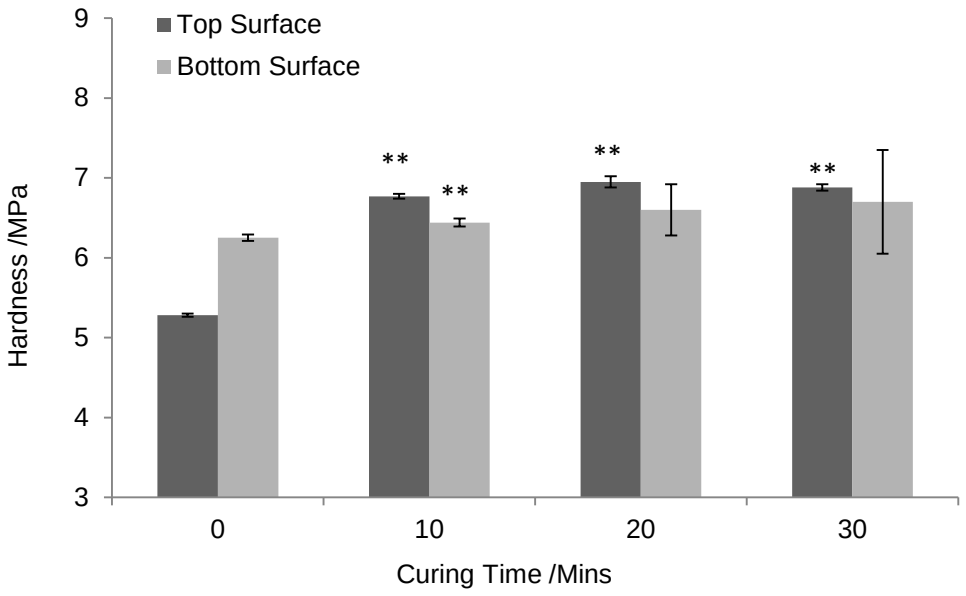

*Figure 5.23: Hardness of the top and bottom surface of the square samples printed in nitrogen environment after different period of post-curing using PCLDMA:PEGDA (70:30) (3 wt% of both photoinitiator and accelerator, Mean ± Standard Deviation n=50, compared with no post curing, *p<0.01, **p<0.001).*

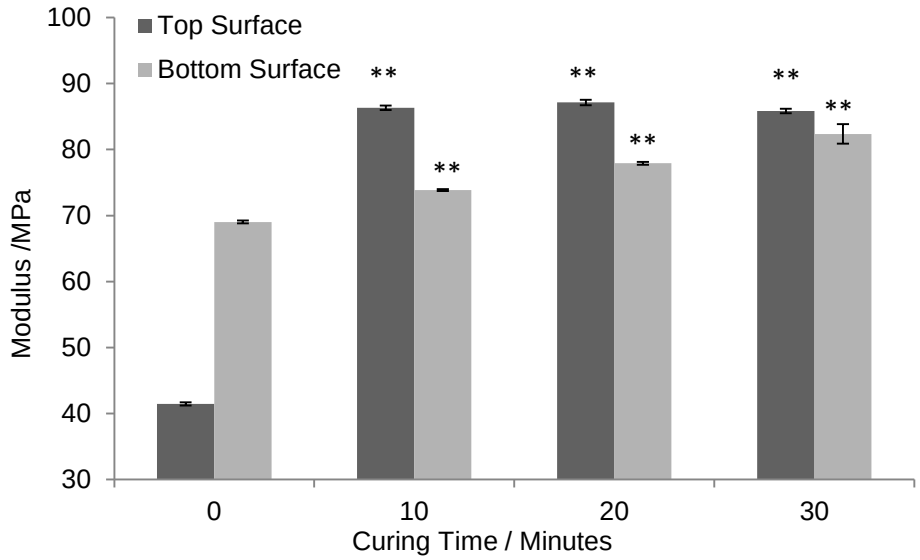

*Figure 5.24: Modulus of the top and bottom surface of the square samples printed in nitrogen environment after different period of post-curing using PCLDMA:PEGDA (70:30) (3 wt% of both photoinitiator and accelerator, Mean ± Standard Deviation n=50, compared with no post curing,*p<0.01, **p<0.001).*

An experiment was performed to assess whether a nitrogen environment would enhance the properties of objects formed using type II photoinitiators. Surprisingly, they all manifest higher hardness and modulus compared to those printed in an air environment, which suggests improved crosslinking (Table 5.8). These signify that inert environments can still help to improve the curability of the ink, even when using type II systems. The accelerator can only protect the excited photoinitiator from being oxidized to a certain extent. The dependence of the material properties on the post-curing process appears similar effect for samples printed in air and in nitrogen. Both hardness and modulus on the top surface increased after being post-cured for 10 minutes but very little increase was seen after further post-curing.

The possible reason for this observation is thata free radical UV curing reaction is a stochastic process. The presence of excited accelerator free

radicals will largely reduce the chance that photoinitiator free radicals react with diffused oxygen and be oxidized. However a small amount of photoinitiator free radicals can still be oxidized and lose reactivity. Also as environmental oxygen concentration increases, more oxygen was diffused into the printed ink and the chance that the excited photoinitiator being oxidized will also increase. This directly influences the progress of the crosslinking reaction, and therefore lowers the hardness and modulus.

The transmission spectrum of the cured ink printed in a nitrogen environment was also characterized and shown in Figure 5.25.

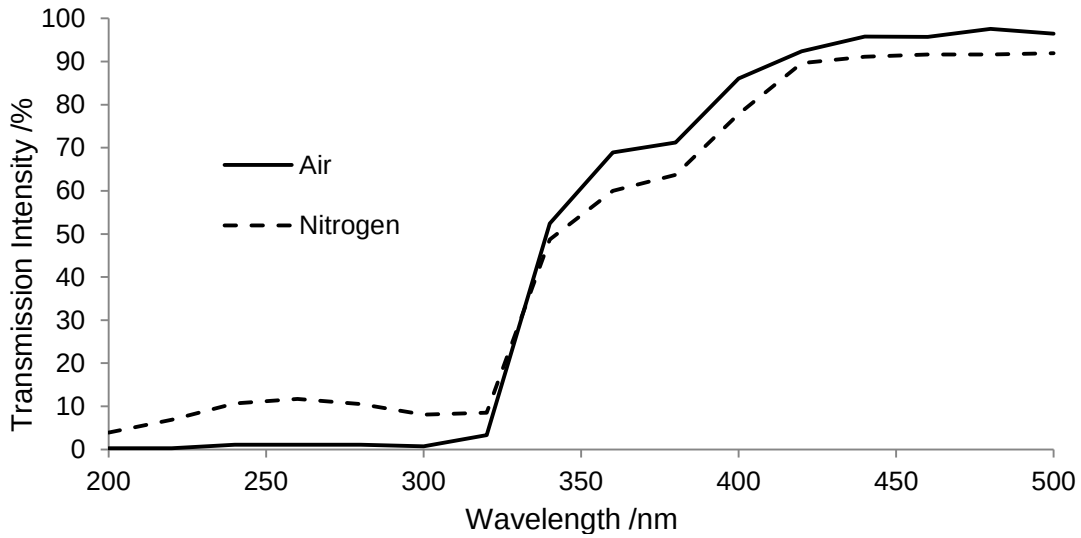

Figure 5.25: Transmission spectrum for one layer of printed PCLDMA: PEGDA ink with 3 wt% photoinitiator and accelerator in both air and nitrogen.

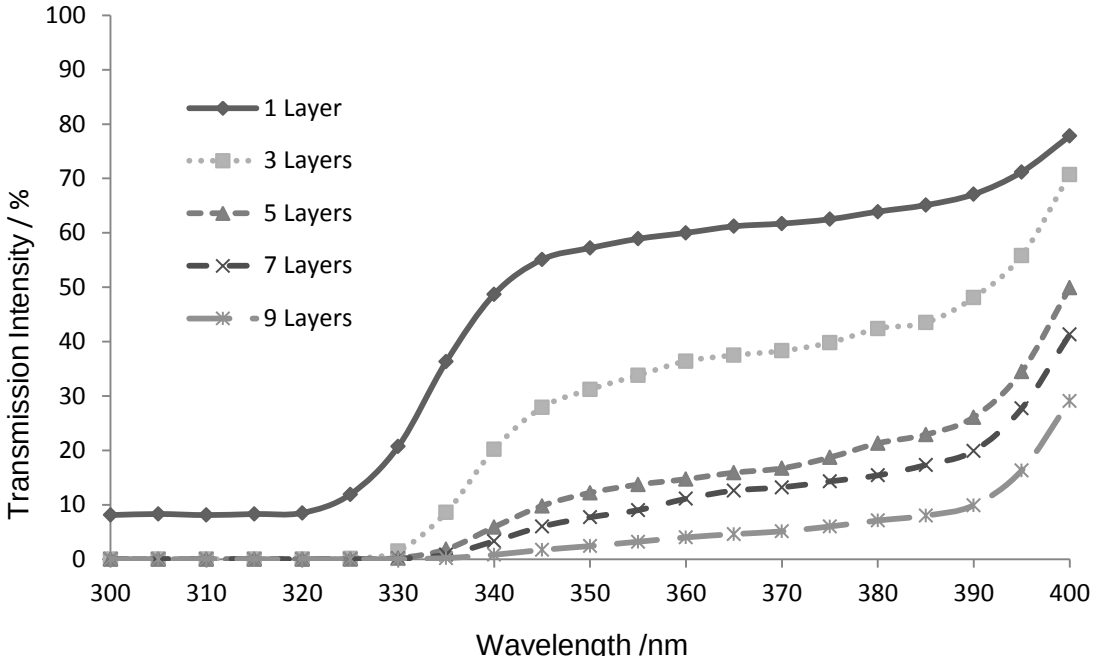

Figure 5.26: Transmission spectrum of PCLDMA: PEGDA ink with 3 wt% photoinitiator and accelerator printed with 1, 3, 5, 7 and 9 layers printed in a nitrogen environment.

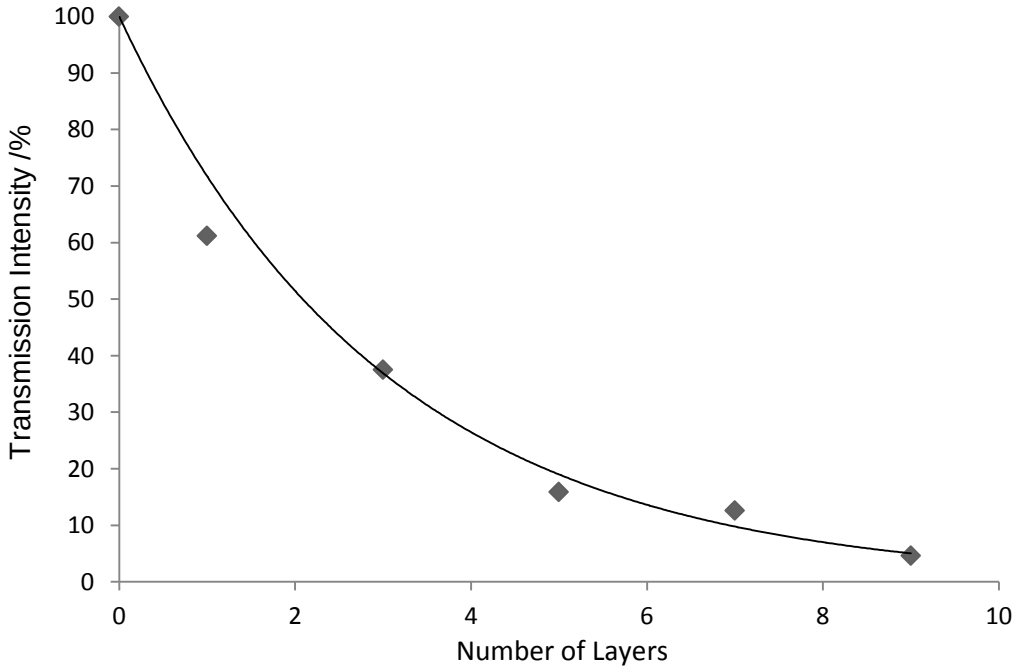

Figure 5.27: Plot of transmission change at 365nm with increment of printed layers for PCLDMA: PEGDA ink (3wt% photoinitiator and accelerator) printed in nitrogen environment.

The spectrum for ink cured in a nitrogen environment shows a similar absorbance to that printed in an air environment, but has slightly lower absorbance for light below 340 nm and higher absorbance for light above 340nm. The plot of absorbance on 365 nm also shows that only around 5% of the 365 nm UV light left after going through 9 layers which significantly inhibits further crosslink happening on the bottom side during post-curing.

In conclusion, the ink with 3 wt% of both photoinitiator and accelerator demonstrated good curability in both air and nitrogen environment. But the samples printed in a nitrogen environment showed greater hardness and modulus after been printed and cured, which suggested that even if the accelerator can provide some protection for the photoinitiator, an oxygen free environment is still preferred for better curability. Post-curing can induce further crosslinking to the sample and increase mechanical properties on the surface that was directly illuminated.

Attenuation of the UV light through the sample was deduced from nano-indentation data and demonstrated by measuring the cured samples' absorbance spectrum. Hardness and modulus for samples printed in both environments showed only small increase on their bottom surface after the post-curing procedure. The absorbance spectrum reveals that the attenuation of UV light at 365 nm reached 95% after going through 9 layers of the printed sample and led to no increase in the properties of the bottom surface of the post-cured samples.

5.2.6 Effect of Curing and Initiator Concentration in Air and Nitrogen Environments

Further experiments were carried out to investigate how photoinitiator and accelerator concentration can influence the sample properties in both air and nitrogen environments. Even though the initiator will be consumed during a curing reaction, it is still a potential source of chemical residuals which may reduce the biocompatibility of the final product. Therefore, it is desirable to investigate whether the inks with lower initiator concentrations can still solidify. This helps decrease the concentration of required photoinitiator as well as potential residual, improves the samples biocompatibility.

Inks with 1, 2 and 3 wt% photoinitiator and accelerator were prepared following the same procedures as before (Section 3.8.2) and printed. Square samples consisting of 100 layers were prepared for each ink. Morphology variations were observed for specimens printed with different inks in both environments (Figure 5.28). For the ink with 1 wt% photoinitiator and accelerator, the printed square samples presented as rounded rectangular shapes after being manufactured in an air environment. But the same inks were able to achieve sharp edges and corners when printed in a nitrogen environment. The likely cause of this is that the curing speed of the ink with 1wt% photoinitiator and accelerator is slower in an air environment in comparison with 3wt% photoinitiator, allowing the droplet to continue spreading and possibly be unable to support drops deposited on to it sufficiently to create sharp edges. In principle, if each droplet can become fully cured as soon as it is deposited, they should be able to stack up

accurately as shown (Figure 5.29). However when there is insufficient curing, the droplet may only be partially cured before another drop is coincident. This effect will be amplified further when the next drop is placed on top, as the partial curing will mean the low viscosity drop will “sag” and slide down the edge of the underneath drop due to gravitational and spreading effects. This caused irregular and rounded edges (e.g., Figure 5.28 (a), (b)). As curing speed is increased, the deposited drops will become more viscous and less mobile, creating a situation where edges will be sharper and less susceptible to spreading effects.

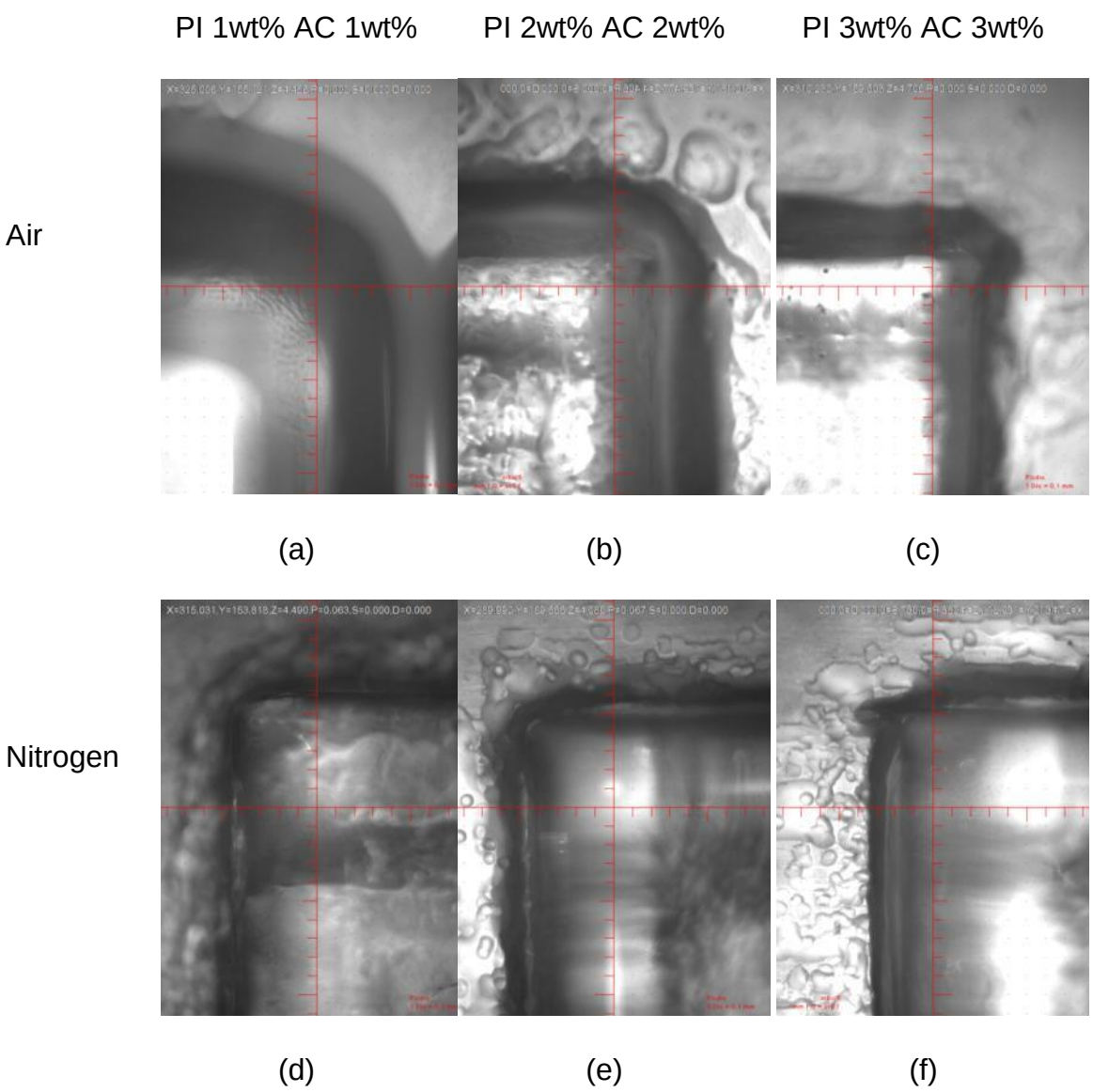

Figure 5.28: Optical microscope pictures of square samples printed with inks with different concentration of photoinitiators (PI) and accelerators (AC) in both air and nitrogen environments.(1 division=100 µm)

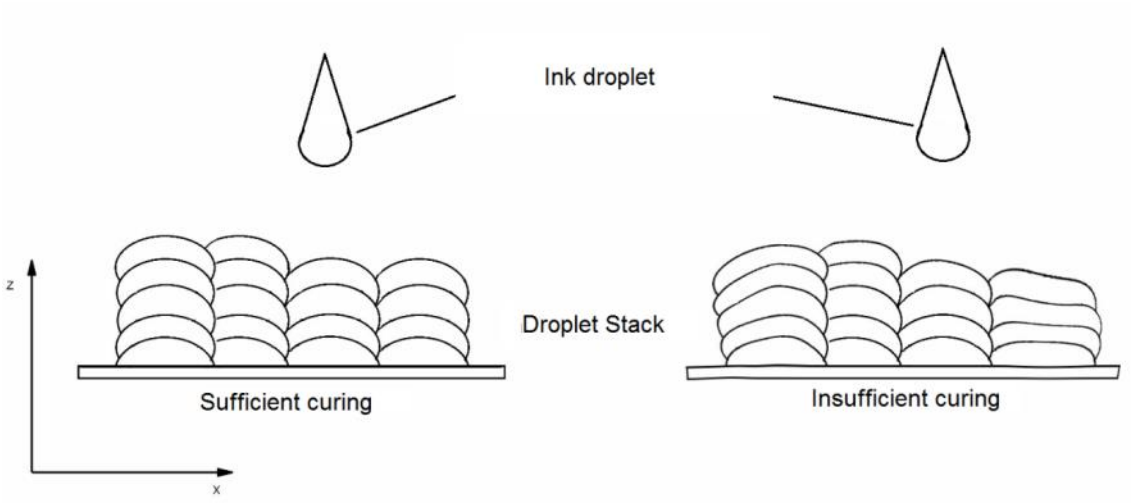

Figure 5.29: Schematic of deposited droplet in Z direction with different curing condition.

The hardness and modulus of these samples were measured by nano-indentation tests on both surfaces following the same protocol established before for investigation of postcuring effects. The results are shown in Table 5.9.

Table 5.9: Hardness and indentation modulus for printed PCLDMA:PEGDA (70:30) with 1 wt%, 2 wt% and 3 wt% of both photoinitiator and accelerator in air environment. (Mean ± Standard Deviation n=50)

Air Environment			
Photoinitiator and Accelerator Concentration		Hardness (MPa)	Indentation Modulus (MPa)
Top Surface	1 wt%	3.09±0.13	20.7±1.1
	2 wt%	3.68±0.52	24.35±3.6
	3 wt%	4.80±0.05	31.22±2.3
Bottom Surface	1 wt%	6.27±0.02	62.29±1.2
	2 wt%	5.71±0.03	44.38±1.4
	3 wt%	4.78±0.32	28.15±0.8

Table 5.10: Hardness and indentation modulus for printed PCLDMA:PEGDA (70:30) with 1wt%, 2wt% and 3wt% of both photoinitiator and accelerator in nitrogen environment. (Mean ± Standard Deviation n=50)

Nitrogen Environment			
Photoinitiator and Accelerator Concentration		Hardness (MPa)	Indentation Modulus (MPa)
Top Surface	1 wt%	6.15±0.02	52.97±1.3
	2 wt%	5.53±0.32	44.85±1.8
	3 wt%	5.15±0.12	40.14±0.6
Bottom Surface	1 wt%	6.99±0.02	96.54±1.2
	2 wt%	6.55±0.03	75.50±1.4
	3 wt%	6.31±0.32	67.45±2.8

Table 5.9 indicates that for the samples printed in an air environment, both hardness and modulus of the top surface show an upward trend with photoinitiator and accelerator concentration increases. This implies that lower photoinitiator and accelerator concentrations will be deleterious for curing rates in air. Raising the photoinitiator and accelerator concentration will generate more excited photoinitiator free radicals when illuminated by the same UV light, as well as producing more excited accelerators to protect the reaction from being inhibited by the oxygen in an air environment, both of which will accelerate the crosslink procedure.

This hypothesis was further tested by carrying out FTIR analysis for all these samples and for an uncured ink (Figure 5.30). The characteristic peak at 810 cm^{-1} was used to track the conversion of the double bond (Xu J. et al., 2006; Hong B.T., 2005). Figure 5.30(b) shows the normalized peak height at 810 cm^{-1} for each sample and it can be seen that the intensity of characteristic peak at 810 cm^{-1} decreased as the photoinitiator concentrations were

increased, indicating more conversion of C=C double bonds and higher levels of curing for samples with higher initiator concentration.

Meanwhile, it is also observed that C=C double bonds are still present in appreciable quantities in the sample, which indicate that acrylate residuals remain. As mentioned in section 3.8.2, these residuals may influence any manufactured product's biocompatibility. The acrylate residual could be minimised by carrying out post-processing (section 2.8.2).

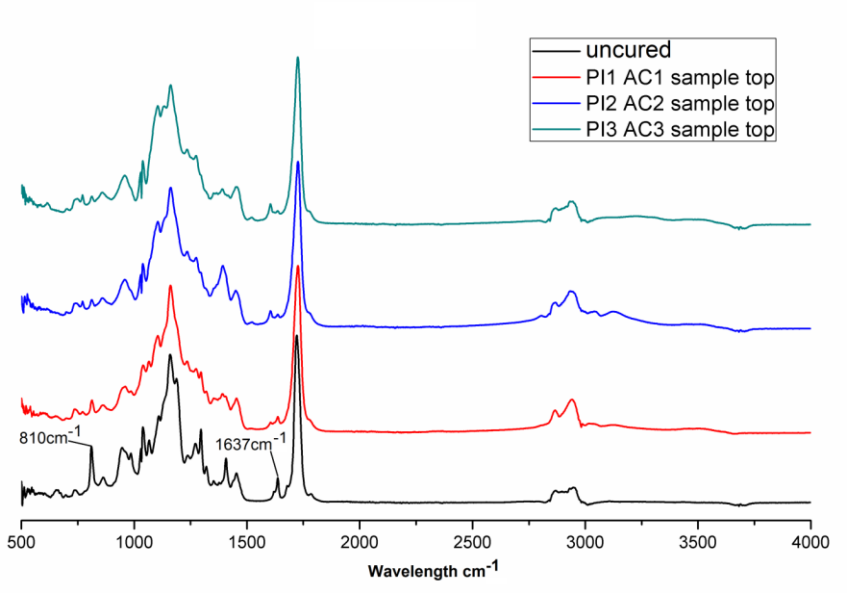

(a)

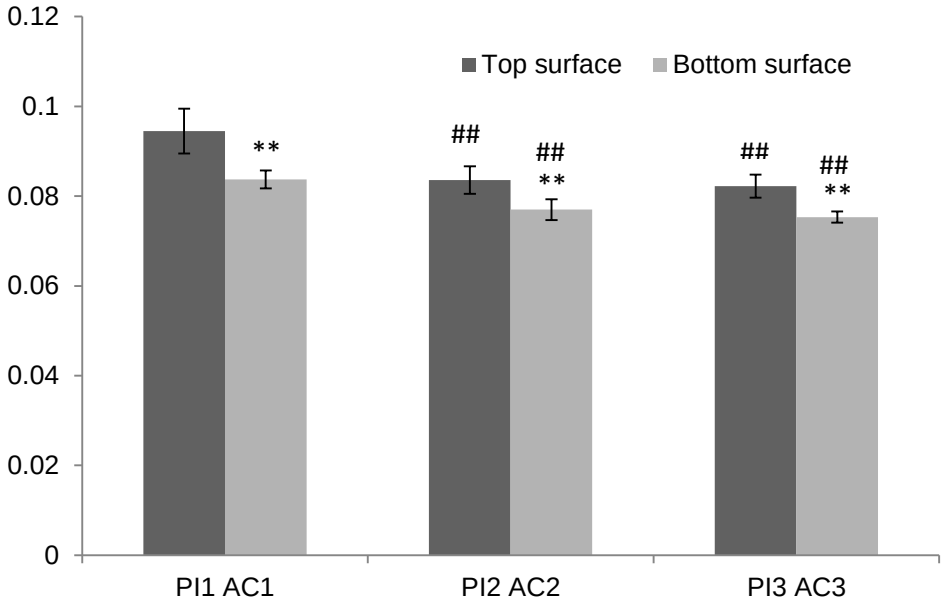

(b)

*Figure 5.30: FITR result of inks with different photoinitiator and accelerator concentrations printed in air environment: (a) FITR results of samples top surface, (b) Comparison of 810cm^{-1} peak height. (PI: photoinitiator concentration wt%; AC: accelerator concentration wt%, Mean ± Standard Deviation n=50, compared between bottom and top surface *p<0.01, **p<0.001, compared with 1wt% initiator concentration #p<0.01, ##p<0.001)*

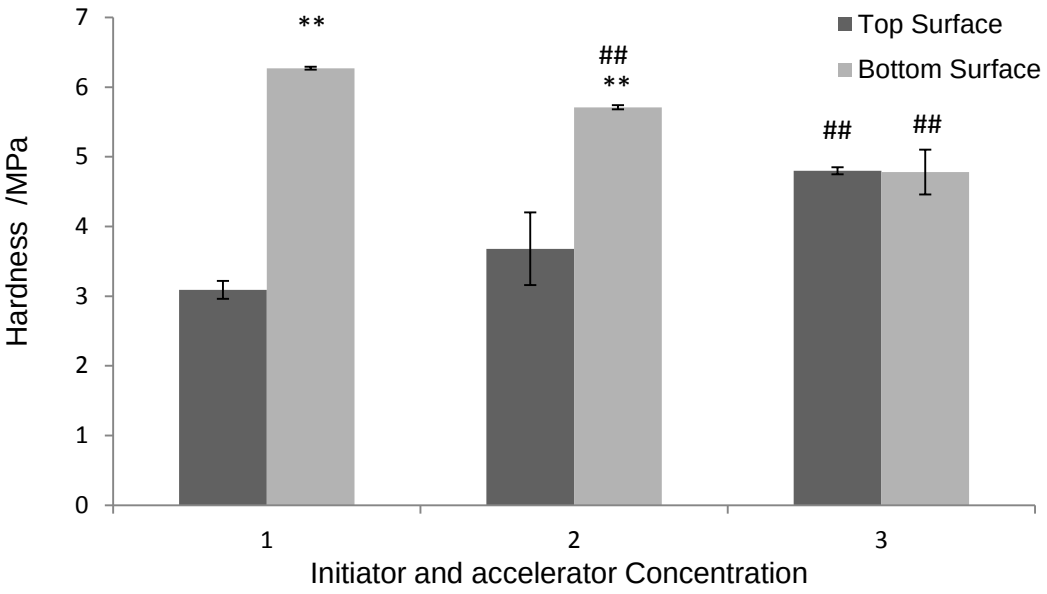

*Figure 5.31: A comparison of the hardness at the top and bottom surface of the square samples printed in air environment using PCLDMA:PEGDA (70:30) with 1wt%, 2wt% and 3wt% initiators (Mean ± Standard Deviation n = 50, compared between bottom and top surface *p<0.01, **p<0.001, compared with 1wt% initiator concentration #p<0.01, ##p<0.001)*

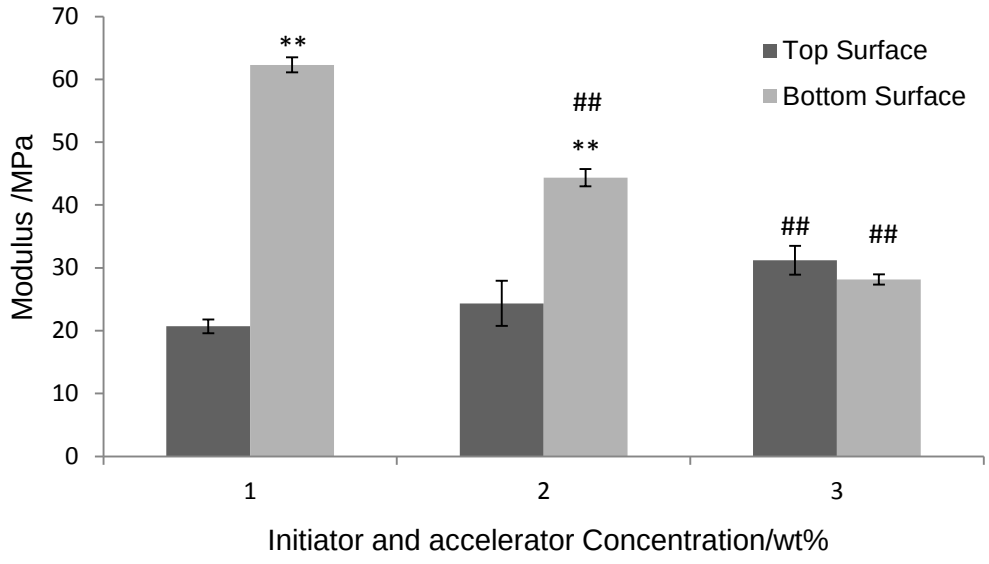

*Figure 5.32: A comparison of the modulus at the top and bottom surface of the square samples printed in air environment using PCLDMA:PEGDA (70:30) with 1wt%, 2wt% and 3wt% initiators. (Mean ± Standard Deviation n = 50, compared between bottom and top surface *p<0.01, **p<0.001, compared with 1wt% initiator concentration #p<0.01, ##p<0.001)*

All the inks printed in a nitrogen environment showed good curability. From the results in Table 5.10, it can also be observed that printed samples show higher hardness and modulus values on the bottom surface, which again can be attributed to a higher UV exposure than the top surface. It was again observed that inks with lower photoinitiator and accelerator concentration showed better hardness and modulus, but this time on both top and bottom surface. This further supports the hypothesis that when the samples can achieve a sufficient curing level, the sample with lower photoinitiator and accelerator concentration will manifest better properties.

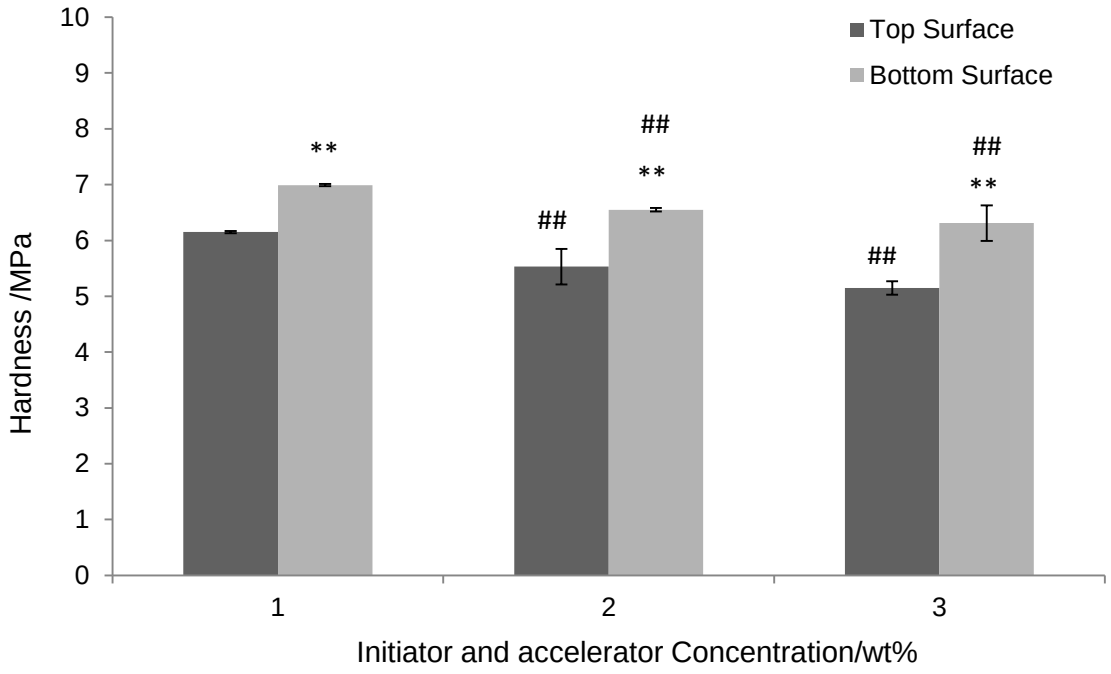

*Figure 5.33: A comparison of the hardness at the top and bottom surface of the square samples printed in nitrogen environment using PCLDMA:PEGDA (70:30) with 1wt%, 2wt% and 3wt% initiators. (Mean ± Standard Deviation n = 50, compared between bottom and top surface *p<0.01, **p<0.001, compared with 1wt% initiator concentration #p<0.01, ##p<0.001)*

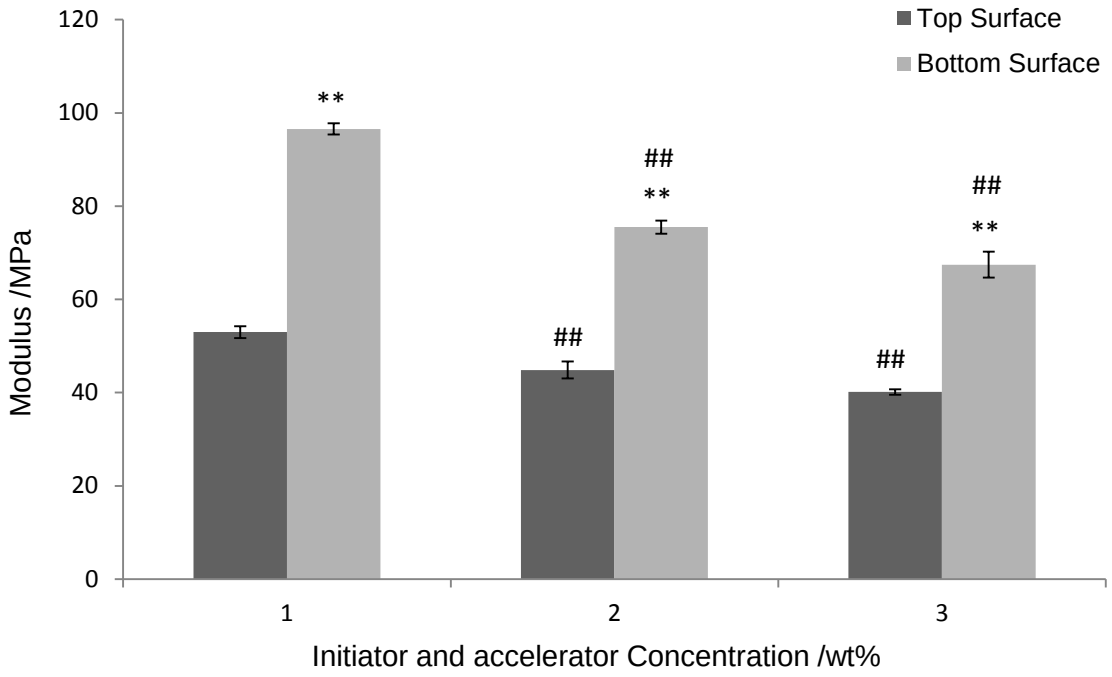

*Figure 5.34: A comparison of the modulus at the top and bottom surface of the square samples printed in nitrogen environment using PCLDMA:PEGDA (70:30) with 1wt%, 2wt% and 3wt% initiators. (Mean ± Standard Deviation n = 50, compared between bottom and top surface *p<0.01, **p<0.001, compared with 1wt% initiator concentration #p<0.01, ##p<0.001)*

The FTIR results in Figure 5.30 showed that samples with only 1wt% and 2 wt% initiators and accelerators did not fully cure on their top surface when printed in an air environment. Further evidence to support this was found when another parameter: the Elastic Recovery Parameter (EPR), *R,* was introduced.

The Elastic Recovery Parameter defines the level of deformation recovery after an applied force is released. It can be calculated by the following equation:

$$R = \frac{h_{max} - h_r}{h_{max}} \qquad \text{Equation 5.3}$$

where h_{max} represents for the maximum deformation when specific force was applied and h_r represents for the residual deformation when the force was fully released. For an ideal elastomer, all the deformation should be able to fully recover after the release of an applied force and the Elastic Recovery Parameter (R) will be equal to 1. Before curing, the ink is in a low viscosity liquid state and most of the deformations are not recoverable. As a crosslinking reaction initiated by UV illumination, crosslinks start to form between monomers and oligomers to create a 3D network which will restrict the chains to retain their state. The ink will then start to solidify and the hardness of the ink will increase. However at an early stage, the crosslink density is low and the crosslinking only restricts a small portion of the molecules and the Brownian motion between the molecules is not significantly disturbed (James and Guth, 1943). Therefore, the ink is rubbery at this stage, but both the ink's hardness and elastic recovery parameter will increase as the amount of crosslink increase.

As the curing goes further, more crosslinks are formed, which will eventually fully restrict the mobility (intra-molecular Brownian motion) of the polymer chain (James and Guth, 1943). At this stage, the hardness of the sample will further increase. However, the value of elastic recovery parameter will start to decrease as the polymer chains are approaching a fully restricted state and any deformations happening in this stage are non-reversible. At this stage, the sample's hardness and ERP will reduce as the amount of crosslink increases.

Table 5.11: Hardness and elastic recovery parameters of both top and bottom surface for the ink with different concentration of initiator printed in air environment. (Mean ± Standard Deviation n=50)

Air Environment			
Photoinitiator and Accelerator Concentration		Hardness (MPa)	Elastic Recovery Parameters
Top Surface	1wt%	3.09±0.13	72.29
	2wt%	3.68±0.52	80.73
	3wt%	4.80±0.05	96.47
Bottom Surface	1wt%	6.27±0.02	71.76
	2wt%	5.71±0.03	87.40
	3wt%	4.78±0.32	94.98

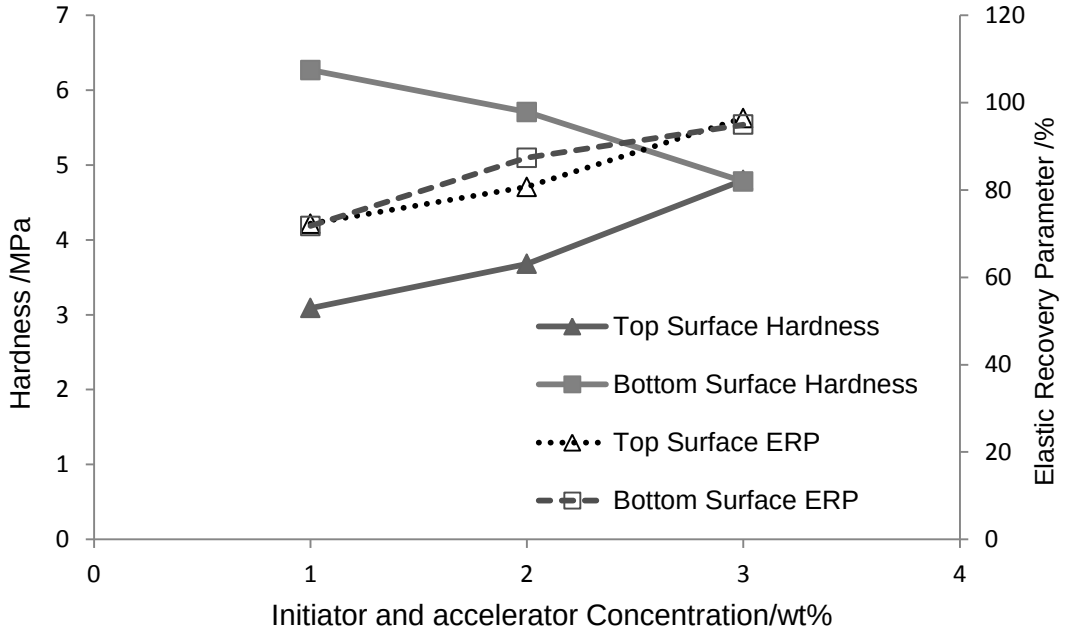

Figure 5.35: Plot of hardness and elastic recovery parameter of both top and bottom surface for the ink with different concentration of initiator printed in air environment.

Table 5.12: Hardness and elastic recovery parameters of both top and bottom surface for the ink with different concentration of initiator printed in nitrogen environment. (Mean ± Standard Deviation n=50)

Nitrogen Environment			
Photoinitiator and Accelerator Concentration		Hardness (MPa)	Elastic Recovery Parameters
Top Surface	1wt%	6.15±0.02	76.88
	2wt%	5.53±0.32	82.23
	3wt%	5.15±0.12	83.09
Bottom Surface	1wt%	6.99±0.02	54.64
	2wt%	6.55±0.03	63.37
	3wt%	6.31±0.32	67.43

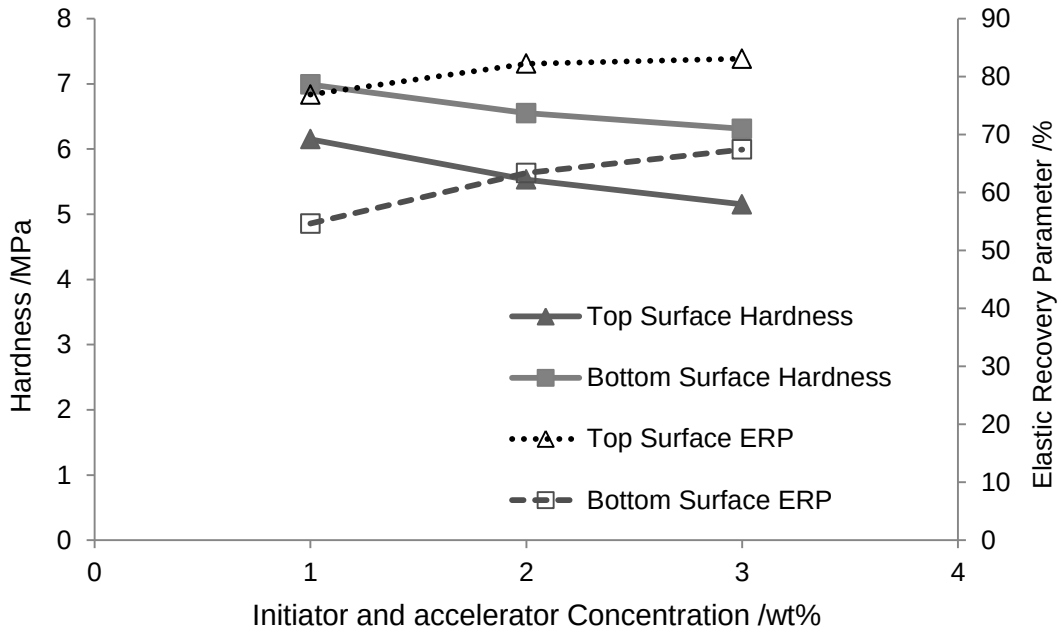

Figure 5.36: Plot of hardness and elastic recovery parameter of both top and bottom surface for the ink with different concentration of initiator printed in nitrogen environment.

From the plot in Figure 5.35 it can be observed that while the hardness at the top surface increases with increasing initiator concentration, the value of elastic recovery parameter was also increases. This trend shows that the ink

at the top surface is in the stage between transforming from liquid into rubbery elastomer and the crosslink density was still at a low level. Meanwhile on the bottom surface, the elastic recovery parameter decreased as the hardness increased which means the ink on the bottom layer had reached the second stage: transforming from elastomer into rigid solid. For the samples printed in nitrogen (Figure 5.36), due to the absence of Oxygen, there was better curing at both top and bottom surface. Both surfaces entered the second stage that the elastic recovery parameter decreases with increasing hardness, which represents that they were transforming from elastomer into rigid solid.

It can also be concluded from both Figure 5.35 and Figure 5.36 that the samples with enough crosslink and having entered the second stage (transforming from rubbery into rigid solid) will show better hardness and modulus at lower initiator concentration level. This is because high initiator concentration will narrow the length of crosslink and therefore reduce the size of the overall crosslinking network which will then reduce the hardness as well as modulus of the final sample (Clay et al., 1995). As mentioned before, the free radical reaction is stochastic. Higher initiator concentration will generate more excited free radicals at the initiation stage (see section 2.6.1, on the basic concepts of UV curing reactions), which largely increased the chance that excited initiators will meet an oligomer and enter the chain propagation stage. This, therefore, can accelerate the crosslink reaction in a less favourable environment, e.g. printed in air environment (Oxygen inhibition), as plenty of backup excited initiators were generated. This assumes better crosslink and higher hardness at the top surface would be achieved for the samples with higher initiator concentration and printed in air environment.

However in the chain propagation stage, high concentration of excited oligomer chain will also have a higher chance to meet another excited oligomer and be terminated instead of meeting another oligomer and propagates. This will lead to more premature polymer chains being terminated, which reduces the total length and completeness of the whole network. A less complete network will lead to lower hardness and modulus for inks with higher initiator concentrations.

From these results, it can also be concluded that if a product is going to be fabricated in an air environment, reducing the photoinitiator will increase the amount of uncured ink and residual amount of acrylate. Although increasing the photoinitiator concentration can increase the degree of curing, it will also increase the possibility of photoinitiator residuals. Both cases will reduce the biocompatibility of the product. Therefore printing in the air is not an optimal choice for the developed ink when considering biocompatibility of the final product. However for the sample prepared in a nitrogen environment, it showed more curability with lower photoinitiator concentration, and as a consequence, printing in the nitrogen environment with lower photoinitiator concentration is a better choice to both improve the sample's mechanical properties and its biocompatibilities.

5.2.7 Further Characterisation

The printed square samples were examined under optical microscope to study the sample surfaces. The optical microscope pictures of all the samples are shown in the appendix. Small pores were found on all the cured samples most of which were around 10μm.

Printed samples showed hardness and modulus differences on their top and bottom surface. This is attributable to the differential UV light exposure. In order to get further evidence, several attempts were made to track the curability on both surfaces by measuring the amount of existing C=C bonds. Both FTIR microscopy and Raman microscopy are characterization methods which could track localized chemical variation. For FTIR microscopy (transmission), the sample was cut into 5 μm slices through the cross-section by using a cryostat microtome and placed on CaF slides. Sample slices with this thickness will allow enough IR to transmit through the sample and be detected. Samples with different initiator concentrations printed in an air environment, the most typical sample set which would show C=C variations on both surfaces were chosen for the characterization trials. The optical microscope pictures of microtomed samples are shown in Figure 5.37.

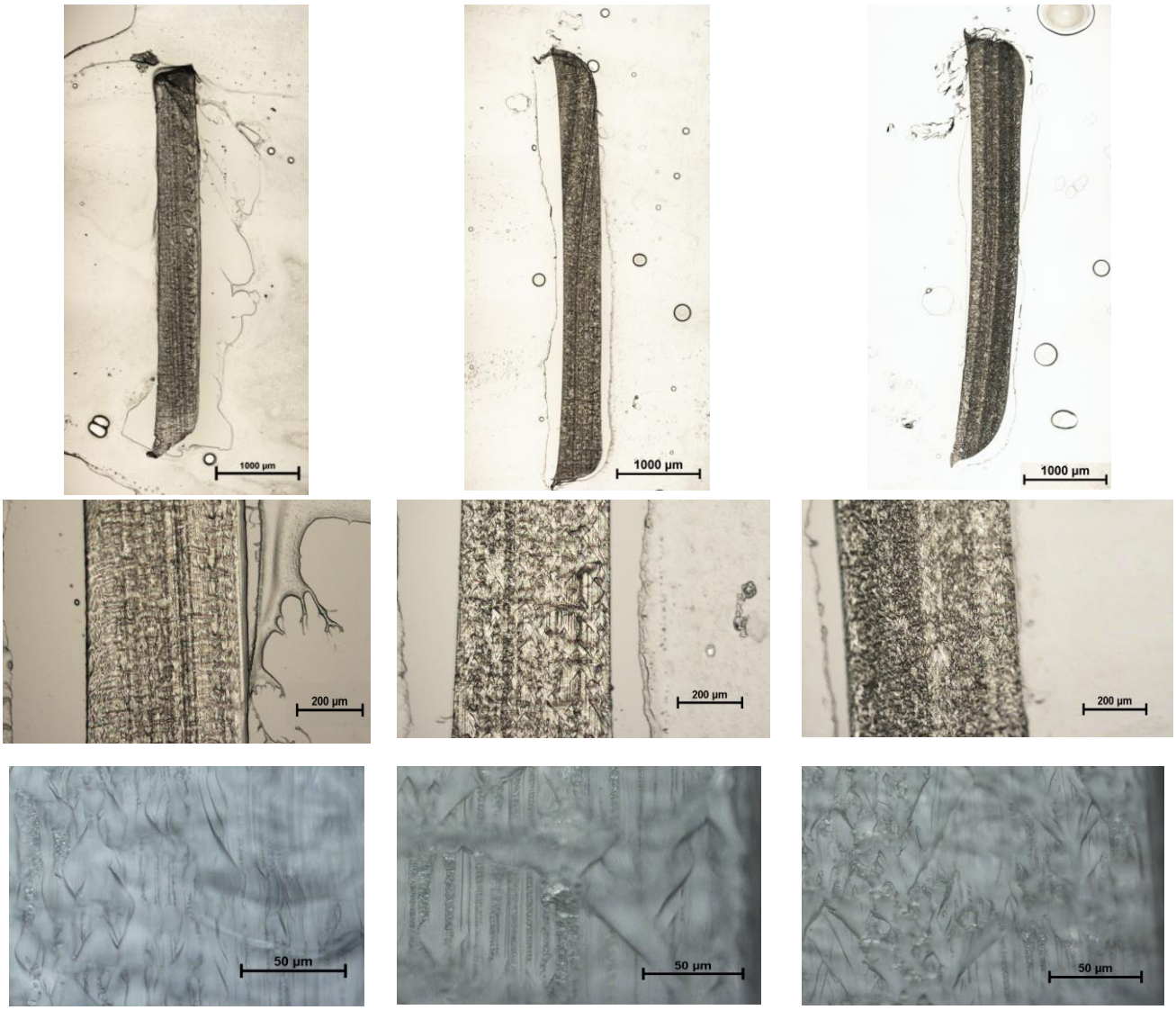

(a) (b) (c)

Figure 5.37: Optical microscope picture of microtomed sample slices with different photoinitiator and accelerator concentrations (a) 1 wt%, (b) 2 wt% (c) 3 wt%.

From the microscope pictures, laminated structures can be observed which indicate the layer by layer printing. Smearing due to the blade cutting motion can be observed in the high magnification images (cutting direction is from bottom of the image to the top). This led to rough surfaces and caused a lot of scattering during the FTIR microscope characterization. The IR received by the detector was then not strong enough to distinguish the characteristic

peaks from the machine noise. The cross-section samples were also characterized by Raman microscopy, however strong fluorescent effects occurred with all available laser wavelengths, which led to no characteristic peaks observable.

5.3 Summary

A novel UV curable PCLDMA:PEGDA ink that is suitable for material jetting for the fabrication of PCL structures has been developed for the first time. For different printer and applications, the proportion of PEGDA and processing temperature can be varied.

PCLDMA:PEGDA (70:30) was suitable for the Dimatix DMP-2830 printer when printed at 60ºC. The prepared ink can be cured sufficiently to retain desired structures during processing and stable products can be produced with 3 wt% initiator and accelerator in an air environment. The printed sample's hardness and modulus increased when a post-curing procedure was applied and the mechanical properties at the top surface increase more than the bottom surface. Further experiments with different concentrations of type II photoinitiator showed that inks with higher concentration of initiator manifested faster curing in air environment while inks with lower concentration of initiator experienced more serious Oxygen inhibition. However, when printed in nitrogen environment, where Oxygen concentration was minimized, higher hardness and modulus were observed within the samples containing lower concentration of initiators. A small amount of uncured PCLDMA was observed on the sample surface during FTIR characterization, which may bring potential risk to the biocompatibility of printed sample and requires further investigation.

Chapter 6 General Discussion

The primary aim of this research is to investigate the possibility of using material jetting technique to produce polycaprolactone based structures which could be potentially used to fabricate high porosity and complex shaped tissue-engineering structures. Through this work, it has been demonstrated that polycaprolactone can be printed through both direct jetting techniques (solvent-based polycaprolactone ink) and reactive jetting techniques (UV-curing based ink). A wide range of processing parameters and ink formulations were studied to achieve printable inks which are able to fabricate structures with desired morphologies. The most significant finding is the demonstration of using synthesised polycaprolactone to prepare a novel UV curing based ink which can be used in both nitrogen and air environments. PCL mesh structures were printed, which showed that the strut size can reach 180 μm-200 μm. The mechanical characterization showed that the ihardness of the solid sample ranged between 5 and 7 MPa with modulus between 50 and 90 MPa.

Although material jetting showed advantages compared to FDM and SLS techniques, the main obstacles were the necessary requirements to develop a printable ink with target material. This limited the materials that could be applied in material jetting, which therefore limited its application as well.

As the viscosity of polymer melt is far above the printable viscosity range, in order to print target polymer, previous researchers have developed solvent based inks by dissolving target polymers into solvents to meet the viscosity requirement and triggering the solidification by evaporating the solvent (Lee et al., 2011, Teichler et al., 2011). A similar principle was used in this research to attempt preparing polycaprolactone based solvent ink. Different kinds of solvents were tried to dissolve polycaprolactone and prepare printable PCL solvent ink with the consideration of both biocompatibility and processability. The performance of the prepared PCL solvent based inks were studied and optimized, by the end of which a multi-layer PCL structure can be fabricated with the developed PCL solvent based ink.

So it is possible to print PCL through solvent based technique, but is this technique suitable for use to fabricate PCL scaffold? From biocompatibility point of view, PCL solvent based ink was prepared from pure PCL polymer, therefore the biocompatibility and degradation of printed structure are promising. The use of solvent will induce the risk of chemical residuals, however this risk can be minimized by carrying out post processing such as vacuum drying, which is a practical method that is widely used in pharmaceutical industry. From processing point of view, a PCL solvent based ink is able to produce a PCL droplet around 70 μm, which provides the potential of fabricating a scaffold with a similar strut width. Compared with the PCL scaffolds presented in the literature, which showed fabricated PCL scaffolds by other additive manufacturing techniques (minimum strut width: 200μm for FDM and 500μm for SLS (Lohfeld et al. 2010, Ahn et al. 2011)), PCL solvent based ink and material jetting technique are superior in resolution

and provide the potential for fabricating a PCL scaffold with more delicate micron-level structures. The main challenge for solvent based ink is the printing efficiency. With the developed PCL solvent based ink in this research, the thickness of each layer was around 0.8 μm and 95 wt% of the ink needs to be evaporated. This limits the practicability of solvent based inks.

The second approach is to use reactive jetting. It is known that commercially available reactive jetting based machines are based on photopolymerisation reactions. However there is little research in this field about developing an ink suitable for this technique. The idea of preparing PCL based solid structure through UV curing based reactive jetting was proposed for the first time in this research. Previous researches have demonstrated that photo reactive groups can be grafted onto a PCL structure through condensation polymerization (Feng and Snaping, 2003; Park et al., 2007; Ferreira et al., 2008). The photo-reactive PCL was synthesized following a method modified from the literature (Feng and Snaping, 2003) and used to develop a suitable ink. The formulation and processing parameters of the ink was optimized with the consideration of processability and biocompatibility as well.

From biocompatibility point of view, UV curing based PCL inks induced more chemical residuals than a solvent based PCL ink. The potential chemical residuals include unreacted photo reactive PCL and unreacted initiator. Therefore the product fabricated with UV curable PCL ink will require more effort in post-processing (e.g.: post curing, vacuum drying) in order to minimize the risk of chemical residuals. These post-processing methods are still practical and achievable. During this research, efforts have also been made in the processing and material selection to minimize the residuals (e.g.,

carrying out post curing, reducing initiator amount, using safer initiators). As investigated by Kweon et al., (2003), crosslinked PCL still retained the ability to degradate, the biodegradabiliy of PCL may vary, which will reqiure furthuer investigate in the future study. The hardness and modulus of the cured PCL (5 to 7 MPa for hardness and 50 to 90 MPa for modulus) are slightly higher than the PCL samples produced by FDM and SLS in the literature. (Ahn et al. 2011, Mazzoli et al. 2015, Shor et al. 2009, William et al. 2005, Zein et al. 2002). Therefore in terms of mechanical properties, UV curable PCL ink could find uses, for example, in the fabrication of scaffold for human trabecular bone application. From a processing point of view, the printing efficiency of UV curable PCL is much higher than solvent based inks, since one can achieve 10μm with almost no weight loss post-deposition. The deposit droplet size was similar to those achieved with solvent based techniques, which means PCL UV based ink can also potentially reach 70 μm strut width as well. Therefore, the processing resolution has surpassed the other two AM based PCL processing techniques (FMD and SLS).

So in summary, this work has demonstrated that fabricating polycaprolactone based product through material jetting technique is mechanically possible. The resolution of PCL structures fabricated by material jetting technique were better than those previously produced by SLS and FDM techniques. This suggests that material jetting technology could be used to fabricate high porosity and high complexity tissue-engineering structures. The mechanical properties of fabricated parts were in the range of human trabecular bone which suggested that it could find applications for trabecular bone scaffolds. Post processing was found necessary to maximise the products'

biocompatibility as unreacted PCLDMA was detected on the sample by FTIR and further systematic studies are required in the future to determine whether the amount of residuals are above the safety limit.

Chapter 7 Conclusion and Future Work

6.1 Conclusion

In this project, two kinds of potential inks: solvent based and UV curing based, were developed and printed. Both of them were printed by a material jetting method, but each showed very different printabilities and stabilities. The PCL based structures fabricated by material jetting showed higher resolution compared with those fabricated by the other AM techniques (FDM, SLS) in available previous studies, whilst also achieving similar mechanical properties. This suggested material jetting is a technique which has potential for use in fabrication of more complex geometries in comparison with currently used AM techniques. Further work is required on studying the influences of chemical residuals on the biocompatibility, and should include assessments of cell viability on printed PCL structures.

Polycaprolactone Solvent Based Ink:

A PCL solvent based ink was developed and successfully printed. The solubility of PCL in different kinds of solvents were firstly studied and 1,4-dioxane was chosen based on both solubility and biocompatibility. During solvent based ink preparation and printing, it was found that high solute concentration (above 10 wt%) and volatile solvent (boiling point below 100 ºC) would easily cause printhead nozzle failure or blockage.

The measured rheology data showed that the viscosity of both 5 wt% and 10 wt% PCL solvent based inks is lower than the suggested optimum viscosity range for a Dimatix DMP 2800 ink jet printer. Therefore, the standard waveform did not allow for stable droplet formation. A double peak waveform was then developed and modified, through which stable droplet formation was achieved.

The morphology of the printed and solidified PCL was studied using a optical microscope. The influences of different droplet speeds, droplet spacings and substrate temperatures on the quality of printed tracks and films were investigated. During the experiments, the influence of the substrate heating was assessed and it was found that substrate heating can accelerate the evaporation of the ink and create more regular printing threads. However, the heated substrate will gradually heat up the printhead nozzle as well as the printing environment which will accelerate the ink's evaporation speed at the nozzles and reduce the ink's stability. The coffee ring effect was observed during printing polycaprolactone solvent based ink and most of the precipitated polymer concentrated to the edge of the droplet or thread. This, to a certain extent, influences the uniformity of printed structure.

Trial of printing multi-layer samples was performed, however, due to limitations associated with the solute concentration, the precipitated polycaprolactone's layer thickness was around 0.8μm only, which limited the efficiency of printing 3D structures with this kind of solvent based ink. In conclusion, solvent based methods could be used to print polycaprolactone layers, but it is not as suitable for the manufacture of 3D structures with sizes in centimetre range or above, due to low printing efficiency and the large

amount of solvent vapour emission. However, it could be used to create delicate PCL layers or patterns which have high requirements on the layer thickness and pattern complexity.

Polycaprolactone UV Curing Based Ink:

Polycaprolactone was chemically modified to graft UV curable methyl acrylate groups onto its chain end based on a method provided by existing literature. A UV curable Polycaprolactone (Polycaprolactone di-methylacrylated, PCLDMA) was synthesized and cured under UV light with the presence of photoinitiator. Several kinds of photoinitiators were studied and it was found that the ink with Irgacure 2959 (a type I photoinitiator) cannot be cured after being printed in air environment due to strong Oxygen inhibition effects. A type II photo initiator was then chosen owing to its reduced sensitivity to oxygen and it was then possible to successfully cure the ink in an air environment.

Viscosity characterization also showed that the viscosity of pure PCLDMA was out of the printable range for Dimatix. Therefore Polyethylene glycol diacrylated (PEGDA), a kind of widely used UV curable material to prepare biocompatible hydrogel, was used as diluent to adjust synthesized UV curable polycaprolactone into the printable range. During the ink preparation, it was also found that deoxygenation was also an indispensable procedure to ensure printed ink was able to be properly cured after jetting.

During the jetting process, it was also found that inks with different initiator concentrations showed very different curability when printed in an air environment. Therefore, the influences of initiator concentrations and printing environments were then studied as well. Inks with different photoinitiator

concentrations were printed under both air and nitrogen atmosphere to assess the influences of a range of conditions on the printed material's mechanical properties. It was found that a nitrogen environment can improve curing reaction and the specimens produced under a nitrogen environment showed higher hardness and modulus comparing with those printed in an air environment. However due to the higher initiator concentration narrowing the length of the crosslink, samples with higher initiator concentrations showed lower hardness and modulus when they were cured.

Post-curing was a post-process which was used in some UV curing based processes to help improve the final properties of the product. Therefore, the influences of post-curing on the final product were also studied. Nevertheless, because of low penetration rate of UV light for this ink, the effect of postcuring was restricted to the top surface of the sample. In conclusion, when comparing with a solvent based polycaprolactone ink, the UV based ink provides better printing efficiency and stability as the ink is less volatile and can fully transfer into a solid without any solvent loss. This principle could be used to prepare inks for material jetting process to create biodegradable polymeric structure in the future.

6.2 Future Work

This project aims to investigate the possibility of fabricating PCL structure through material jetting technique based AM, which can potentially produce more complex structures for tissue engineering applications compared with currently used FDM and SLS based AM techniques. This work mainly developed and studied PCL base inks for use with material jetting.

Short term

Residual chemicals characterization

Chemical residuals may exist in the fabricated sample, which will influence the biocompatibility of the final product and requires further investigation. The amount of chemical residual can be analysed by Gas Chromatography or NMR. The concentration of chemical residuals between samples with different post process strategies can be compared to help find an optimum method for fabricating products with acceptable biocompatibility.

Biodegradability test

Biodegradability can be carried out by a weight loss method. Samples with different polycaprolactone proportions can be printed and characterized to study the influence of ink formulations on the degradability. SEM and nanoindentation tests can be applied to study the surface morphology change as well as mechanical properties changes during the degradation.

Irgacure 2959 curing system

Currently, the ink was printed using a type II photoinitiator in both air and nitrogen environment. Additional experiments to investigate the curability of the ink with type I photoinitiator (Irgacure 2959, a widely used photoinitiator in to prepare biocompatible hydrogels) in nitrogen environment, as well as how photoinitiator concentration influences the properties of the final cured sample, can be performed as a comparison to existing results.

In vitro test

After confirming the residual chemicals are within the safety range and degradation speed of the product, an *in vitro* test can be carried out first to study the compatibility of the sample surface with target cells as well as the cytotoxicity of the material and any chemicals leaching during degradation.

Long term

Manipulation of the product properties

PCL has a high compatibility with other polymers and as a consequence other alternative, biodegradable, materials can be used to manipulate the product properties and investigate potential applications. This may require other printing systems or printheads that allow higher processing temperature or ink viscosity tolerance, which would enable wider range of printable materials.

There are also other biodegradable polymers which can be chemically modified into a UV curable polymer. These polymers, such as PLA, PLGA, have different degradation speeds and/or biocompatibility, and can be investigated to build up a material library for 3D material jetting of

biodegradable materials. This approach will also allow selection of materials for production of multi-functional product by multi-material printing.

Optimization of Curing Efficiency

Inks with better curing efficiency can help improve processing accuracy by minimizing the droplet sagging and secure deposited droplets at the target location. This can be achieved by optimizing the initiation system as well as the curing system. Optimizing the initiation system can be achieved by looking for more effective photoinitiators and also use acrylated polymers instead of methyl acrylated polymers. Increasing the UV curing system can be achieved by attaching a stronger UV curing unit, customize UV curing strategy as well as printing in an inert atmosphere with lower oxygen concentration (less than 1% oxygen).

Scaling Up the Process

This project has developed a jettable ink which can then be scaled up to make real 3D objects with more complicated functions. The Dimatix DMP2830 printer used in this project is a basic machine with only one printhead and 16 nozzles. This machine was mainly used for ink development. More advanced printers such as Pixdro LP50 or Toucan, which runs up to 6 printheads where each printhead consists of 512 nozzles, can hugely increase the processing speed. Meanwhile, by using more than one printhead, multi-functional, multi-material and graded products can be produced.

References

Ahn S.H., Hyeoong J.J., Kim G.H., 2011, Polycaprolactone scaffold fabricated with an advanced Electrohydrodynamic direct-printing method for bone tissue regeneration, *Biomacromolecules*, volume 12, pp. 4256-4263.

Aimetti, A.A., Machen, A.J., Anseth, K.S., 2009, Poly(ethylene glycol) hydrogels formed by thiol-ene photopolymerization for enzyme-responsive protein delivery. *Biomaterials,* volume 30(30), pp. 6048-6054.

Ainsley, C., Reis, N., Derby, B., 2002, Freeform Fabrication by Controlled Droplet Deposition of Powder Filled Melts, *Journal of Material Science,* volume 37, pp. 3155-3161.

Albrecht, D., Tsang, V.L., Sah, R.L., Bhatia, S.N., 2005, Photo- and electropatterning of hydrogel-encapsulated living cell arrays. *Royal Society of Chemistry,* volume 5, pp. 111-118

Aldrich, S., 2014. *Photoinitiators - Sigma-Aldrich.* [Online] Available at: http://www.sigmaaldrich.com/content/dam/sigma-aldrich/docs/Aldrich/General_Information/photoinitiators.pdf
[Accessed 15 10 2014].

Arceneaus, J. and Willard K.,2014, *RadTech Printer's Guide.* [Online] Available at: http://72.52.184.8/~radtecho/pdfs/PrinterGuideChemistry.pdf
[Accessed 11 9 2014].

ASTM, 2012, *Standard Terminology for Additive Manufacturing Technology,* ASTM Interinational.

Baround, C.N., 2013, *Encyclopedia of Microfluidies and Nanofluidies*, New York, Springer Science+Bussiness Media.

Bhola R., Bhola S.M., Liang H., Mishra B., 2010, Biocompatible denture polymers-A review, *Trends in biomaterials and artificial organs*, volume 23(3), pp. 129-136

Bohlin Instruments, 1994, *A basic introduction to rheology-section 3:flow characterisation*, Glasgow, pp. 21-22

Bobyn, J.D., Stackpool, G.J., Hacking, S.A., 1999, Characteristics of bone ingrowth and interface mechanics of a new porous tantalum biomaterial. *The Journal of Bone and Joint Surgery,* volume 81(5), pp. 907-914.

Bobyn, J.D., Pilliar, R.M., Binnington, A.G., Szivek J.A., 2005, The effect of proximally and fully porous-coated canine hip stem design on bone modeling. *Journal of Orthopaedic Research,* volume 5, pp. 393-408.

Brunahl, J., 2003, Physics of Piezoelectric Shear Mode Inkjet Actuators. *PhD thisis,* Royal Insitute of Technology.

Chan, C., 1993, *Polymer Surface Modification and Characterization,* New York, Hanser

Chen D.R., Bei J.Z., Wang S.G., 2000, Polycaprolactone microparticles and their biodegradation, *Polymer Degradation and Stability*, volume 67(3), pp. 455-459

Chen, X.S., Ashcroft, I.A., Wildman, R.D., Tuck, C.J., 2015, A inverse analysis method for the depth profiling and characterisation of 3D printed objects, Accepted by *Proceedings of Royal Society*.

Cho., J.D., Kim, H.K., Kim, Y.S., Hong, J.W., 2003, Dual curing of cationic UV-curable clear and pigmented coating systems photosensitized by thioxanthone and anthracene. *Polymer Testing*, volume 22(6), pp. 633-645.

Ciapetti, G., Ambrosio, L., Savarino, L., Granchi, D., Cenni, E., Baldini, N., Pagani, S., Guizzardi, S., Causa, F., Giunti, A., 2003, Osteoblast Growth and Function in Porous Poly ε-caprolactone Matrices for Bone Repair: a Preliminary Study, *Biomaterials*, volume 24, pp. 3815-3824.

Clay, P., Gilbert, R.G., 1995, Molecular Weight Distributions in Free-Radical Polymerizations. 1. Model Development and Implication for Data Interpretation. *Macromolecules,* volume 28, pp. 552-569.

Coran, A., 1978, *Science and Technology of Rubber.* New York: Academic Press.

Cuchiara, M.P., Allen, A.C.B., Chen, T.M., Miller, J.S., West, J.L., 2010. Multilayer microfluidic PEGDA hydrogels. *Biomaterials,* volume 31, pp. 5491-5497.

Davidson, R., 1999, Exploring the Science, Technology and Applications of UV and EB Curing, *SITA Technology,* pp. 67-85.

Deegan, R., Bakajin, O., Dupont, T.F., Huber, G., Nagel, S.R., 1997, Capillary flow as the cause of ring stains from dried liquid drops. *Nature,* volume 389, pp. 827-829.

Deegan, R., Bakajin, O., Dupont, T.F., Huber, G., Nagel, S.R., 2000. Contact Line Deposits in An Evaporation Drop, *Physical Review E,* volume 62(1), pp. 756-765.

Deipold, T., Obermeier, E., Berchtold, A., 1998, A micro machined continuous inkjet printhead for high resolution printing. *Journal of Micromechanicals and Microengineering,* volume 8, pp. 144-147.

Dimatix, 2014, *Dimatix Material Printer,* [Online], Available at: http://www.fujifilmusa.com/products/industrial_inkjet_printheads/deposition-products/dmp-2800/index.html
[Accessed 11 9 2014].

Dimatix, 2010, *DMP 2800 User's Guide Version 2.0*, U.S.A, Fujifilm Dimatix.

Dimitrov, D., Schreve, K., De Beer, N., 2006, Advances in Three Dimensional Printing-State of the Art and Future Perspectives, *Rapid Prototyping*, volume 12(3), pp. 136-147.

Dong, H., Carr, W.W., Morris, J.F., 2006, Visualization of drop-on-demand inkjet: Drop formation and deposition. *Review of Scientific Instruments,* volume 77.

Ebewele, R., 2000, *Polymer Science and Technology.* London, Boca Raton.

Eggers, J., Villermaux, E., 2008. Physics of Liquid Jets. *Reports on Progress in Physics,* Volume 71.

EOS, 2015, *FORMIGA P 110 Technical data.* [Online] Available at: http://www.eos.info/systems_solutions/plastic/systems_equipment/formiga_p_110
[Accessed Jan 2015].

Eshraghi, S., Das, S., 2010, Mechanical and Microstructural Properties of Polycaprolactone Scaffolds with One-dimensional, Two-dimensional and Three-dimensional Orthogonally Oriented Porous Architectures Produced by Selective Laser Sintering, *ActaBiometerialia*, volume 6, pp. 2467-2476.

Fedorovich, N.E., Oudshoom, M.H., van Geemen, D., 2009, The effect of photopolymerization on stem cells embedded in hydrogels. *Biomaterials,* volume 30, pp. 344-353.

Feng, Z., Sanping Z., 2003 , Synthesis and characterization of biodegradable hydrogels based on photopolymerizable acrylate-terminated CL-PEG-CL macromers with supramolecular assemblies of a-cyclodextrins. *Polymer,* volume 44, pp. 5177-5186.

Ferreira, P., Coelho, J.F.J., Gil, M.H., 2008, Development of a new photocrosslinkable biodegradable bioadhesive. *International Journal of Pharmaceutics ,* volume 352, pp. 172-181.

Gan, H.Y., Shan, X., Eriksson, T., Lok, B.K., Lam, Y.C., 2009, Reduction of droplet volume by controlling actuating waveforms in inkjet printing for micro-

pattern formation, *Journal of Micromechanics and Microengineering,* volume 19(5). pp. 1-8

Gao, F., Sonin, A.A., 1994, Precise Deposition of Molten Microdrops: the physics of digital microfabrication. *Proceedings of the Royal Society A,* volume 444, pp. 533-554.

Gardel, M.L., Shin, J.H., MacKintosh, F.C., Mahadevan, L., 2004, Elastic behaviour of cross-linked and bundled actin networks. *Science,* volume 304(5675), pp. 1301-1305.

Gauthier, M., Stangel, I., Ellis, T.H., 2005, Oxygen Inhibition in Dental Resins. *Journal of Dental Research,* volume 84(8), pp. 725-729.

Giannatsis, J., Dedoussis, V., 2009, Additive Fabrication Technology Applied to Medicine and Health Care: A Review, *The International Journal of Advanced Manufacturing Technology ,* volume 40, pp. 116-127.

Gibson, I., 2010, *Additive Manufacturing Technologies,* Springer Science.

Gibbons, G., Williams, R., Purnell, P., Farahi, E., 2010, 3D Printing of Cement Composites, *Advanced in Applied Ceramics*, volume 109(5), pp. 287-290.

Goncalves T.S., Schmitt V.M., Thomas M., Lopes de Souza M.A., Macedo de Menezes L., 2008, Cytotoxicity of two autopolymerized acrylic resin used in orthodontics, *Angle Orthodontist*, volume 78(5), pp. 926-930

Gong, C.Y., Wu, Q.J., Dong, P.W., Shi, S., 2009, Acute Toxicity Evaluation of Biodegradable In Situ Gel-Forming Controlled Drug Delivery System Based

on Thermosensitive PEG-PCL-PEG Hydrogel,. *Journal of Biomedical Materials Research Part B: Applied Biomaterials,* volume 91B(1), pp. 26-36.

Gowariker, V., 1986, *Polymer Science.* New York, Wiley.

Goulet R.W., Goldstein S.A., Ciarelli M.J., Kuhn J.L., Brown M.B., Feldkamp L.A., 1994, The relationship between the structural and orthogonal compressive properties of trabecular bone, *Hournal of biomechanics*, volume 27(4), pp. 375-389

Grodowska K., Parczewski A., 2010, Organic solvents in the pharmaceutical industry, *Acta Poloniae Pharmaceutica-Drug Research*, volume67 (1), pp.3-12

Gunatillake P.A., Adhikari R., 2003, Biodegradable Synthetic Polymers for Tissue Engineering, *European Cells and Materials*, volume 5, pp.1-16.

Hacking, S.A., Bobyn, J.D., Toh, K.K., Tanzer, M., 2002, Fibrous tissue ingrowth and attachment to porous tantalum, *Journal of Biomedical Material Research,* volume 52, pp. 631-638.

Hahn, M.S., Miller, J.S., West, J.L., 2005, Laser Scanning Lithography for Surface Micropatterning on Hydrogel, *Advanced Materials,* volume 17, pp. 2939-2942.

Hahn, M.S., Taite, L.J., Moon, J.J., Rowland, M.C., Ruffino, K.A., 2006, Photolithographic patterning of polyethylene glycol hydrogels. *Biomaterials,* volume 27, pp. 2519-2524.

Harrison A., Huggett R., 1992, Effect of the curing cycle on residual monomer levels of acrylic resin denture base polymers, *Journal of Dentistry*, volume 20(6), pp. 370-374

Hoffman, A.S., 2012. Hydrogels for Biomedical Applications. *Advanced Drug Delivery Reviews,* volume 64, pp. 18-23.

Hogue, M.E., San, W.Y., Wei, F., Li, S., 2009, Processing of polycaprolactone and polycaprolactone-based copolymers into 3D scaffolds, and their cellular responses. *Tissue Engineering,* volume 15(10), pp. 3013-3024.

Hong, B T, Shin, K S, Kim, D S., 2005, Ultraviolet‐curing behavior of an epoxy acrylate resin system, *Journal of Applied Polymer Science*, volume 98(3): pp. 1180-1185.

Hopkinson, N., 2006, *Rapid Manufacturing: An Industrial Revolution for the Digital Age,* West Sussex, John Wiley and Sons Ltd.

Huang M., Li S., Hutmacher D.W., Schantz J., Vacanti C.A., Braud C., Vert M., 2004, Degradation and cell culture studies on block copolymers prepared by ring opening polymerization of epsilon-caprolactone in the presence of poly(ethylene glycol), *Journal of Biomedical Materials Research*: Part A, volume 69A(3),pp. 417-427

Hymer C.B., 2002, Residual solvent testing: a review of gas-chromatographic and alternative techniques, *Pharmaceutical Research*, volume 20(3), pp. 337-344

Iroh J.O.,1999, in *Polymer Data Handbook*, Oxford University Press, New York, pp.361-362

Ivkovic N., Bozovic D., Ristic S., Mirjanic V., Jankovic O., 2013, the residual monomer in dental acrylic resin and its adverse effects, *Contemporary Materials*, volume 4(1), pp/ 84-91.

James, H.M., Guth, E., 1943, Theory of the Elastic Properties of Rubber. *Jounral of Chemical Physicals,* volume 11(10), pp. 455.

Jette, K.K., Law, D., Schmitt, E.A., Kwon, G.S., 2004, Preparation and drug loading of Poly(Ethylene Glycol)-block-Poly(ε-caprolactone) micelles through the evaporation of cosolventazeotrope, *Pharmaceutical Research,* volume 21(7), pp. 1184-1191.

Jiang, C.P., Huang, J.R., Hsieh, M.F., 2011, Fabrication of synthesized PCL-PEG-PCL tissue engineering scaffolds using an air pressure-aided deposition system. *Rapid Prototyping,* volume 17(4), pp. 288-297.

Juszczak, L.J., Friedman J.M., 1999, UV resonance Raman spectra of ligand binding intermediates of sol-gel encapsulated hemoglobin. *The Journal of Biological Chemistry,* volume 274, pp. 30357-30360.

Kajiya, T., Doi, M., 2011, Dynamics of Drying Process of Polymer Solution Droplets: Analysis of Polymer Transport and Control of Film Profiles, *Journal of the Society of Rheology Japan,* volume 39(1-2), pp. 17-28.

Kim, D., Jeong, S., Park, B.K., Moon, J., 2006, Direct Writing of Silver Conductive Pattern: Improvement of Film Morpholigy and Conductace by Controlling Solvent Composition, *Applied Physics Letters,* volume 89.

Kweon, H.Y., Yoo, M.K., Park, I.K., Kim, T.H., Lee, H.C., Lee, H.S., 2003, A novel degradable polycaprolactone networks for tissue engineering. *Biomaterials,* volume 24, pp. 801-808.

Kwon, K., Kim, W., 2007, A waveform design method for high-speed inkjet printing based on self-sensing measurement,*Sensors and Actuators,* volume 140, pp. 75-83.

Labet M., Thiele,ams W., 2009, Synthesis of Polycaprolactone: a review, *Chemical Society Review*, volume 38, pp.3484-3504

Lam C.X.F., Savalani M.M., Teoh S., Hutmacher D.W., 2008, Dynamics of invitro polymer degradation of polycaprolactone-based scaffolds: accelerated versus simulated physiological conditions, *Biomedical Materials*, volume 2008(3), pp. 1-15

Leach, J.B., Schmidt, C.E., 2005, Characterization of protein release from photocrosslinkable hyaluronic acid-polyethylene glycol hydrogel tissue engineering scaffolds, *Biomaterials,* volume 26(2), pp. 125-135.

Lee, J.K., Lee, U.J., Kim, M.K., Lee, S.H., Kang, K.T., 2011, Direct writing of semiconducting polythiophene and fullerene derivatives composite from bulk heterojunction solar cell by inkjet printing, *Thin Solid Films,* volume 519, pp. 5649-5653.

Li S., Garreau H., Pauvert B., McGrath J., Toniolo A., Vert M., 2002, Enzymatic degradation of block copolymers prepared from epsilon-caprolactone and poly(ethylene glycol), *Biomacromolecules,* volume 3, pp.525-530.

Lohfeld S., Tyndyk M.A., Cahill S., Flaherty N., Barron V., McHugh P.E., 2010, A Method to fabricate small features on scaffolds for tissue engineering via selective laser sintering, *Journal of biomedical Science and Engineering*, volume 3, pp. 138-147.

Makerbot, 2015, *Makerbot Replicator 3D printer.* [Online] Available at: http://store.makerbot.com/compare [Accessed Jan 2015].

Mazzoli A., Ferretti C., Gigante A., Salvolini E., Mottioli-Belmonte M., 2015, Selective Laser Sintering Manufacturing of Polycaprolactone bonne scaffolds for applications in bone tissue engineering, *Rapid Prototyping Journal*, volume21(4),pp. 386-392

Merkli A., Tabatabay C., Gurny R., Heller J., 1998, Biodegradable Polymers for the Controlled Release of Ocular Drugs, *Progress in Polymer Science*, volume 23(3), pp. 563-580.

Middleton. C.J., Tipton J.A., 2000, Synthetic biodegradable polymers as orthopedic devices, *Biomaterials*, volume 21, pp. 2335-2346.

Nicodemus, G.D., Bryant, S.J., 2007, Cell Encapsulation in Biodegradable Hydrogels for Tissue Engineering Applications, *Tissue Engineering Part B: Reviews,* volume 14(2), pp. 149-165.

Norman, S., 1996, Photoinitiators for UV and visible curing of coatings:Mechanisms and properties. *Journal of Photochemistry and Photobiology A:Chemistry,* volume 100(1-3), pp. 101-107.

Objet, 2012, *Polyjet Technology.* [Online] Available at: http://www.objet.com/PRODUCTS/PolyJet_Technology [Accessed Jan 2012].

O'D onnell P.B., McGinity J.W., 1997, Preparation of microspheres by the solvent evaporation technique, *Advanced Drug Delivery Reviews*, volume 28(1), pp.25-42

Ramanath, H.S., Chua, C.K., Leong, K.F., 2008, Melt Flow Behaviour of Poly-ε-caprolactone in Fused Deposition Modelling, *Journal of Material Science*, volume 19, pp. 2541-2550.

Ovsianikov, A., Malinauskas, M., Schlie, S., Chichkow, B., 2011, Three-dimensional laser micro- and nano-structuring of acrylated poly(ethylene glycol) materials and evaluation of their cytoxicity for tissue engineering applications. *Acta Biomaterialia,* volume 7(3), pp. 967-974.

Palit, S.R., 1956. Thermodynamic Interpretation of the Eötvös Constant, *Nature,* volume 177(4521), p. 1180.

Pappas, P., 1980, *UV Curing Science and Technology,* Stamford, USA: Technology Marketing Corporation.

Partee B., Hollister S.J., Das S., 2006, Selective laser sintering process optimization for layered manufacturing of CAPA 6501 polycaprolactone bone

tissue engineering scaffolds, *Journal of manufacturing science and engineering*, volume 128, pp. 531-540

Parisse, F., Allain, C., 1996, Shape Changes of Colloidal Suspension Droplets During Drying, *Journal of Physicals II,* volume 6, pp. 1111-1119.

Park, J., Woo, D.G., Sun, B.K., Chung, H.M., Im, S.J., 2007, In vitro and in vivo test of PEG/PCL-based hydrogel scaffold for cell delivery application. *Journal of Controlled Release,* volume 124, pp. 51-59.

Park S. Kim G., Jeon Y.C., Koh Y. Kim W., 2009, 3D Polycaprolactone scaffolds with Controlled pore structure using a rapid prototyping system, *Journal of materials Science: Materials in Medicine*, volume 20(1), pp. 229-234.

Pimbley, W.T., Lee, H.C., 1977, Satellite Droplet Formation in a Liquid Jet. *IBM Journal of Research and Development ,* volume 21(1), pp. 21-30.

Schwalm, R., 2006, *UV Coatings: Basics, Recent Developments and New Applications,* Elsevier Science.

Seeton C.J., 2006, Viscosity–temperature correlation for liquids, *Tribology Letters,* volume 22(1), pp. 67-78.

Shin, P., Sung, J., Lee, M.H., 2011, Control of droplet formation for low viscosity fluid by double waveforms appliedto a piezoelectric inkjet nozzle. *Microelectronics Reliability,* volume 51, pp. 797-804.

Shor, L., Güçeri, S., Chang, R., Gordon, J., Kang, Q., Hartsock, L, Sun, W. 2009. Precision extruding deposition (PED) fabrication of polycaprolactone

(PCL) scaffolds for bone tissue engineering, *Biofabrication*, volume 1(1), pp. 1-10

Sinha V.R., Bansal K., Kaushik R., Kumria R., Trehan A., 2004, Poly-epsilon-caprolactone microspheres and nanospheres:an overview, Internal Journal o fPharmaceutics, volume 278(1), pp. 1-23.

Stopp, S., Wolff, T., Irlinger, F., Lueth, T., 2008, A new Method for Printer Calibration and Contour Accuracy Manufacturing with 3D-print Technology, *Rapid Prototyping*, volume 14(3), pp. 167-172.

Stjerndahl A., Finne-Wistrand A., Albertsson A.C., Backesjo C.M., Lindgren U., 2007, Minimization of residual tin in the controlled Sn(II)octoate-catalyzed polymerization of epsilon-caprolactone, *Journal of Biomedical Materials Research Part A*, volume 87A(4), pp. 1086-1091

Stratasys, 2014, *Production Series.* [Online] Available at: http://www.stratasys.com/3d-printers/production-series/ [Accessed 07 July 2014].

Stringer, J., Derby B., 2010. Formation and stability of lines produced by injet printing. *Langmuir,* volume 26(12), pp. 10365-10372.

Sun H., Mei L., Song C., Cui X., Wang P., 2006, The in vivo degradation, absorption and exceretion of PCL-based implant, *Biomaterials*, volume 27(9), pp. 1735-1740.

Tang, Z.G., Black, R.A., Curran, J.M., Hunt, J.A., Rhodes, N.P., Williams D.F., 2004. Surface properties and biocompatibility of solvent-cast poly[e-caprolactone films. *Biomaterials,* Volume 25, pp. 4741-4748.

Teichler, A., Eckardt, R., Friebe, C., Perelaer, J., Schubert, U.S., 2011, Film Formation Properties of Inkjet Printed Poly(phenylene-eth ynylene)-poly(phenylene-vinylene)s, *Thin Solid Films,* volume 519, pp. 3695-3702.

Toti, U.S., Kariduraganavar, M.Y., 2000. Density, Viscosity, Refractive Index, and Speed of Sound of Ternary Systems: Polystyrene in 1,4-Dioxane + Tetrahydrofuran Mixtures at (298.15, 303.15, and 308.15) K. *Journal of Chemical&Engineering Data,* 45(5), pp. 920-925.

Tsuchiya H., Hoshino Y., Tajima K., Takagi N., 1994, Leaching and cytotoxicity of formaldehyde and methyl methacrylate from acrylic resin denture base materials, *The Journal of prosthetic dentistry*, volume 71(6), pp.618-624.

Wang, D., 2001, *UV curing materials: Theory and Application,* Science Publisher.

Wang, X., Carr, W.W., Bucknall, D.G., 2010, High-shear-rate capillary viscometer for inkjet inks. *Review Of Scientific Instruments,* Volume 81.

Williams, D., 1971, *Polymer Science and Engineering,* Prentice-Hall.

Williams, J., Adewunmi, A., Schek, R.M., Flanagan, C.L., 2005, Bone Tissue Engineering using Polycaprolactone Scaffold Fabricated via Selective Laser Sintering, *Biomaterials*, volume 26, pp. 4817-4827.

Wohlers, T., 2007, *Wohlers Report 2007,* Colorado, Wohlers Associates Inc.

Woodruff M.A., Hutmacher D.W., 2010,The return of a forgotten polymer-Polycaprolactone in the 21st century, *Progress in Polymer Science*, volume 35, pp.1217-1256

Woodward S.C., Brewer P.S., Moatamed F., Schindler A., Pitt C.G., 1985, The intracellular degradation of poly (epsilon‐caprolactone), *Journal of biomedical materials research*, volume 19(4),pp. 437-444.

Xu, J., Pang, W, Shi W., 2006, Synthesis of UV-curable organic–inorganic hybrid urethane acrylates and properties of cured films, *Thin Solid Films*, volume 514(1): pp. 69-75

Yamaguchi, K., Sakai, K., Yamanaka, T., Hirayama, T., 2000, Generation of three-dimensional micro structure using metal jet, *Precision Engineering,* volume 24, pp. 2-8.

Yamaguchi, K., Sakai, K., Yamanaka, T., Hirayama, T, 2003, Generation of 3-dimensional micro-structure by metal jet, *Microsystem Technology,* volume 9, pp. 215-219.

Yeong W.Y., Sudarmadji N., Yu H.Y., Chua C.K., Leong K.F., Venkatraman S.S., Boey Y.C.F., Tan L.P., 2009, Porous polycaprolactone scaffold for cardiac tissue engineering fabricated by selective laser sintering, *Acta Biomaterialia,* volume 6, pp. 2028-2034.

Yin, H.B., Gong, C.Y., Shi, S., Liu, X.Y., 2010, Toxicity evaluation of biodegradable and thermosensitive PEG-PCL-PEG hydrogel as a potential in

situ sustained ophthalmic drug delivery system. *Journal of Biomedical Materials Research Part B: Applied Biomaterials,* volume 92B(1), pp. 129-137.

Zein, I., Hutmacher, D.W., Tan, K.C., Teoh, S.H., 2002, Fused Deposition Modeling of Novel Scaffold Architectures for Tissue Engineering Application. *Biomaterials,* volume 23, pp. 1169-1185.

Zhang, T., Oyama, T., Aoshima, A., Hidaka, H., 2001, Photooxidative N-demethylation of methylene blue in aqueous TiO2 dispersions under UV irradiation. *Journal of Photochemistry and Photobiology A: Chemistry,* volume 140(2), pp. 163-172.

Zhu, J., 2010. Bioactive Modification of Poly(ethylene glycol) hydrogels for tissue engineering. *Biomaterials,* volume 31(17), pp. 4639-4656.

Appendix I

Optical Microscope Pictures of Samples printed in air environment

	5X	10X	100X
PI1 AC1	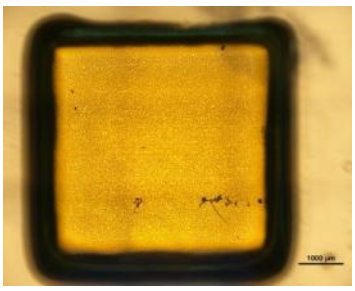	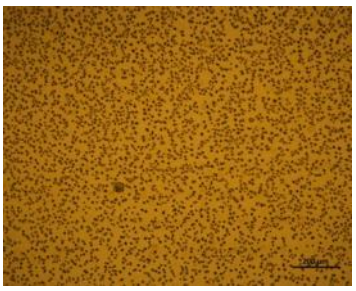	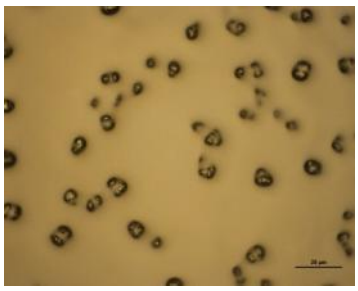
	(a)	(b)	(c)
PI2 AC2	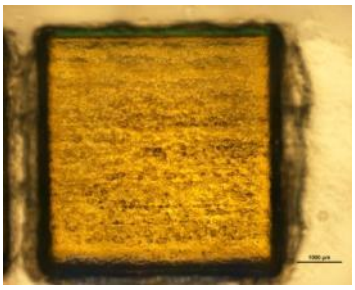	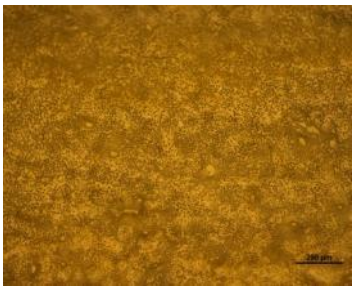	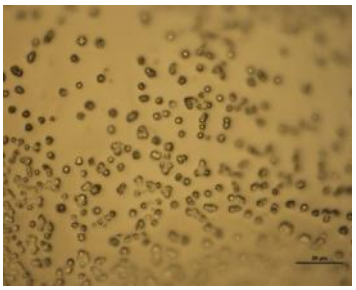
	(d)	(e)	(f)
PI3 AC3	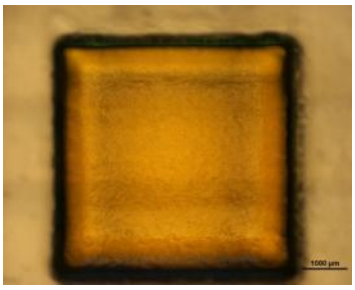	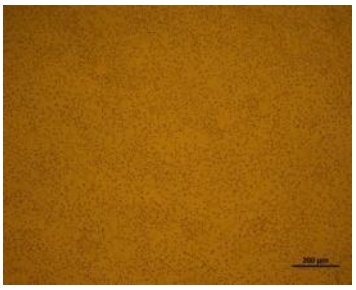	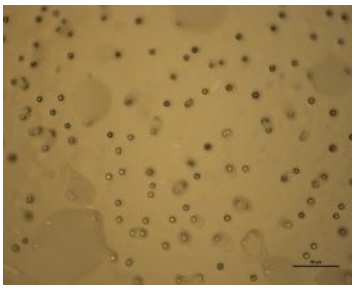
	(g)	(h)	(i)

Optical Microscope Pictures of Samples printed in nitrogen environment

	5X	10X	100X
PI1 AC1	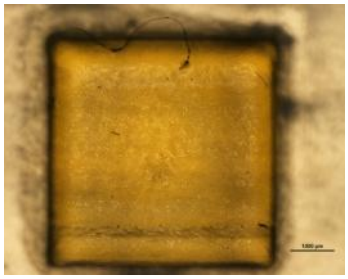	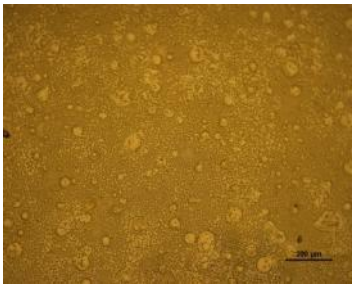	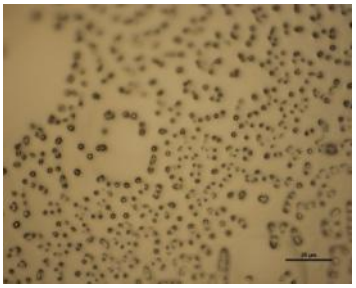
	(a)	(b)	(c)
PI2 AC2	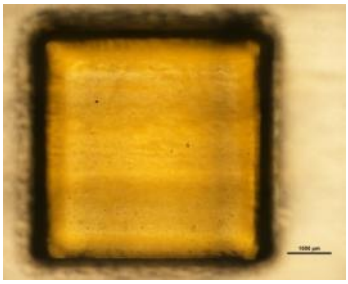		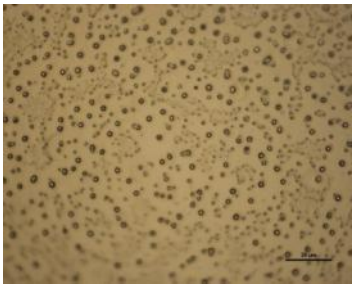
	(d)	(e)	(f)
PI3 AC3	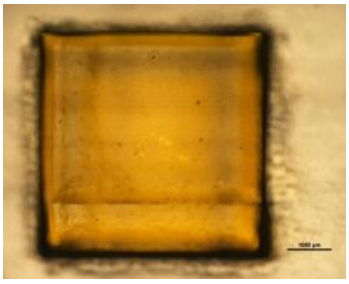	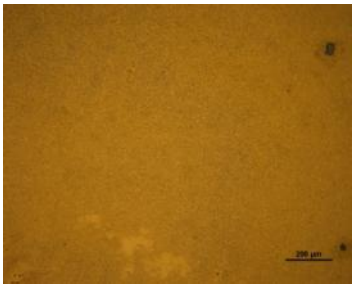	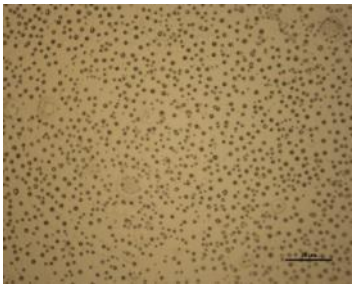
	(g)	(h)	(i)

Optical Microscope Pictures of Samples printed in air environment after different length of post-curing

	5X	10X	100X
10mins	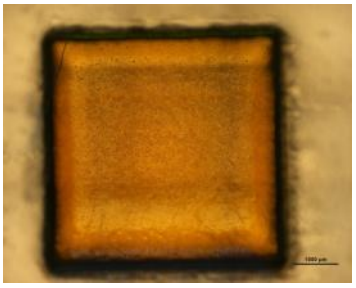 (a)	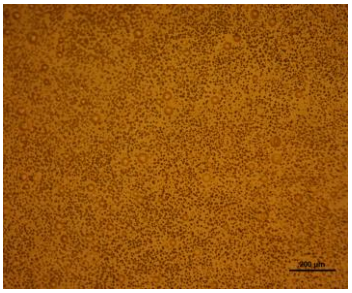 (b)	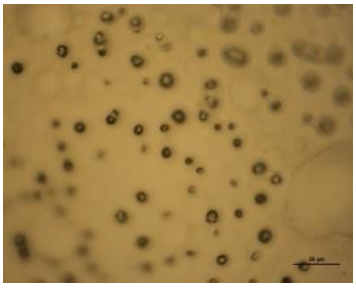 (c)
20mins	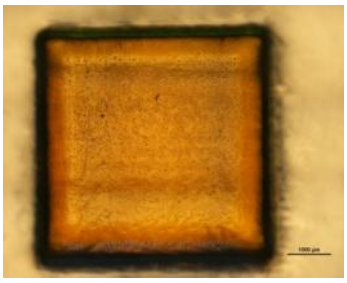 (d)	 (e)	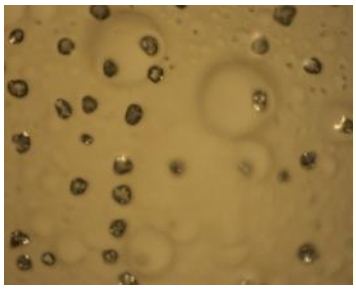 (f)
30mins	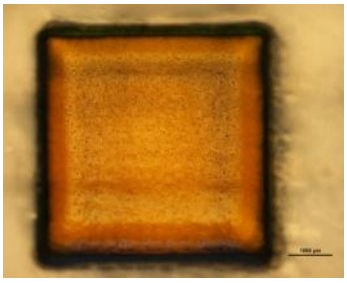 (g)	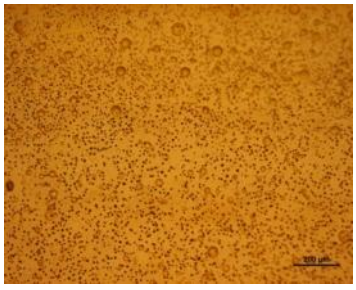 (h)	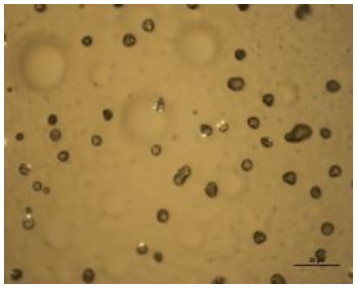 (i)

Optical Microscope Pictures of Samples printed in nitrogen environment after different length of post-curing

	5X	10X	100X
10mins	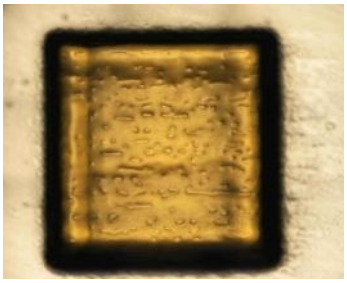		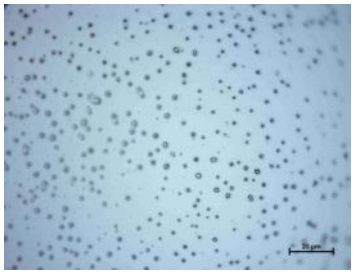
	(a)	(b)	(c)
20mins	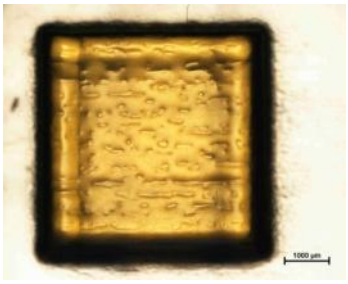		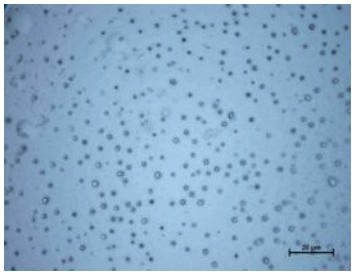
	(d)	(e)	(f)
30mins	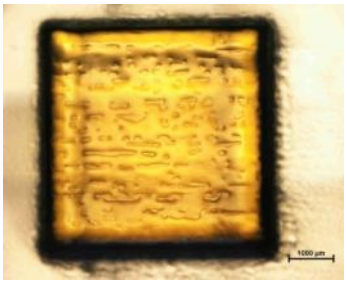	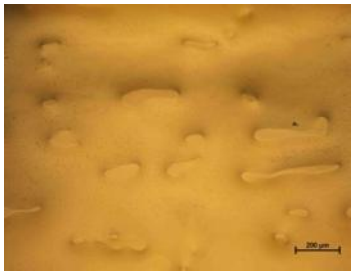	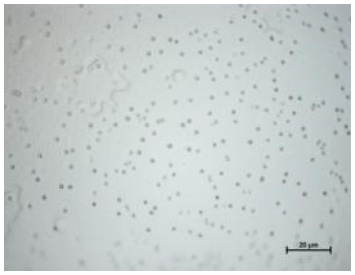
	(g)	(h)	(i)

Appendix II

Cross-section Nano-indentation data through the sample's cross-section measured by mounting into epoxy

0 minute				
Distance from top surface (µm)	Hardness (MPa)		Indentation Modulus(MPa)	
	Avg	STDV	Avg	STDV
50	6.77	0.15	63.77	0.86
100	6.17	0.13	54.4	1.05
150	5.85	0.17	48.81	0.7
200	5.97	0.24	47.89	0.75
250	5.88	0.13	46.43	0.61
300	5.81	0.08	45.57	0.37
350	5.81	0.13	43.76	0.53
400	5.73	0.12	42.98	0.72
450	5.8	0.16	44.6	0.78
500	5.6	0.07	45.17	0.78
550	5.64	0.17	46.66	0.87
600	5.89	0.18	49.86	0.8
650	6.55	0.15	61.87	2.45

30 minutes				
Distance from top surface (µm)	Hardness (MPa)		Indentation Modulus(MPa)	
	Avg	STDV	Avg	STDV
50	6.52	0.20	67.97	2.30
100	5.86	0.42	53.25	1.68
150	5.45	0.20	46.12	0.73
200	5.61	0.30	44.81	1.36
250	5.43	0.35	43.52	1.66
300	5.64	0.21	42.99	1.05
350	5.5	0.23	42.38	0.79
400	5.33	0.15	41.95	0.39
450	5.35	0.17	42.00	0.84
500	5.39	0.11	43.08	0.90
550	5.31	0.25	44.62	0.92
600	5.87	0.17	50.49	0.85
650	5.92	0.26	57.81	2.01

60 minutes				
Distance from top surface (µm)	Hardness (MPa)		Indentation Modulus(MPa)	
	Avg	STDV	Avg	STDV
50	6.17	0.5	56.03	2.59
100	5.84	0.36	48.5	0.94
150	5.84	0.18	47.31	0.95
200	5.70	0.32	45.59	1.25
250	5.53	0.17	44.22	0.72
300	5.62	0.13	44.64	0.74
350	5.52	0.08	43.95	0.38
400	5.47	0.23	43.62	0.84
450	5.55	0.15	43.06	0.74
500	5.40	0.13	42.15	1.22
550	5.48	0.25	42.63	1.06
600	5.68	0.31	46.41	0.44
650	6.11	0.38	53.21	1.30

90 minutes				
Distance from top surface (µm)	Hardness (MPa)		Indentation Modulus(MPa)	
	Avg	STDV	Avg	STDV
50	6.89	0.61	66.71	2.1
100	6.83	0.43	56.8	1.71
150	6.73	0.55	52.21	2.11
200	5.76	0.36	45.04	1.32
250	5.51	0.31	43.33	1.21
300	5.36	0.6	42.29	2.76
350	5.28	0.31	42.33	2.65
400	5.5	0.54	41.06	1.75
450	5.55	0.49	42.17	1.13
500	5.66	0.4	43.58	1.29
550	5.74	0.62	45.57	2.31
600	5.91	0.31	47.49	0.9
650	6.72	0.38	53.43	0.48